Dear Editor,

Following suggestions from the two co-authors, we have now modified the original manuscript, taking on board all suggestions. All changes to the manuscript are highlighted as track changes (see attachment). Please also find attached a point-by-point response to each reviewer comment.

Yours faithfully,

Adil Shah

Response 1 to Reviewer 1

We thank the reviewer for taking the time to submit a very fair and useful review. This review has greatly helped to improve our manuscript in terms of clarity and our presentation of the key outcomes of this work. We have taken all of the comments on board and have submitted our responses below (red text) to each reviewer comment (black text).

General comments: The paper is a useful addition to the growing body of literature around these low-cost sensors. In particular, the discussion of ambient vs. synthetic air for calibration and the power-law model presented in section 3 are interesting contributions. I found the paper's narrative somewhat difficult to follow, and had difficulty keeping track of the different systems and variables (e.g. System A vs. System B; the various resistance values). Possibly some minor restructuring to center the novel findings and more explicit terminology/notation throughout would help with readability.

We are grateful to the reviewer for their kind comments. We have taken this opportunity to rename certain variables to avoid ambiguity. We have also improved the conclusion section (as suggested by the reviewer) to better emphasise the key findings of this work.

Specific comments by line number:

110-130: While these previous studies report usable results with TGS2600, they used different models and system designs, and it is unclear whether the results are generalizable or tied to specific characteristics of the research sites or experiments. In our previous study (https://amt.copernicus.org/articles/15/5117/2022/) we did not find TGS2600 to respond to low levels of methane in a laboratory setting. This section would be improved by mention of some of the papers' caveats; for example, Eugster and Kling (2012) note in section 3.5 an R^2 of less than 0.20; Collier-Oxandale et al. found different models necessary for their different sites and note that some overfitting was observed, and so on.

We value the reviewer's advice to elaborate on the limitations of the various Figaro testing studies, discussed in the introduction. We have therefore expanded the end of section 1 to highlight specific limitations of previous studies using the TGS 2600. Yet we have remained cautious to limit the level of detail, to avoid this section becoming over-exhaustive.

It is unfortunate that we previously overlooked the interesting outcomes within Furuta *et al.* (2022), due to its recent publication. We thank the reviewer for highlighting its publication and have taken this opportunity to incorporate its valuable findings into our manuscript.

While we recognise that the reviewer did not observe strong TGS 2600 or TGS 2611-C00 methane sensitivity, we suggest that this may be due to dominant effect of variability in [H_2O] in their tests. As the reviewer suggests in their own manuscript (Furuta et al., 2022), condensation and evaporation may have occurred from their chamber walls, which we now discuss in section 5.2. In fact, we encountered a similar issue during our own chamber testing work, when we first conducted tests with humidity control

turned off. For this reason, we had no choice but to use humidity control, resulting in vast variations in [H_2O] (see section 3.3), albeit about a central targeted humidity level.

172 & 184: The 5k resistor choice needs justification. As you note at line 165, the reference resistor should be close in value to the expected sensor resistance. Around background methane levels one would expect a sensor resistance an order of magnitude larger than your 5k choice, as can be seen in your supplemental information (which is consistent with our observations).

The reviewer is right to suggest that a load resistor with a higher resistance would have been more appropriate in this work, based on typical resistance measurements made by the Figaro sensors. However, we chose to use the same load resistance in both System A and System B, to make measurements and systematic errors from both loggers as comparable as possible. Thus, we were effectively bound by the resistance selected by the System A manufacturer.

Therefore, we now clarify that the System A load resistor was hard-wired into the logging box in section 2.2. We now also state that we chose the load resistance in System B to mirror System A, in section 2.3.

The choice of a 5 kΩ load resistor used by the System A manufacturer can be justified by looking to load resistors used in pervious work. For example, Jørgensen *et al.*, 2020 used a 10 kΩ resistor. We now make this additional point in the manuscript in section 2.2. We also include a short discussion on this point in section 4.2, where measurements from the Amailloux landfill site are presented. Although a higher load resistance would improve sensitivity, 5 kΩ is sufficient to detect resistance variations in response to changes in the surrounding environment.

169-179: More detail about the logging system would be useful, particularly the ADC resolution, noise floor, and so on, as these can be expected to determine sensitivity in combination with the reference resistor choice. I would be interested in a brief sensitivity calculation using the ADC resolution/noise floor and the 5k reference resistor to show the ability to detect small changes in the sensor resistance. The logger's power supply stability is also a critical detail for your system's performance.

This is a useful suggestion. We have provided additional details on the ADC resolution in section 2.3. We now specify that although it has a maximum resolution of 18 bit, we set it to sample at 16 bit (for improved sampling frequency), resulting in 0.15 mV resolution. This translates into a resistance precision of 0.6 Ω, assuming 5 kΩ Figaro resistance.

According to the manufacturer data sheet, the System B power supply has rated ripple and noise effects of less than ±1 mV. In reality, we observed a standard deviation of ±0.1 mV, when tested with the ADC. We now also provide this additional detail in section 2.3.

We thank the reviewer for the suggestion to include these details, which we previously overlooked in terms of importance. We hope that these useful resolution values support our measurement setup.

194: For the application 35mV is possibly not good enough; is this value referring to the accuracy of the setting, ripple, drift, or a combination of all of them? 35mV ripple would swamp any sensor response to small methane changes, for example. You have some discussion of supply voltage sensitivity in your supplemental information, but a short quantitative discussion of what this supply voltage tolerance means in terms of sensor response/detection capability would be illuminating, as it's not immediately obvious to me how big of a concern the supply voltage accuracy is for your experiment.

We agree that an actual 35 mV power supply accuracy (including ripple effects) would be insufficient in this work. In reality, this 35 mV value refers to a read-back setting accuracy, which we now clarify in the manuscript in section 2.3. As we adjusted the supply voltage using an independent measurement of potential difference across the Figaro circuit board, the power supply voltage accuracy has no effect on our testing. To further augment our confidence in the stability of our power supply unit, we measured the circuit board potential difference on many occasions on different days, finding no change in voltage. Nevertheless, the reviewer raises an important point here which we hope we have now resolved in the manuscript in section 2.3.

311-318: The H2O fluctuations within each period are substantial (from the chart, up to 0.5%) and appear to continue over the whole of each sampling period. If the sensors require hours to stabilize at a given humidity level, will they stabilize at all given this large fluctuation?

The reviewer makes a valuable observation regarding the large fluctuations in [H_2O] during our environmental chamber tests. Our work shows that the key issue associated with unstable water, is the associated lengthy Figaro stabilisation time, whereby resistance gradually exponentially decays towards a stable resistance (see Appendix B). We showed that this resistance decay occurs immediately following a step-change in [H_2O].

In the case of the environmental chamber, rather than a single step transition in [H_2O], there is periodic variability about a central point. This phenomenon occurred because the humidity control system constantly works to rectify humidity towards a target setting. As this water variability occurred both above and below the target [H_2O] setting, the water resistance delay effect effectively occurred in both directions simultaneously, thus cancelling itself out.

This can be observed in the top pane of Fig. 7, where after the initial temperature change, Figaro resistance appears to stabilise within 8 hours. Thus, resistance delay effects due to changes in [H_2O] cancel each other out. This argument is now explicitly clarified in the manuscript, where suggested by the reviewer in section 3.3.

316 and throughout: Could you remind the reader what R2 indicates or use a more descriptive subscript? I had difficulty remembering the resistance notation, much of which is similar - R2, Rb, Rl, etc.

To reduce ambiguity, R_l has been renamed to R_{load}, R_b has been renamed to $R_{baseline}$ and R_2 has been renamed to $R_{2\ ppm}$. We hope that these changes make these different resistance terms easier to follow.

337: As the sensors are much more responsive to humidity than to methane, is 3% uncertainty good enough?

This 3% uncertainty value represents the uncertainty in the $R_{2\ ppm}$ resistance baseline (at 2 ppm [CH_4]). $R_{2\ ppm}$ is calculated as a first step, before subsequently calculating [CH_4] enhancements above the 2 ppm [CH_4] level. As $R_{2\ ppm}$ and [CH_4] are calculated separately, and as different steps, it is difficult to compare the two uncertainties and to aggregate them. Therefore, it is not straightforward to make a direct link between uncertainty in $R_{2\ ppm}$ and a theoretical resulting uncertainty in [CH_4]. Each uncertainty for each model must be treated independently. We now emphasise the significance of this 3% value more clearly in the manuscript in section 3.3, to avoid confusion.

As we were unable to derive [CH_4] estimates during field deployment, it is difficult to know whether this 3% uncertainty in $R_{2\ ppm}$ had a significant influence on the overall [CH_4] uncertainty.

355: Fig 10 shows some fluctuation in sensor response in the last two minutes, and it looks like the sensors stabilize at the new methane levels quite quickly. Why is it better to select the last two minutes of each methane level rather than the last 10 minutes, which appear to already be stable?

Our original Figure 10 was used to highlight the general stability of our logging system, rather than the stability of individual Figaro sensors. This figure did not therefore well-illustrate Figaro stabilisation issues, as LSCE001 (shown in the original figure) in one of the more stable sensors that we tested. On the other hand, LSCE009 took longer to stabilise in response to changes in [CH_4]. We have therefore updated Figure 10 with an example of a LSCE009 methane transition, which shows a longer stabilisation period.

Based on the delayed stabilisation effect illustrated in this figure, we used a 2-minute averaging period for all five sensors, for consistency. Furthermore, Figure 11 justifies our choice of averaging time, as the [CH_4] points fit the model curve very well. This satisfies the ultimate aim of this test to characterise methane sensor response. In theory, taking the final minute instead of the final two minutes, would probably produce the same result with no advantage either way. We have added a sentence to section 3.4, to support this reasoning.

361: Why is Eq. 3 only valid for system A?

We thank the reviewer for raising the ambiguity in this statement. In fact, Eq. 3 is an entirely empirical logger-specific model used to relate measured temperature and derived [H_2O] to measured resistance. However, Figaro resistance is also influenced by logger-specific parameters such as airflow and thus associated cooling effects. Furthermore, the gradient between the point of each temperature measurement and each Figaro sensor is also logger-specific, especially for System B, where five

different Figaro sensors were tested in the same logging cell. Therefore, Eq. 3 model parameters can only be used for the logger in which they have been derived. We now clarify these points in section 3.4 and section 3.3.

Table 4: The variation in the alpha values for the sensors is surprising to me - our previous work found TGS2611-E00 to be quite consistent, at least within the same production batch. Were your sensors taken from the same batch, or is there some other component in the system that might be causing this variation? You mention this at line 641, but it would be good to also indicate whether your sensors have the same or different batch codes (printed on the side of the component).

Unfortunately, it is difficult to satisfy this point directly at this moment, as the sensors are currently deployed in the field. However, we know that LSCE001, LSCE003 and LSCE005 were purchased by Scientific Aviation in the USA, whereas LSCE007 and LSCE009 were purchased by us at a later date in France. So, we are fairly certain that at least two different batches were tested, but there may have been more. We now add the point that the sensors likely come from at least two batches in section 5.2 of the manuscript. Unfortunately, if is difficult for us to elaborate any more on this without certainty on specific sensor batches.

421: Again, why the last five minutes? It looks like the sensors stabilize more quickly than that, as far as I can see from Fig. 12.

The averaging duration was chosen as a compromise between maximal stability and maximal averaging points. As the sensors stabilised much faster in this carbon monoxide test compared to the methane test (see response above), a longer averaging period of 5 minutes was more appropriate here, than 2 minutes used for the methane test.

We now highlight this point in section 3.5 of the manuscript and explain our rationale for selecting a 5-minute averaging period. In any case, we do not feel that prolonging the averaging time would have a significant impact on the outcomes of this test: choosing a 10-minute averaging time instead of a 5-minute averaging time would probably yield the same qualitative conclusion.

Section 5.1: Your field and lab tests presumably used different power arrangements. Could you add some discussion of the steps taken to ensure consistent electrical operating conditions between the field and lab tests (particularly 5V supply stability)? In the supplemental information you show that different supply voltages cause different sensor responses; is this possibly involved in the differences?

The reviewer makes an interesting point which we previously failed to clarify. The System A logging system converts battery voltage into a stable 5 V Figaro power supply over a wide battery supply voltage range. Therefore, despite the 12 V lithium ion phosphate battery being connected to a charger instead of a solar panel, the Figaro power supply remained unaffected. We now make this point clear in section. 5.1 and also in section. 2.2, where we introduce the System A field logger.

Section 6: This section is difficult to read to me, and doesn't highlight the major contributions of the paper. It would be more clear to me if broken into multiple paragraphs, and with stronger emphasis on the findings you believe to be particularly important.

We appreciate this useful suggestion and have broken section 6 up into smaller paragraphs. We have rephrased the existing points in this section to improve clarity. We have also included additional key points, to emphasise the key findings of our work, as suggested by the reviewer. For example, we now stress the value of the laboratory testing results, where we characterised methane response using an adapted power fit.

Response 1 to Reviewer 2

We thank the reviewer for taking the time to read our paper and for making a number of useful suggestions to improve the manuscript. This review has helped to reduce ambiguity in the manuscript and improve the presentation of our work. We have taken all of the comments on board and have submitted our responses below (red text) to each reviewer comment (black text).

"Characterising Methane Gas and Environmental Response of the Figaro Taguchi Gas Sensor (TGS) 2611-E00" introduces two field and laboratory logging systems (System A, System B), which were used for an extended deployment at a landfill site with Picarro reference and in an environmental chamber setup, respectively. Resistance of the Figaro sensor in relation to methane, temperature, and water vapor were modeled. Both phases resulted in unexplained variability (ambient air vs synthetic air under lab conditions; and ambient air resistance model in field conditions). A thorough discussion of the issues, including literature discussion, is presented. I think the work is sound and have only minor comments:

We appreciate that the reviewer recognises the value of our work. We hope to have improved the manuscript further by following their suggestions.

L88 Is 'trialed' meant here instead of 'trailed'?

We thank the reviewer for spotting this error which we have now rectified, as suggested.

The references to needing to operate in 'wet air' (L111) and elsewhere should be clarified. The Riddick et al. 2020 paper specifically talks about high uncertainty below 40% relative humidity. Additionally [H2O] is defined as the 'water mole fraction' on L19 but that this is usually specified as water vapor mole fraction since solid and liquid phases are also possible.

We agree that greater clarity is required here. Having reviewed the cited literature again, we have improved the details provided on the effect of water vapour on sensor behaviour. Rivera Martinez *et al.* (2021) showed that resistance was abnormally high at 0% [H_2O] compared to 1% [H_2O]. Eugster and Kling (2012) showed that TGS resistance was unpredictable below 35% relative humidty. Riddick *et al.* (2020) remarked that based on the Eugster and Kling (2012) study, calibrations must be performed in wet conditions. Following our changes, we hope that these points are now more accurately incorporated in the manuscript in section 1.

We have also now changed "water mole fraction" to "water vapour mole fraction" to avoid confusion and to make it clear that we are referring to water in the vapour phase.

Fig 4: Is the Raspberry Pi 3B+ computer outside of the cell pictured? This is important for understanding the data logging configuration

This is a good point. We now clarify in the caption for Figure 4 that the photograph only depicts the logging cell and not the entire logging system, with the logging computer and power supply not shown.

The figure has been updated with an arrow pointing towards the cable which both supplies power and provides connections to the analogue-to-digital converter. We also now explicitly clarify the external placement of the logging computer in section 3.3.

L200 Is Picarro serial feed sent to the Raspberry Pi? It is minor, but simultaneous logging on a computer does not automatically solve timing issues because the Picarro and ADC board used for the Figaro still have separate clocks.

The Picarro streams data to System B using a serial data connection. This detail has now been added to the manuscript. When the Picarro data reaches the System B logger, it is written directly into the System B data file. Therefore, only the System B timestamp is used. There is no use for the Picarro timestamp, which is not recorded by System B, so it does not matter if the Picarro has a separate clock. We apologise for any confusion here and have made efforts to make this point clearer in section 2.3.

As the Picarro data is simply written into the datafile alongside the Figaro data, it does not matter whether the time is accurate or not. So long as a single time stamp is being used, the laboratory experiment is not affected. We acknowledge that this does not solve timing accuracy issues (*i.e.* if System B time in not precisely equal to UTC). However, it eliminates any issues with a time offset (*i.e.* if the Picarro time is different to the System B time), which may become an issue if attempting to combine two separate data files.

L233 suggest moving the statement "All synthetic air cylinders contain a natural balance of nitrogen, oxygen and argon." to the paragraph starting L254 once it is mentioned that multiple synthetic air cylinders were used

This is a good idea. We have followed the reviewer's suggestion.

L239 Does stabilization of [H2O] in the 'large environmental chamber' also play a role, or the settling can simply be attributed to the Figaro?

As this test was conducted with System B in the laboratory and not in the environmental chamber, we can be certain that the observed effect was due to the Figaro itself. We apologise for any confusion here and added a sentence in section 3.2 describing how System B testing was performed in an air-conditioned laboratory. We have also added a sentence in section 2.3 to clarify that this test took place in System B, where [H_2O] was held constant, thanks to the dew-point generator. Only System A was tested in the environmental chamber.

L345 How was the dilution from 5% [CH4] in argon all the way down to 2 ppm achieved? The accuracy of the dilution seems somewhat important, since the agreement with the 2 ppm synthetic air and disagreement with ambient laboratory air is a key area of discussion in the manuscript

In this methane characterisation test, ambient air was used as a standard reference gas, which naturally contains about 2 ppm [CH_4]. Therefore, 2 ppm [CH_4] was quite simply achieved by sampling pure ambient air, with no dilution. In order to increase [CH_4] up to 1 000 ppm, we used mass-flow controllers to add small quantities of gas from a 5% [CH_4] cylinder. We now direct the reader to section 2.3 in section 3.4, where the mass-flow controllers are discussed. The Picarro G2401 reference instrument was used to deduce the resulting [CH_4] from the gas blend.

In section 3.2, where different 2 ppm [CH_4] sources were compared, a 2 ppm [CH_4] sample was achieved by diluting 5% [CH_4] gas with zero-air generator gas, which contains 0 ppm [CH_4]. This was also achieved using mass-flow controllers. As all Figaro laboratory testing was conducted alongside a Picarro G2401 reference instrument, we can be sure that the mass-flow controllers successfully produced a 2 ppm gas blend during this test. Thus, we were always aware of the [CH_4] level in the gas stream, regardless of uncertainty in the mass-flow controller flow rate.

L522 ‘model yielded excellent R2 agreement during chamber testing (see Fig. 8)’ This is not shown in Figure 8

The reviewer is right to highlighted that Figure 8 is a visual representation of the background resistance model and does not allow the reader to evaluate model agreement. We instead direct the reader to Table 2 here, where R^2 and RMSE values are given.

L568 I think the statement ‘chamber testing may not be suited for SMO sensors in general.’ is stronger than what is said in Eugster et al. 2020. Moreso that lab calibration can, and ideally should, be incorporated, but field calibration is simpler to do accurately

This is a good point. We have rewritten this sentence more factually, without drawing general conclusions from the work of Eugster *et al.* (2020). We simply state that Eugster *et al.* (2020) yielded unsatisfactory results from chamber testing, as stated in their section 3.5.

The figure font sizes / arrangement could use some work, as Figures 1, 7, and others are relatively hard to read even while spanning a full page in this version

We have updated most of the figures in the manuscript, with improvements including higher resolution and fewer white spaces. Regarding Figure 1, we have changed the background colour to white, making the text easier to read, which we have also emboldened. We have made a number of improvements to Figure 7 including increasing the size of the axis labels and titles. We have also plotted all environmental chamber resistance measurements as coloured dots, instead of black dots, to make them easier to distinguish. The periods used to derive 30-minute averages are now shown as black bars at the top of the plot. In the previous version of this plot, individual SHT85 temperature and water mole fraction measurements from each System A logger were plotted as overlapping dots. We have now changed this by presenting average temperature and water mole fraction values from all five System A

boxes, as they are almost identical. The average standard deviation in temperature was 0.14° C and the average standard deviation in [H_2O] was 0.01%, between the different System A boxes.

On Fig 18, the number of data points is high so using a stripplot for the individual data does not add much information versus just showing a standard boxplot. A swarmplot may be preferable for showing the individual points

The reviewer makes a good suggestion. We attempted to produce a swarm plot here, but there were too many densely packed measurements in the centre of each data range, making it impossible to present this figure nicely. However, we fully agree with the reviewer's suggestion that a box plot is otherwise more apt here. We have therefore updated this figure as a simple box plot.

Modified manuscript

Characterising Methane Gas and Environmental Response of the Figaro Taguchi Gas Sensor (TGS) 2611-E00

Adil Shah[1], Olivier Laurent[1], Luc Lienhardt[1], Grégoire Broquet[1], Rodrigo Rivera Martinez[1], Elisa Allegrini[2], Philippe Ciais[1]

[1]Laboratoire des Sciences du Climat et de l'Environnement (CEA-CNRS-UVSQ), Institut Pierre-Simon Laplace, Université Paris-Saclay, Site de l'Orme des Merisiers, 91191 Gif-sur-Yvette, France
[2]SUEZ Smart Solutions, 15-27 Rue de Port, 92000 Nanterre, France

Correspondence to: Adil Shah (adil.shah@lsce.ipsl.fr)

Abstract. In efforts to improve methane source characterisation, networks of cheap high frequency in situ sensors are required, with a parts-per-million level methane mole fraction ($[CH_4]$) precision. Low-cost semiconductor-based metal oxide sensors, such as the Figaro Taguchi Gas Sensor (TGS) 2611-E00, may satisfy this requirement. The resistance of these sensors decreases in response to the exposure of reducing gases, such as methane. In this study, we set out to characterise the Figaro TGS 2611-E00, in efforts to eventually yield $[CH_4]$ when deployed in the field. We found that different gas sources, containing the same ambient 2 ppm $[CH_4]$ level, yielded different resistance responses. For example, synthetically generated air containing 2 ppm $[CH_4]$ produced a lower sensor resistance than 2 ppm $[CH_4]$ found in natural ambient air, due to possible interference from supplementary reducing gas species in ambient air, though the specific cause of this phenomenon is not clear. TGS 2611-E00 carbon monoxide response is small and incapable of causing this effect. For this reason, ambient laboratory air was selected as a testing gas standard, to naturally incorporate such background effects into a reference resistance. Figaro TGS 2611-E00 resistance is sensitive to temperature and water vapour mole fraction ($[H_2O]$). Therefore, a reference resistance using this ambient air gas standard was characterised for five sensors (each inside its own field logging enclosure) using a large environmental chamber, where logger enclosure temperature ranged between 8° C and 38° C and $[H_2O]$ ranged between 0.4% and 1.9%. $[H_2O]$ dominated resistance variability in the standard gas. A linear $[H_2O]$ and temperature model fit was derived, resulting in a root-mean-squared error (RMSE) between measured and modelled resistance in standard gas of between ±0.4 kΩ and ±1.0 kΩ for the five sensors, corresponding to a fractional resistance uncertainty of less than ±3% at 25° C and 1% $[H_2O]$. The TGS 2611-E00 loggers were deployed at a landfill site for 242 days before and 96 days after sensor testing. Yet the standard (*i.e.* ambient air) reference resistance model fit based on temperature and $[H_2O]$ could not replicate resistance measurements made in the field, where $[CH_4]$ was mostly expected to be close to the ambient background, with minor enhancements. This field disparity may have been due to variability in sensor cooling dynamics, a difference in ambient air composition during environmental chamber testing compared to the field or variability in natural sensor response, either spontaneously or environmentally driven. Despite difficulties in replicating a standard reference resistance in the field, we devised an excellent methane characterisation model up to 1 000 ppm $[CH_4]$, using the ratio between measured resistance with $[CH_4]$ enhancement and a reference resistance in standard gas. A bespoke power-type fit between

resistance ratio and [CH_4] resulted in a RMSE between modelled and measured resistance ratio of no more than ±1% $\Omega\ \Omega^{-1}$ for the five sensors. This fit and its corresponding fit parameters were then inverted and the original resistance ratio values were used to derive [CH_4], yielding an inverted model [CH_4] RMSE of less than ±1 ppm, where [CH_4] was limited to 28 ppm. Our methane response model allows other reducing gases to be included if necessary, by characterising additional model coefficients. Our model shows that a 1 ppm [CH_4] enhancement above the ambient background results in a resistance drop of between 1.4% and 2.0%, for the five tested sensors. With future improvements in deriving a standard reference resistance, the TGS 2611-E00 offers great potential in measuring [CH_4] with a parts-per-million precision.

1. Introduction

Methane (CH_4) is a potent greenhouse gas (Mitchell, 1989) with many poorly characterised sources (Jackson *et al*, 2020). Yet as atmospheric methane mole fraction ([CH_4]) is increasing (Rigby et al., 2007, Nisbet et al., 2014), improved source flux quantification is required (Saunois et al., 2016, Nisbet et al., 2019, Turner et al., 2019). This necessitates improvements in fast-response (less than 1 minute) and high frequency (at least 0.1 Hz) in situ [CH_4] sampling. CH_4 is a trace gas with a low natural ambient atmospheric background (defined to be (2±1) ppm hereon), which is two orders of magnitude lower than carbon dioxide mole fraction ([CO_2]) (Dlugokencky et al., 1994, Lan et al., 2023~~Dlugokencky, 2022~~).

Fast-response in situ [CH_4] sampling techniques span many capabilities and costs (Hodgkinson and Tatam, 2013, Schuyler and Guzman, 2017). The best measurements are achieved using tuneable infrared (IR) lasers (Baer et al., 2002, Frish, 2014), but cheaper broad-band IR can also be used in techniques such as non-dispersive IR spectroscopy (Hummelgård *et al*, 2015), at expense of precision (Shah et al., 2019). Alternatively, semiconductor-based metal oxide (SMO) sensors have been available for several decades (Fleischer and Meixner, 1995, Barsan et al., 2007, Reinelt et al., 2017, Ponzoni et al., 2017). Though they are marketed for low-precision applications, their sub-10²€ cost (Eugster and Kling, 2012, Riddick et al., 2020) merits a thorough assessment of their fast-response [CH_4] sampling capability (Collier-Oxandale et al., 2018, Honeycutt et al., 2019).

SMO sensor resistance is influenced by gas exposure (Kohl 1990). For n-type sensors containing metal lattices in their most oxidised state (Kohl, 2001), oxygen surface chemisorption forms O^{2-}, O_2^- or O^- (depending on temperature), thus decreasing near-surface electron density in the conduction band (Barsan et al., 2007, Das et al., 2014). This catalyses SMO surface oxidation of reducing gases, thereby releasing electrons into the conduction band to lower resistance (Kohl, 1989, Ponzoni et al., 2017). For CH_4, this initially produces a hydrogen atom and methyl radical (Kohl, 1989), before eventual formation of carbon dioxide (CO_2) and water (Suto and Inoue, 2010, Chakraborty et al., 2006, Glöckler et al., 2020).

n-type SMO sensors may contain tin, vanadium or zinc oxides (Hong et al., 2020). As tin oxides (SnO_x) are poorly CH_4-selective (Kim et al., 1997, Collier-Oxandale et al., 2018), catalysts may be introduced (Hong et al., 2020). Noble metals such as platinum (Pt) and palladium (Pd) influence sensitivity and selectivity (Kohl, 1990, Xue et al., 2019), often by catalysing

oxygen dissociation (Kim et al., 1997, Navazani et al., 2020, Wang et al., 2010). For example, Haridas and Gupta (2013) improved CH_4 detection by uniformly applying Pd clusters to SnO_x, whereas Suto and Inoue (2010) employed a Pt-black catalyst layer, to block hydrogen and carbon monoxide (CO). This yielded ±0.004 ppm [CH_4] agreement with a high-precision reference (HPR) instrument in background conditions (Suto and Inoue, 2010). Elsewhere, Yang et al. (2020) printed zeolite film on their Pd-loaded SnO_x sensor, to catalytically oxidise CO and ethanol.

Most SMO sensors contain packed grains (Ponzoni et al., 2017, Hong et al., 2020), with sufficient touching grains to facilitate bulk conduction (Kohl, 2001). Smaller grains or more pores amplify surface area and thus, sensitivity (Wang et al., 2010). This was achieved by Kim et al. (1997) who mixed SnO_x powder with alumina or silica supported noble metals (detecting 500 ppm [CH_4]). Some SMO sensors instead utilise films (Suto and Inoue, 2010, Haridas and Gupta, 2013, Yang et al., 2020), for example Moalaghi et al., (2020) applied SnO_x layers on alumina chips, whereas Chakraborty et al. (2006) painted iron-doped SnO_x layers on alumina tubes. The Chakraborty et al. (2006) sensor exhibited peak 1 000 ppm CH_4 sensitivity at 350° C, but peak 1 000 ppm butane sensitivity at 425° C (depending on Pd content). Xue et al. (2019) printed a Pt flower pattern on silicon dioxide film, for maximal surface area. Zhang et al. (2019) decorated 2% SnO_x on uniform hexagonal nickel oxide sheets in their p-type CH_4 sensor, to optimise sensitivity and selectivity. Gagaoudakis et al., (2020) developed a transparent 100 nm thick polycrystalline p-type nickel oxide sensor, using aluminium. However, ultraviolet radiation was required to restore resistance, after gas exposure (Gagaoudakis et al., 2020).

Nanotubes and graphene structures may alternatively be used (Ponzoni et al., 2017, Hong et al., 2020) for better surface adsorption (Navazani et al., 2020). Kooti et al. (2019) tested one-dimensional nanoscale rods, to be mixed with porous graphene nanosheets, where CH_4 could diffuse into the small pores, improving selectivity. Navazani et al. (2020) made an SnO_x sensor 28 times more CH_4-sensitive (at 100 ppm), by combining it with Pt-doped multi-walled carbon nanotubes. Elsewhere, Das et al. (2014) used 2.4 nm SnO_x quantum dots to detect as little as 50 ppm [CH_4]. A high surface to volume ratio and quantum effects enabled low-temperature (150° C) CH_4 sensitivity (Das et al., 2014).

Most SMO sensors operate at up to 400° C (Barsan et al., 2007), to enable oxygen vacancies to diffuse into the bulk material (Kohl, 1990). Airflow may consequently cause indirect sensor effects (Eugster et al., 2020). Cooler 150° C sensors have also been developed, for example by Das et al. (2014) or by Kooti et al. (2019), which detected down to 1 000 ppm [CH_4]. Elsewhere, Xue et al. (2019) sampled 500 ppm [CH_4] with their 100° C sensor. Room temperature sensors have also been trialled (Navazani et al., 2020), for example, Haridas and Gupta (2013) developed a sensor using ultraviolet radiation to generate photo-induced oxygen ions. This improved 200 ppm CH_4 sensitivity by three orders of magnitude (Haridas and Gupta, 2013). Conversely, Moalaghi et al. (2020) developed a hot (700° C up to 850° C) SnO_x thermal decomposition sensor, to theoretically detect 50 ppm [CH_4]. The thermal stability of CH_4 enhanced its selectivity compared to hydrogen and CO (Moalaghi et al., 2020).

Water also influences SMO sensors (Collier-Oxandale et al., 2019, Navazani et al., 2020, Rivera Martinez et al., 2021) by competing for oxygen absorption sites (Kohl, 1989) at the expense of sensitivity (Wang et al., 2010, Yang et al., 2020). This effect may be temperature-dependent, whereby heat enhances water desorption (Kohl, 2001). While dry sampling may resolve this (Kohl, 1989, Suto and Inoue, 2010, Sasakawa et al., 2010), some sensors require wet air for normal operation (Eugster and Kling, 2012, Riddick et al., 2020).

Following robust physical sensor characterisation, empirical gas testing may then be performed in preparation for field deployment (Kim et al., 1997, Barsan et al., 2007, Honeycutt et al., 2019, Zhang et al., 2019, Daugela et al., 2020). A field-ready SMO sensor includes a sensitive layer, a substrate, electrodes (Barsan et al., 2007, Kooti et al. 2019, Glöckler et al., 2020) and a logger (Ferri et al., 2009, Collier-Oxandale et al., 2018). Concurrent measurement~~logging~~ of environmental conditions is invaluable (van den Bossche et al., 2017, Daugela et al., 2020, Cho et al., 2022). As an example of actual field application, Sasakawa et al. (2010) deployed nine Suto and Inoue (2010) sensors in Siberian wetlands. Thanks to regular calibrations, [CH_4] measurements contributed towards regional surface flux emission estimates (Sasakawa et al., 2010). Gonzalez-Valencia et al. (2014) mapped landfill surface fluxes using flux chambers containing a suite of IR and SMO sensors. Daugela et al. (2020) used Hanwei Electronics Co., Ltd. MQ2 and MQ4 sensors, to crudely localise landfill emission hotspots. Honeycutt et al. (2021) utilised MQ4 sensors within a sampling network for autonomous deployment, with a 1 000 ppm [CH_4] targeted detection limit. Kim et al. (2021) exploited low SMO sensor mass for unmanned aerial vehicle deployment, to derive landfill CH_4 hotspots and surface fluxes. The sensor was laboratory-tested up to a maximum [CH_4] of 200 ppm (Kim et al., 2021).

Figaro Engineering Inc. (Mino, Osaka, Japan) produce fast-response grain-based SMO sensors (Ferri et al., 2009, Eugster and Kling, 2012), which have been shown to be~~are~~ more stable than the MQ4 (Honeycutt et al., 2019). Figaro sensors require wet air for normal operation, for example, Rivera Martinez et al. (2021) found Figaro Taguchi Gas Sensor (TGS) resistance to be abnormally high at 0% water vapour mole fraction ([H_2O]) compared to 1% and 2.3% [H_2O]. Meanwhile, Eugster and Kling (2012) reported that TGS response is unpredictable at a relative humidity of below 35%. This therefore rules out the possibility of conducting ~~(Rivera Martinez et al., 2021), thereby ruling out~~ dry calibrations (Riddick et al., 2020). Eugster and Kling (2012) therefore performed Figaro ~~Taguchi Gas Sensor (~~TGS~~)~~ 2600 field characterisation with an HPR~~,~~ over an Arctic lake, yielding a deterministic model capable of discerning diurnal features, but with a coefficient of determination (R^2) of 0.2 compared to the HPR. CO cross-sensitivity caused complications (Eugster and Kling, 2012), as encountered by Collier-Oxandale et al. (2018), elsewhere. The TGS 2600 sensor is also hydrogen-sensitive (Ferri et al., 2009). Eugster et al. (2020) yielded ±0.1 ppm model agreement with an HPR, from 7 years of background [CH_4] Arctic sampling with a TGS 2600, although this model was not valid below freezing, where [H_2O] was naturally very low. Riddick et al. (2020) deployed the TGS 2600 for 3 months at a gas extraction site, sampling up to ~~a~~ 6 ppm [CH_4]~~ maximum~~, with a derived ±0.01 ppm [CH_4] measurement uncertainty, following laboratory HPR characterisation. They initially attempted to use the Eugster and Kling (2012) model but could not derive a fit, either due to model shortcomings or due to the sensor-specific nature of this model,

and instead opted for a different non-linear deterministic model which also resulted in an R^2 of 0.2 (Riddick et al., 2020). The Collier-Oxandale et al. (2018) study, which sampled in background [CH_4] conditions (*i.e.* at 2 ppm), used a period of HPR sampling for model training and a period for model testing, although a sufficient training dataset is required to avoid model overfitting. They found that different models are suited to different sampling environments, deriving a root-mean-squared error (RMSE) range of between ±0.2 ppm and ±0.6 ppm [CH_4], compared to an HPR (Collier-Oxandale et al., 2018).

Collier-Oxandale et al. (2019) found that the TGS 2600 is additionally highly responsive to CO, benzene and acetaldehyde. They therefore also used training and testing periods from a combined dataset of Figaro TGS 2600 and TGS 2602 (non-CH_4) sampling~~sensor~~ to improve CH_4 selectively and to combat cross-sensitivities~~. A subset of field sampling was used for HPR training, with the remainder for model testing~~ (Collier-Oxandale et al., 2019). They obtained a deterministic model with an R^2 of 0.6 and an RMSE of ±0.24 ppm, when sampling up to 5 ppm [CH_4] (Collier-Oxandale et al., 2019). Casey et al. (2019) applied a similar field HPR training and testing approach to ten packages containing various sensors (including a TGS 2600 and TGS 2602), which were deployed across an oil and gas extraction region. Linear and artificial neural network (ANN) models were both able to derive [CH_4], but correlated gas emissions from the same source may have confounded model output in this multi-sensor approach (Casey et al., 2019). Eugster et al. (2020) also tested an ANN model, which performed better in warmer conditions. Rivera Martinez et al. (2021) used 47 days of TGS 2600, TGS 2611-C00 and TGS 2611-E00 sampling to derive background [CH_4] with ANN models. 70% of sampling was used for HPR training, typically resulting in less than ±0.2 ppm ~~root-mean-squared error (~~RMSE~~)~~, but the position in time of the 30% testing window effected model performance (Rivera Martinez et al., 2021). Elsewhere, Rivera Martinez et al. (2022) produced laboratory-generated methane spikes of between 3 ppm and 24 ppm over 130 days, which were sampled by four different TGS 2611-C00 and TGS 2611-E00 loggers. 70% of the data was used to train linear, polynomial and ANN models to replicate the spikes, using an HPR, with a target RMSE [CH_4] of ±2 ppm (Rivera Martinez et al., 2022).

The Figaro TGS 2611-E00 is a more CH_4-selective sensor as it incorporates a CO filter (van den Bossche et al., 2017, Bastviken et al., 2020, Figaro Engineering Inc., 2021, Furuta et al, 2022), at the expense of CH_4 sensitivity (Eugster et al., 2020). Furuta et al. (2022) found that the both the Figaro TGS 2611-E00 and the MQ4 exhibited a better general correlation with [CH_4] from an HPR, than the TGS 2600, TGS 2606 and TGS 2611-C00, when tested up to 10 ppm [CH_4], though this may in part be due to the dominant effect of [H_2O] variability on these other sensors during testing. van den Bossche et al. (2017) tested a TGS 2611-E00 in background [CH_4] (*i.e.* at 2 ppm) for 31 days, following laboratory calibration, resulting in −1 ppm accuracy and ±1.7 ppm precision, where variations in [CH_4] were, in reality, no more than ±0.2 ppm. Cho et al. (2022) sampled simulated gas leaks using 19 TGS 2611-E00 units, for four days, applying a universal laboratory calibration to all sensors, with a 100 ppm [CH_4] targeted detection limit. Jørgensen et al. (2020) sampled up to 90 ppm [CH_4] while HPR field testing a TGS 2611-E00 for 100 hours on the Greenland Ice Sheet, resulting in ±1.69 ppm RMSE. It then sampled autonomously for 18 days in very stable environmental conditions, where [CH_4] estimates were in a similar range to those observed during HPR testing (Jørgensen et al., 2020). Bastviken et al. (2020) tested various TGS 2611-E00 calibration models up to 700 ppm [CH_4], for use

in surface flux chambers. Sieczko et al. (2020) deployed TGS 2611-E00 flux chambers over three boreal lakes to characterise CH_4 emission variability. Although they calibrated each sensor, strong diurnal environmental outcomes were inferred from this imprecise sensor (Sieczko et al., 2020).

Due to its superior CH_4 selectivity, we characterised the TGS 2611-E00, with the eventual objective of measuring [CH_4] during outdoor field deployment. In order to derive [CH_4] with confidence, we conducted a series of robust laboratory characterisation tests, to understand the core principles of sensor response to various external factors. Our sensor characterisation approach was thoroughly tested using 338 days of field sampling. Two logging systems were used, as described in Sect. 2: one for autonomous field sampling and the other for controlled testing of multiple sensors. Our overall characterisation process is outlined in Fig. 1. As a first step, sensor response to different standard gas samples was characterised, in the absence of CH_4 enhancements (see Sect. 3.1 and Sect. 3.2). ~~Water mole fraction (~~[H_2O]~~)~~ and temperature response were then characterised in a large environmental chamber in Sect. 3.3. A specific [CH_4] enhancement model fit was derived in Sect. 3.4. Sensor CO, CO_2 and oxygen response were also tested (see Sect. 3.5, Sect. 3.6 and Sect. 3.7). Then, to test sensor applicability in field conditions, ten sensors were deployed at a landfill site, providing a prolonged dataset with which to test our characterisation approach. [H_2O] and temperature measurements were used to model field resistance for five of these sensors, for comparison with actual resistance measurements (see Sect. 4). The quality of the environmental resistance model fit is discussed in Sect. 5 and we summarise our outcomes in Sect. 6.

2. Materials and logging methods

2.1 Sensor overview

Here we describe the basic operating principles of the Figaro TGS 2611-E00, referred to hereafter as "Figaro", unless otherwise stated. The Figaro is an SMO sensor, sensitive to hydrogen and light hydrocarbons (including CH_4), featuring an incorporated CO and ethanol filter (Figaro Engineering Inc., 2021). The Figaro internal heater and SMO element both operate at a (5.0±0.2) V supply voltage (V_s). Figaro resistance (R) reactsponds to surrounding gas exposure, which can be inferred by measuring the precise voltage drop (V_d) across a resistor of fixed load resistance (R_{load}), connected in series with the Figaro sensor electrodes (see Fig. 2), using Eq. (1) (Collier-Oxandale et al., 2018).

$$R = R_{load} \cdot \left(\frac{V_s}{V_d} - 1\right) \quad (1)$$

V_d is effectively used to gauge current flow, thereby quantifying resistance at a set V_s. R_{load} may take a minimum value of 0.45 kΩ (Figaro Engineering Inc., 2021). However, tofor maximiseal sensitivity, R_{load} should be selected to target a similar order of magnitude to R, depending on the sensor type and the predicted sampling conditions. A higher R_{load} permits better sensitivity at lower [CH_4], but limits precision when detecting larger [CH_4] enhancements.

2.2 Field logging system

To measure Figaro resistance in the field, we used ten Systematic Observations of Facility Intermittent Emissions (SOOFIE) logging systems (referred to hereafter as System A), manufactured by Scientific Aviation, Inc (Boulder, Colorado, USA). The ten systems (illustrated in Fig. 3, for example) are labelled from LSCE001 to LSCE010 ~~(see Fig. 3, for example)~~. Each system enclosure includes a Figaro sensor, hard-wired ~~connected~~ in series with a 5 kΩ load resistor. This 5 kΩ load resistance is similar in order of magnitude to load resistors used in previous work (van den Bossche et al., 2017, Jørgensen et al., 2020, Furuta et al., 2022). Air is drawn towards the Figaro, using a downwards facing fan, in a similar style to Cho et al. (2022). An SHT85 environmental sensor (Sensirion AG, Staefa, Switzerland) records System A temperature (T_A) and relative humidity. The logging system is powered by a 12 V rechargeable lithium-ion phosphate battery, connected to a solar panel. This is converted to a stable Figaro 5 V power supply on an internal circuit board, using a high-precision low-temperature-coefficient voltage regulator, with a stability of ±3 mV; this maintains a constant Figaro supply voltage regardless of changes in ambient temperature or input battery voltage. The battery can power the logging system for 3 days from full charge. An Arduino data logger records minute-average V_d, T_A and relative humidity measurements, which are wirelessly transmitted to an Internet server using a cellular network board inside each box, similar to Honeycutt et al. (2021). Three systems (LSCE005, LSCE006 and LSCE007) also transmit minute-average wind speed and direction measurements from their own two-dimensional Gill WindSonic anemometers (Gill Instruments Ltd., Lymington, Hampshire, UK), connected to each of these three System A enclosures.

2.3 Laboratory testing logging system

A bespoke laboratory logger was designed, with five sockets, to facilitate simultaneous Figaro testing (referred to hereafter as System B). The 0.1 dm^3 cell has a glass exterior with a stainless steel head (see Fig. 4), which was adapted from a filter (FS-2K-D, M&C TechGroup Germany GmbH, Ratingen, Germany). Each Figaro socket is connected in series with a high-precision (5.00±0.05) kΩ load resistor (Vishay Intertechnology, Inc., Malvern, Pennsylvania, USA). This System B load resistance was selected so as to be identical to the load resistor in System A (which was determined by the System A manufacturer and beyond our control). 18 bit analogue-to-digital converter chips (MCP3424, Microchip Technology Inc., Chandler, Arizona, USA) measure 1 Hz V_d for each Figaro. This chip is ready-mounted onto an ADC Pi board (Apexweb Ltd, Swanage, Dorset, UK), which is connected to a Raspberry Pi 3B+ logging computer (Raspberry Pi Foundation, Cambridge, UK), using similar logging software to Rivera Martinez et al. (2021). A cable enters the top of the cell to provide connections between the Figaro circuit board and both the logging computer and ADC Pi board, which are outside the cell. The ADC Pi board is configured to sample at 16 bit, resulting in a 0.154 mV resolution, which, assuming a 5 kΩ Figaro resistance, is equivalent to an optimum resistance resolution of 0.6 Ω. A raw ADC Pi board V_s measurement is recorded, alongside raw Figaro V_d, to linearly calibrate the ADC Pi. Furthermore, a ground reference offset correction between the Figaro sensors and the ADC Pi board is applied to V_d.

Preliminary tests with a single power supply yielded unstable V_d measurements, as background activity on the logging computer influences total current draw. V_s also influences Figaro CH_4 sensitivity (see Appendix A). Therefore, the logging computer and Figaro power supplies are split, with a common ground, as suggested elsewhere (van den Bossche et al., 2017, Daugela et al., 2020). A high-precision power supply unit (T3PS23203P, Teledyne LeCroy Inc., Chestnut Ridge, New York, USA) provides Figaro power, with rated ripple and noise effects of below ±1 mV (root-mean-squared) between 5 Hz and 1 MHz. A ±0.1 mV voltage standard deviation of was observed when the power supply was tested with the ADC Pi board. The power supply unit also has a supply voltage read-back accuracy of at least 35 mV. Yet this rated accuracy does not affect our measurements, as the supply voltage setting was independently adjusted from the potential difference measured directly across the Figaro circuit board. This additionally corrects for voltage drop between the power supply unit and the Figaro sensors.

An SHT85 sensor measures System B temperature and relative humidity at 1 Hz inside the cell. In addition, the Figaro cell air outlet is fed through towards a Picarro G2401 gas analyser (Picarro, Inc., Santa Clara, California, USA), serving as an HPR. It records [CH_4], [H_2O], carbon monoxide mole fraction ([CO]) and [CO_2] at a maximum sampling frequency of 0.32 Hz, although the rate at which gas measurements are made~~this frequency~~ decreases~~lines~~ depending on the complexity of the gas mixture, with the Picarro G2401 designed to sample optimally in ambient gas conditions. The Picarro G2401 offers sampling with a high temporal stability (Yver Kwok et al., 2015), with a 0.2 Hz precision of less than ±0.001 ppm, ±0.0030%, ±0.015 ppm and ±0.050 ppm for [CH_4], [H_2O], [CO] and [CO_2], respectively (Picarro, Inc., 2021). The Picarro G2401 streams data directly to the logging computer using a serial data connection; this simultaneous HPR logging eliminates time offset issues (if the Picarro G2401 clock is not synchronised with the System B clock), as the Picarro G2401 timestamp is not used. Any sensor response lag time between the System B sampling cell and the Picarro G2401 was measured and corrected for (typically a few seconds).

As Figaro sensors naturally operate in wet conditions, a dew-point generator (LI-610, LI-COR, Inc., Lincoln, Nebraska, USA) was employed during all System B testing. In addition, a variety of mass-flow controllers (Bronkhorst High-Tech B.V., AK Ruurlo, Netherlands) were utilised~~,~~ to produce various gas blends by combining different gas sources, all at a constant net 1 dm^3 min^{-1} flow rate. This is essential to maintain a consistent Figaro cooling effect inside the System B cell.

3. Sensor characterisation

3.1 Sensor gas response

Here we describe the general sampling strategy, used to derive [CH_4]. According to the Figaro sensor characterisation strategy of van den Bossche et al. (2017) and Jørgensen et al. (2020), [CH_4] can be derived by comparing measured resistance to a baseline reference resistance ($R_{baseline}$) measured in the presence of~~with~~ a standard gas (Eugster and Kling, 2012). If this

reference resistance is well-characterised to account for environmental changes (independent of gas composition), a gas derivation function (f) may be used to yield [CH_4], as in Eq. (2), where [CH_4]$_{baseline}$ is the baseline reference [CH_4] in standard gas. This function is independent of environmental variables, as they are already incorporated in the reference resistance and thus, cancel out. Therefore, this ratio is solely a function of gas enhancement.

$$f(([CH_4] - [CH_4]_{baseline}), \ldots) = \frac{R}{R_{baseline}} \quad (2)$$

The f function may be dependent on various reducing or oxidising gases, though only CH_4 is explicitly included here, for simplicity.

3.2 Choice of standard reference gas

In order to conduct repeatable testing, a reliable reference gas is first required. This gas must produce a consistent Figaro resistance response. Our initial candidate was gas from a zero-air generator (UHP-300ZA-S, Parker Hannifin Manufacturing Limited, Gateshead, Tyne and Wear, UK); this catalytic oven oxidises hydrocarbons and CO, resulting in a clean air stream containing 0.00 ppm [CH_4] and 0.00 ppm [CO], as recorded by the Picarro G2401. This reference gas was initially selected for testing due to enhanced Figaro environmental sensitivity expected in the absence of all reducing gases (Bastviken et al., 2020). Zero-air has also been employed as a reference gas by Jørgensen et al. (2020).

But before this zero-air source could be used as a standard gas in subsequent testing, it was important to verify that we could predict the resistance change under a [CH_4] transition from 0 ppm to 2 ppm (ambient background), which would be a crucial step in working with zero-air as a standard reference. This test was conducted with various gas samples containing the same 2 ppm [CH_4] from different sources, which were sampled with five sensors (LSCE001, LSCE003, LSCE005, LSCE007 and LSCE009) in System B. This System B testing was conducted in an air-conditioned laboratory. First, a cylinder containing 5% [CH_4] in argon (P5-Gas ECD, Linde Gas AG, Höllriegelskreuth, Germany) was diluted with 99.996% zero-air generator gas, targeting 2 ppm [CH_4], using mass-flow controllers (discussed in Sect. 2.3). This was sampled twice. Next, a synthetic air cylinder containing 2 ppm [CH_4] (Deuste Gas Solutions GmbH, Schömberg, Germany) was sampled twice. Although this cylinder also contained 5 000 ppm [CO_2], this is irrelevant in the context of Figaro resistance response (see Sect. 3.6). ~~All synthetic air cylinders contain a natural balance of nitrogen, oxygen and argon.~~ This was directly followed by sampling two ambient air sources once: ambient laboratory air from the room surrounding the instruments was sampled for 5 minutes, before finally sampling an ambient target gas cylinder, filled with outdoor air from next to our laboratory building some months previous. Ambient is defined here to be any natural air acquired from the surrounding environment.

A dew-point setting of 8° C was applied throughout this test, resulting in (0.970±0.002)% [H_2O]. This was possible thanks to the closed cell nature of System B with a fixed inlet, which allows precise gas samples to be delivered to the sensors with a constant [H_2O]. The sensors were allowed to stabilise in response to this [H_2O] setting for at least 24 hours directly preceding

the test, until there was no noticeable resistance drift. This stabilisation period is essential, as Figaro sensors exhibit a delayed response to [H_2O] changes (see Appendix B).

Results of this 2 ppm [CH_4] transition test are presented in Fig. 5. The Picarro G2401 recorded 2 ppm [CH_4] for all four gas samples, with consistently low [CO], which confirms the accuracy of diluting 5% [CH_4] in argon, using mass-flow controllers. However, Figaro resistance decrease varied considerably (see Table 1 for fractional decrease values). Resistance drop (compared to zero-air generator gas) when sampling both ambient target gas and ambient laboratory air was smaller (on average 4% for all five sensors) than when sampling synthetic air and diluted 5% [CH_4] (on average 12% for all five sensors), although there was considerable variability between the different sensors (see Table 1). This suggests that there may be one (or many) additional species in ambient air, causing an unexpectedly high Figaro resistance drop. Such a substance may be absent in synthetic air and combusted by the zero-air generator. However, identifying such species remains a challenge (see Sect. 5.2 for discussion), with us unable to identify any obvious alternative ambient reducing candidates from previous Figaro testing work. Moreover, the consistent resistance drops for both synthetic 2 ppm [CH_4] and zero-air blended with 0.004% of 5% [CH_4], suggests that synthetic 2 ppm [CH_4] contains no reducing contaminants.

methane source	LSCE001	LSCE003	LSCE005	LSCE007	LSCE009
diluted 5% methane	−3%	−4%	−3%	−3%	−3%
synthetic air	−4%	−5%	−3%	−3%	−3%
ambient laboratory air	−19%	−23%	−7%	−8%	−4%
ambient target gas	−19%	−23%	−6%	−8%	−4%

Table 1: Fractional Figaro resistance decrease in response to different sources of 2 ppm methane mole fraction, compared to zero-air generator gas. The final 120 s of each 2 ppm sampling period was used to derive these values. A zero-air reference resistance was derived by taking the average of all 120 s zero-air averages, preceding a 2 ppm transition.

Although this test infers the presence of an interfering substance in ambient natural air (both target gas and laboratory air), it is important to verify that the zero-air generator is not itself a source of such components. It is also useful to test that different synthetic air cylinders (filled at different times) from the same supplier (Deuste Gas Solutions GmbH) behave in the same way, compared to zero-air generator gas. All synthetic air cylinders from this supplier contain a natural balance of nitrogen, oxygen and argon, to which trace quantities of other gases are added. System B was used to sample a synthetic 50 ppm [CH_4] cylinder filled in 2019 (old), a synthetic 50 ppm [CH_4] cylinder filled in 2021 (new), a synthetic zero-air cylinder filled in 2014 (old) and a synthetic zero-air cylinder filled in 2021 (new~~old~~), which were all sampled twice. Four sensors were tested (LSCE002, LSCE004, LSCE006 and LSCE008) at a fixed dew point, resulting in (0.652±0.010)% [H_2O] for this test. A sufficient [H_2O] stabilisation period preceded this test.

Fig. 6 shows Figaro and HPR observations from this test. The two synthetic 50 ppm [CH_4] cylinders (old and new) both produced identical resistance decreases, compared to gas from the zero-air generator, when filled two years apart. This suggests

that the quality of synthetic 50 ppm [CH_4] cylinders is consistent and that CH_4 is the dominant reducing species in these cylinders. The second part of the test shows that synthetic zero-air has a negligible effect on Figaro resistance, compared to gas from the zero-air generator. Though synthetic zero-air causes a small resistance variability (particularly for LSCE006; see Fig. 6), this is insignificant in the context of the resistance decrease values presented in Table 1, for different 2 ppm [CH_4] sources. This consistency in zero-air resistance response suggests that the zero-air generator successfully burns Figaro-sensitive species. This supports the conclusions derived from Fig. 5 that there may be an additional reducing substance in natural air, otherwise absent in zero-air from multiple sources (both synthetic and from the zero-air generator).

To summarise, these two tests infer that zero-air (either synthetic or from a zero-air generator) is an unsuitable standard reference gas. Figaro resistance is abnormally high in zero-air, due to the possible absence of (non-CH_4) interfering reducing species otherwise present in ambient air. The fact that the resistance drop in ambient laboratory air was almost identical to the resistance drop in ambient target gas (filled some months previous), suggests that any unidentified background reducing species are stable, with a long lifetime. Elsewhere, Jørgensen et al. (2020) found that a laboratory calibration conducted with zero-air could not be applied to ambient air sampling, which required its own calibration (attributing this to power supply issues). van den Bossche et al. (2017) also found that applying a calibration made in synthetic air to ambient air resulted in larger sensor disparity, compared to an HPR. They attributed this to ±2% oxygen mole fraction ([O_2]) variability in their synthetic air source (van den Bossche et al., 2017), however our oxygen test (see Sect. 3.7) shows that this is unlikely and an interfering species was probably responsible. Yet, during our tests, we were unable to identify such interfering species from our HPR and there are no other obvious reducing candidates in ambient air (see Sect. 5.2 for discussion). The oxidising capacity of air is unlikely to vary, as surface [O_2] is near constant. Furthermore, Collier-Oxandale et al. (2018) observed no ozone sensitivity for the similar Figaro TGS 2600 sensor.

Therefore, to incorporate this natural background effect into any subsequent models or analysis, natural ambient air should be employed as a standard gas instead of zero-air, assuming that the ambient air background composition remains consistent in various characterisation tests. Although natural air contains both CH_4 and CO, their variability is typically small, when not in the close vicinity of emission sources. Hence all subsequent testing assumes an ambient 2 ppm [CH_4] background.

3.3 Reference resistance characterisation

Having selected natural ambient air as a standard gas, the next step is to characterise a standard 2 ppm [CH_4] baseline reference resistance ($R_{2\,ppm}$) in response to environmental variables (independent of gas composition), which dominate Figaro performance (Eugster and Kling, 2012, Collier-Oxandale et al., 2019, Rivera Martinez et al., 2021, Furuta et al., 2022). The most important environmental factors (discussed in Sect. 1) are temperature and [H_2O] (Eugster et al., 2020), which were characterised using a large environmental chamber (UD500 C, Angelantoni Test Technologies Srl, Massa Martana, Italy) to simultaneously test five System A loggers. The chamber was slowly replenished (at less than 0.5 $dm^3\,min^{-1}$), to avoid the

~~Figaro waste gas~~ accumulation~~,~~ of waste gas species, such as~~which is slightly enhanced in~~ CO, which can be formed due to some incomplete CH_4 ~~surface~~ combustion on the Figaro sensor surface (Glöckler et al., 2020). Rather than using a solar panel, each System A battery was connected directly to a battery charger, to maintain a stable battery voltage and hence, a stable Figaro supply voltage. System A data was remotely accessed by connecting the cellular board inside each enclosure to an antenna outside the environmental chamber. The Picarro G2401 HPR continuously sampled inside the chamber during testing. All System A data was interpolated to the shorter Picarro G2401 timestamp.

Chamber testing was conducted across a temperature and $[H_2O]$ range expected in the field, as suggested elsewhere (Barsan et al., 2007), to optimise time resources with limited chamber access. $[H_2O]$ of 0.4%, 0.7%, 1.0%, 1.4% and 1.9% were targeted, by adjusting relative humidity inside the chamber, according to the temperature setting. Relative humidity control was essential in this test, as residual liquid water evaporated from the chamber walls with a temperature setting increase. Following each new $[H_2O]$ change, the chamber was first given one 7-hour adjustment period, to augment $[H_2O]$ stabilisation, as required in response to sharp $[H_2O]$ changes (see Appendix B). Next, at least four different temperature settings were sampled at each $[H_2O]$ level in 4-hour intervals (including time for each temperature ramp). Finally, temperature was varied in 8-hour sampling intervals at the same fixed $[H_2O]$ level. Then the entire process was repeated at a different targeted $[H_2O]$.

Chamber observations from each System A logger are presented in Fig. 7, alongside~~.~~ c~~C~~orresponding HPR measurements~~,~~ There was a data transmission gap between 17:14 UTC on 7 December 2021 and 00:46 UTC on 8 December 2021. Average SHT85 T_A measurements and derived SHT85 $[H_2O]$ values from all five System A boxes are also shown in Fig. 7. $[H_2O]$ values~~averages~~ were derived using SHT85 T_A and relative humidity measurements from inside each System A enclosure, where saturation vapour pressure was derived using Teten's equation, given by Murray (1967), and pressure was assumed to be 10^5 Pa, which can be simplified to Eq. (3). M_1 and M_2 are equal to 17.2693882 and 35.86 K, respectively, over water and 21.8745584 and 7.66 K, respectively, over ice.

$$[H_2O] = \text{relative humidity} \cdot 0.000061078 \cdot e^{M_1 \cdot \frac{(T_A - 273.16)}{T_A - M_2}} \quad (3)$$

The average standard deviation in T_A and $[H_2O]$ was (0.14±0.13)° C and (0.0089±0.0063)%, respectively, between the five System A logging systems as a function of time, showing that the boxes were exposed to almost identical conditions for the duration of this experiment. ~~There was a data transmission gap between 17:14 UTC on 7 December 2021 and 00:46 UTC on 8 December 2021.~~

~~The 4-hour intervals presented in Fig. 7 are of insufficient duration for Figaro stabilisation.~~ Despite our efforts to maintain a fixed $[H_2O]$ level during temperature variations, there was a sharp $[H_2O]$ change at each temperature transition with ~~regular~~periodic $[H_2O]$ fluctuations ~~in $[H_2O]$ during each sampling period~~ (see Fig. 7), as the environmental chamber constantly worked to rectify itself to achieve its target environmental settings. $[H_2O]$ therefore fluctuated both above and below a central point periodically, following an initial larger variability associated with each pre-programmed step. Although many hours of

stable sampling are required for sufficient Figaro stabilisation following a [H_2O] step change (see Appendix B), regular periodic fluctuations in [H_2O] should cancel each other out over a sufficient averaging period, as the resistance decay behaviour occurs in both a positive and negative direction. Nevertheless, Fig. 7 shows that 4 hours of sampling was insufficient for resistance stabilisation following the initial step change. Therefore, these 4-hour sampling periods were discarded (thus, conveniently avoiding the data transmission gap). Instead, ~~Thus~~ 30-minute averages were taken towards the end of each 8-hour sampling period, ~~for optimal sensor stabilisation,~~ ranging between 10 kΩ and 47 kΩ for the five sensors. Fig. 7 shows that despite [H_2O] variability resulting in noisy resistance measurements, there was no overall upwards or downwards resistance drift after 8 hours of sampling, with small resistance variations (due to direct [H_2O] fluctuations) superimposed on a larger water stabilisation effect. ~~Averages from 4-hour intervals were discarded, thus conveniently avoiding the data transmission gap.~~

These chamber averages showed that [H_2O] is the dominant factor influencing $R_{2\,ppm}$, as observed in other work (Bastviken et al., 2020, Rivera Martinez et al., 2021), exhibiting a linearly decreasing relationship. Therefore, Eq. (~~43~~) was proposed to model $R_{2\,ppm}$ in the environmental chamber. This equation is analogous to Eq. (2), where $R_{2\,ppm}$ is specifically used in place of a general $R_{baseline}$ value.

$$R_{2\,ppm} = A \cdot \left(1 - \left([H_2O] \cdot \left(B - (T_A \cdot C)\right)\right) - (T_A \cdot D)\right) \quad (43)$$

A is a baseline reference resistance offset in kΩ, B is a water correction coefficient in $\%^{-1}$, C is a temperature-water correction coefficient in $kK^{-1}\,\%^{-1}$ and D is temperature correction coefficient in kK^{-1}, where "%" is a percentage water vapour mole fraction. [H_2O] here represents a derived value from the SHT85 inside each System A enclosure.

A non-linear regression was applied between $R_{2\,ppm}$, T_A and [H_2O] from all 30-minute averages from the 8-hour sampling periods for each sensor. It is worth noting that any empirical model parameters derived from this test are specific to the logging system in which they were derived, as flow dynamics in each logging system are different, resulting in a different Figaro cooling effect. Furthermore, T_A is specifically influenced by the temperature gradient between the Figaro sensor and the point of temperature measurement in System A. Model results are presented in Fig. 8 and corresponding model coefficients in Table 2. As Eq. (~~43~~) contains four free parameters, with a limited number of sampling data points, we evaluated the suitability of parameterisation. An Akaike information criterion (AIC) and Bayesian information criterion (BIC) score was derived for simplified variations of Eq. (~~43~~), with one, two and three free parameters. Results are presented in Table 3, where a lower AIC and BIC score represents a better compromise, providing a good model fit without over-parameterisation. The results in Table 3 is show that, on average, the full version of Eq. (~~43~~) with four free parameters results in the lowest AIC and BIC score, supporting our four-parameter approach.

sensor	A (kΩ)	B (%$^{-1}$)	C (kK^{-1} %$^{-1}$)	D (kK^{-1})	R^2	RMSE (kΩ)	$R_{2\,ppm}$ at 25° C T_A and 1% [H_2O] (kΩ)	RMSE as a fraction of $R_{2\,ppm}$ at 25° C T_A and 1% [H_2O] (%)
LSCE001	30.7	0.389	0.924	1.46	0.961	±0.39	13.9	±2.8
LSCE003	29.5	0.377	0.833	1.24	0.959	±0.43	14.8	±2.9
LSCE005	75.8	0.419	1.135	2.10	0.980	±0.52	22.2	±2.4
LSCE007	44.7	0.317	0.680	1.45	0.970	±0.51	20.3	±2.5
LSCE009	164.3	0.443	1.295	2.40	0.974	±0.99	37.4	±2.6

Table 2: Eq. (43) model parameters for five System A enclosures, derived from 30-minute averages (of 8-hour testing windows), whilst sampling natural ambient air in the environmental chamber. The R^2 and RMSE is given for each model fit and the RMSE is given as a fraction of $R_{2\,ppm}$ at 25° C T_A and 1% [H_2O], for each sensor.

equation ($R_{2\,ppm}$ =)	$A \cdot (1 - ([H_2O] \cdot (B - (T_A \cdot C))) - (T_A \cdot D))$		$A \cdot (1 - ([H_2O] \cdot B) - (T_A \cdot D))$		$A \cdot (1 - ([H_2O] \cdot B))$		$A \cdot (1)$	
test	**AIC**	**BIC**	**AIC**	**BIC**	**AIC**	**BIC**	**AIC**	**BIC**
LSCE001	424	431	424	429	423	427	509	512
LSCE003	429	436	428	434	427	431	513	515
LSCE005	440	447	447	452	454	458	544	546
LSCE007	439	445	438	443	439	443	531	534
LSCE009	476	482	487	493	497	501	571	574
average	441±18	448±18	445±23	450±23	448±27	452±27	534±23	536±23

Table 3: AIC and BIC scores for simplified variations of the Eq. (43) model for five System A enclosures, derived from 30-minute averages (of 8-hour testing windows), whilst sampling natural ambient air in the environmental chamber.

Having selected the four-parameter model given by Eq. (43), the RMSE in $R_{2\,ppm}$ when modelling environmental chamber sampling was derived and is provided in Table 2, spanning between ±0.4 kΩ and ±1.0 kΩ. This represents less than ±3% fractional uncertainty in $R_{2\,ppm}$ at 25° C T_A and 1% [H_2O], for all five sensors (assuming that the sensor has reached a stable level in response to [H_2O] changes). This means to say that the Eq. (4) model can predict Figaro resistance to within ±3% in standard conditions based solely on temperature and [H_2O], when sampling natural air containing 2 ppm [CH_4]. This low model error suggests that Eq. (43) provides good temperature and [H_2O] constraint to $R_{2\,ppm}$. Furthermore, an ~~coefficient of determination (R^2)~~ of 0.97±0.01 for the five model fits illustrates the suitability of Eq. (43) in characterising $R_{2\,ppm}$, with respect to environmental conditions (see Table 2 for values). By accurately modelling $R_{2\,ppm}$ as a first step, this resistance value can then be used to derive [CH_4] from its change in the presence of enhanced levels of CH_4.

3.4 Methane characterisation

In order to derive a Figaro CH_4 response function, the effect of adding CH_4 to standard gas (natural ambient air) was characterised by testing five Figaro sensors (LSCE001, LSCE003, LSCE005, LSCE007 and LSCE009), using System B. Ambient laboratory air (which naturally contains 2 ppm [CH_4]) was blended with gas from a cylinder containing 5% [CH_4] in argon (P5-Gas ECD, Linde Gas AG), in 15-minute intervals from 2 ppm (pure ambient laboratory air) up to a target level of

1 000 ppm ~~target~~ [CH_4], using a pre-programmed mass-flow controller flow script (see Sect. 2.3 for details). This maximum 1 000 ppm [CH_4] gas blend has an argon mole fraction enhancement of 145% and an oxygen and nitrogen mole fraction diminution in of 1.44%, compared to natural ambient air. This 1 000 ppm level represents a realistic upper limit on typical [CH_4] enhancements expected in the vicinity of most methane sources, such as large leaks from oil and gas extraction infrastructure. This high upper [CH_4] limit also facilitates better sensor characterisation over an extended range. Following at least 1 hour of ambient laboratory air sampling, [CH_4] was gradually raised up to its maximum level and then lowered, step-wise, in three cycles. After each cycle, ambient laboratory air was sampled for 1 hour to provide an $R_{2\,ppm}$ reference. This approach is similar to that of Jørgensen et al. (2020), who instead transitioned back to their standard gas following each individual gas enhancement. Throughout our test, an 8° C dew-point setting was applied, which was sampled from at least 24 hours in advance to facilitate the necessary water stabilisation (see Appendix B).

Full Figaro resistance results are presented in Fig. 9. Fig. 10 provides an example of a single [CH_4] transition for LSCE0091, where the final 2 minutes of a 15-minute sampling interval~~s~~ is~~are~~ highlighted. This shows that the final 2 minutes is a suitable representation of stable Figaro resistance, thanks to efficient cell flushing, unlike a long cell residence time observed in other work (Rivera Martinez et al., 2022). Fig. 10 also shows that there is little noise in System B Figaro measurements~~response~~. Therefore a 2-minute resistance average was derived at the end of each 15-minute sampling period (highlighted in Fig. 9). Although a longer averaging period could have been used, we decided to minimise this duration to 2 minutes, for maximal possible stability. A specific $R_{2\,ppm}$ reference baseline was then derived for this test by fitting a second order polynomial to the final 15 minutes of each 1-hour standard (ambient laboratory air) sampling period, except the first period, where 45 minutes of sampling was instead used (see Fig. 9). $R_{2\,ppm}$ was not derived from Eq. (~~4~~3) in this test, as~~,~~ derived empirical Eq. (~~4~~3) model parameters from Sect. 3.3 are~~is~~ only valid in System A, under specific System A flow dynamics and with a specific System A T_A measurement. By instead using a~~This~~ polynomial~~dynamic~~ $R_{2\,ppm}$ fit,~~incorporates~~ any reference resistance variability was incorporated into $R_{2\,ppm}$ during the test, which may occur due to small environmental changes. In any case, temperature and [H_2O] both remained stable: [H_2O] was on average (1.002±0.001)% during $R_{2\,ppm}$ sampling periods, according to the Picarro G2401 HPR, and System B temperature was on average (34.2±0.2)° C, according to the SHT85 inside the System B cell.

For each 2-minute Figaro resistance average, corresponding Picarro G2401 [CH_4] averages were derived. Wet [CH_4] is used here and throughout this manuscript, to minimise errors associated with the internal Picarro G2401 water correction, especially at higher [CH_4], where spectral overlap becomes more prominent and [H_2O] measurements become less reliable. For [CH_4] of over 100 ppm, [CH_4] was instead derived from the mass-flow controller setting, as the Picarro G2401 is less precise at high [CH_4]. Water was then reintroduced into these dry [CH_4] estimates. The ratio between each measured resistance average and its corresponding polynomial $R_{2\,ppm}$ estimate was then deduced and plotted against its respective [CH_4] value in Fig. 11.

Fig. 11 suggests that resistance ratio follows a power law decay behaviour, whereby resistance ratio slowly tends towards zero, as [CH_4] enhancement (above the 2 ppm standard) tends to infinity. However, a simple power law fit cannot be used here: when mole fraction enhancement is equal to zero (*i.e.* when [CH_4] is equal to the 2 ppm standard), the resistance ratio must be equal to unity (*i.e.* $R_{2\,ppm}$ must equal R). Therefore, Eq. (54) is proposed, where one is added to the CH_4 gas term to satisfy this requirement.

$$R = R_{2\,ppm}(T_A, [H_2O]) \cdot \left(1 + \left(\frac{[CH_4] - 2\ ppm}{a}\right)\right)^{-\alpha} \cdot \prod_g \left(1 + \left(\frac{[M_g] - [M]_{0_g}}{c_g}\right)\right)^{-\gamma_g} \quad (54)$$

a is the characteristic methane mole fraction and α is the methane power. Other reducing gases (g) may be included in Eq. (4) depending on sampling conditions, where [M] is the mole fraction of g, $[M]_0$ is the standard mole fraction of g (in ambient air), c is the characteristic mole fraction of g and γ is the power of g. Eq. (54) is a general equation which allows any potential reducing gases to be incorporated in Figaro resistance response. However, for a more specific case when [M] is equal to $[M]_0$, as in standard gas, these multiplicative terms tend to unity and can be ignored from Eq. (54), thus simplifying to Eq. (65).

$$R \approx R_{2\,ppm}(T_A, [H_2O]) \cdot \left(1 + \left(\frac{[CH_4] - 2\ ppm}{a}\right)\right)^{-\alpha} \quad (5)$$

Thus, rather than deriving c and γ for each potential reducing gas, Eq. (65) only focuses on a single variable gas (CH_4, in this case) responsible for most resistance variability.

This model fits the System B measurements of resistance ratio (*i.e.* measured resistance averages divided by their corresponding polynomial $R_{2\,ppm}$ estimates) from the CH_4 characterisation test very well (see Table 4 for a and α for the five tested sensors), which justifies our 2-minute averaging experimental approach. This model resulting in an RMSE resistance ratio of no more than ±1% Ω Ω^{-1} and an R^2 of 0.9993±0.0005, for the five sensors. This means that over a 1 000 ppm [CH_4] range, the ratio between measured Figaro resistance and standard reference resistance can be predicted to within ±1%, thus allowing [CH_4] estimates to be derived by comparing measured resistance to $R_{2\,ppm}$. Eq. (65) was also inverted to make [CH_4] the subject. Using the same original fitting parameters provided in Table 4, this revealed an inverted [CH_4] RMSE of no more than ±31 ppm for the model fit, over the full 1 000 ppm range (see Table 4 for individual values). Applying a [CH_4] threshold reduced this uncertainty further, as [CH_4] is more accurate at lower [CH_4], where there were more data points. Taking [CH_4] values of 28 ppm and lower (nine targeted [CH_4] levels) and using the same fitting parameters from the extended [CH_4] range, resulted in a reduced inverted [CH_4] RMSE uncertainty of no more than ±0.85 ppm. Though it is possible to derive better fitting parameters in this reduced [CH_4] range, the extended [CH_4] range permits better characterisation of the natural power decay behaviour. Furthermore, characterising only small [CH_4] enhancements limits the model to such circumstances; this may be desirable in cases where there is certainty that sampled [CH_4] enhancements will remain low.

sensor	α (ppm)	α	R^2	RMSE ($\Omega\,\Omega^{-1}$)	inverted RMSE (ppm)	inverted RMSE with 28 ppm [CH_4] threshold (ppm)	resistance ratio at 3 ppm [CH_4] ($\Omega\,\Omega^{-1}$)	resistance ratio at 50 ppm [CH_4] ($\Omega\,\Omega^{-1}$)
LSCE001	26.3	0.368	0.9997	±0.0038	±12	±0.37	0.986	0.683
LSCE003	23.2	0.357	0.9997	±0.0041	±16	±0.41	0.985	0.670
LSCE005	30.2	0.461	0.9993	±0.0068	±15	±0.68	0.985	0.645
LSCE007	31.3	0.439	0.9993	±0.0065	±13	±0.69	0.986	0.665
LSCE009	24.7	0.502	0.9986	±0.0099	±31	±0.85	0.980	0.582

Table 4: Eq. (65) methane model parameters for five Figaro sensors, with the R^2 and RMSE for each model fit. Inverted methane mole fraction RMSE values are also given over the full 1 000 ppm range and with a 28 ppm threshold. The expected ratio between measured resistance and $R_{2\,ppm}$ is also provided for a 1 ppm and 48 ppm [CH_4] enhancement above the 2 ppm background.

Although there is a good CH_4 model fit for the extended [CH_4] range, in practice, [CH_4] can only be derived from the ratio between measured resistance and $R_{2\,ppm}$. The resistance ratio for a 1 ppm enhancement above the background (to 3 ppm [CH_4]) would be between 0.980 $\Omega\,\Omega^{-1}$ and 0.986 $\Omega\,\Omega^{-1}$ for the five tested sensors, while resistance ratio for a 48 ppm enhancement above the background (to 50 ppm [CH_4]) would be between 0.582 $\Omega\,\Omega^{-1}$ and 0.683 $\Omega\,\Omega^{-1}$ (see Table 4 for individual values). This makes small [CH_4] enhancements difficult to detect; a transition from 2 ppm to 3 ppm [CH_4] results in a resistance drop of as little as 1%. Thus, [CH_4] estimation using Eq. (65) requires good modelled $R_{2\,ppm}$ estimates (from ~~s~~Sect. 3.3), in order to derive a reliable resistance ratio.

3.5 Carbon monoxide influence

[CO] can vary in natural ambient air depending on nearby pollution (*e.g.* petrol and diesel cars), but is typically of the order of 10^{-1} ppm. As CO is a potent reducing gas, the importance of CO variations within standard ambient air was tested with four sensors (LSCE002, LSCE004, LSCE006 and LSCE008) in System B. Figaro resistance at 0.1 ppm [CO] was compared to a 0.0 ppm [CO] standard baseline reference (with only CO removed). An ambient target gas cylinder, filled with outside air (2 ppm [CH_4] and 0.15 ppm [CO]) was split into two gas streams: one stream was directly from the cylinder and the other stream passed through a chemical CO scrubber (Sofnocat 514, Molecular Products, Limited, Harlow, Essex, UK). The 0.0 ppm [CO] reference was first sampled for at least 1 hour. Then, 0.1 ppm [CO] was sampled in four 15-minute intervals. Each 0.1 ppm interval was followed by 15 minutes sampling the 0.0 ppm [CO] reference. A fixed 8° C dew point setting was applied and a sufficient [H_2O] stabilisation period preceded this test.

Figaro resistances and corresponding HPR measurements are presented in Fig. 12. [CH_4] remained fixed at 2 ppm throughout this test, allowing us to assess the independent influence of CO on Figaro resistance, in the standard gas (natural ambient air). A 5-minute average was taken from the end of each 15-minute 0.1 ppm [CO] sampling period (highlighted in Fig. 12). Although Fig. 12 shows that the sensors stabilise relatively quickly in response to CO, we decided to err on the side of caution

and to limit the averaging period to the final 5 minutes out of 15 minutes, based on the observed resistance delay in the CH_4 test (see Fig. 10). A baseline reference was then derived by fitting a second order polynomial to the final 5 minutes of each 15-minute reference (0.0 ppm [CO]) sampling period, except the first period where 45 minutes was used (see Fig. 12). [H_2O] was on average (0.983±0.001)% during these reference sampling periods, according to the Picarro G2401, and System B temperature was on average (31.3±0.1)° C, according to the SHT85 sensor inside the cell.

The resistance ratio between each 5-minute 0.1 ppm [CO] average and its corresponding modelled reference (0.0 ppm [CO]) resistance was derived. Four individual resistance ratios were acquired and then averaged for each sensor: (0.9922±0.0006) $\Omega\,\Omega^{-1}$ for LSCE002, (0.9936±0.0006) $\Omega\,\Omega^{-1}$ for LSCE004, (0.9960±0.0009) $\Omega\,\Omega^{-1}$ for LSCE006 and (0.9950±0.0005) $\Omega\,\Omega^{-1}$ for LSCE008. Thus, a standard gas transition from 0.0 ppm to 0.1 ppm [CO] results in less than 1% resistance decrease. This low CO sensitivity is likely due to the incorporation of an internal CO filter. This small CO resistance effect could become important in the context of small [CH_4] variations accompanied by an incredibly stable $R_{2\,ppm}$ baseline, allowing miniscule resistance variations can be observed. However, in typical applications, less than 1% resistance change will not be an important factor and thus CO can usually be excluded from Eq. (54). Furthermore, gas sensitivity declines with increasing mole fraction (*i.e.* a [CO] transition from 0.1 ppm to 0.2 ppm will result in an even smaller resistance decrease).

3.6 Carbon dioxide response

Figaro sensors naturally respond to reducing gases. As CO_2 is the most oxidised gaseous form of carbon (with no reducing potential), it is not expected to influence Figaro resistance. To verify a null CO_2 effect, two synthetic air cylinders (Deuste Gas Solutions GmbH) containing 5 000 ppm [CO_2] and 1 000 ppm [CO_2] were sampled, using System B. Both cylinders contained similar ambient quantities of CH_4 and CO. After sampling gas from the zero-air generator, each cylinder was sampled for two short intervals, before returning to zero-air generator gas. Then an ambient target gas cylinder, filled with outside air, was sampled. Four sensors were tested (LSCE002, LSCE004, LSCE006 and LSCE008) at a fixed dew point, resulting in [H_2O] of (0.649±0.006)% for this test. A sufficient water stabilisation period preceded this test.

Figaro sampling results are presented in Fig. 13, alongside corresponding HPR measurements. Fig. 13 shows that both synthetic air sources result in the same Figaro resistance decrease. This consistent decrease is principally due to the similar [CH_4] content of both cylinders. Meanwhile ambient target gas results in a much larger resistance decrease, as observed in Sect. 3.2. Therefore, CO_2 can rightly be eliminated as a species of concern when interpreting~~dealing with~~ Figaro resistance measurements~~output~~.

3.7 Oxygen response

Oxygen naturally forms 20.95% of dry air, at sea level. As an oxidising gas, increasing [O_2] should elevate Figaro resistance, in contrast to the opposite effect of reducing gases, such as CH_4. To verify this behaviour and to quantify the importance of

[O_2] variability, zero-air generator gas was diluted with nitrogen gas (99.999%, Air Products SAS, Saint Quentin Fallavier, France), using System B. Following at least 1 hour of zero-air sampling, [O_2] was gradually depleted to half its ambient atmospheric background level, stepwise, in 15-minute intervals in three cycles. Each cycle was concluded with a 45-minute period of sampling zero-air generator gas. Five Figaro sensors were tested (LSCE002, LSCE004, LSCE006, LSCE008 and LSCE010) at an 8° C dew point. A sufficient water stabilisation period preceded this test.

2-minute average resistances were taken from the end of each 15-minute sampling period (see Fig. 14). Corresponding wet [O_2] estimates were derived for each resistance average, using the mass-flow controller setting and [H_2O]. An [H_2O] value of (1.008±0.002)% was derived from the Picarro G2401 during 2-minute averages at the maximum [O_2] level (other HPR measurements could not be used due to peak broadening effects at lower [O_2]). Average Figaro resistance is plotted against [O_2] in Fig. 14~~.~~, which shows that ~~D~~decreasing [O_2] leads to a reduced Figaro resistance, in agreement with other SMO sensors (Yang et al., 2020). This behaviour is expected for Figaro sensors (van den Bossche et al., 2017, Glöckler et al., 2020), as desorbing oxygen from the SMO surface releases electrons into the bulk semiconductor material~~conduction band~~. For the five tested Figaro sensors, a 1.8% [O_2] drop results in a (0.8±0.1)% Figaro resistance decrease. Furthermore, inferring a linear fit between the highest two [O_2] points reveals a (0.0021±0.0003)% Figaro resistance decrease corresponding to a [O_2] decrease of 0.001% (10 ppm), typical of natural ambient [O_2] variability. This small effect means that oxygen can be ignored from most Figaro characterisation work, as near-surface changes in ambient [O_2] are negligible. This test also shows that Figaro sensors are insensitive to small changes in oxygen partial pressure (which is directly proportional to [O_2], at fixed atmospheric pressure). Oxygen partial pressure is also directly proportional to net atmospheric pressure (at fixed [O_2]). Thus, we can infer from this test that Figaro resistance response is insensitive to small changes in net atmospheric pressure.

4. Field testing

4.1 Field deployment

Here we discuss Figaro autonomous field testing. All ten System A loggers were deployed at the SUEZ Amailloux landfill site in the west of Metropolitan France (46.7568° N, 0.3547° E). A landfill site served as an ideal initial field testing location, as it is a large area emission source producing methane throughout the year, with occasional [CH_4] enhancements above the background of the order of 10^1 ppm. SUEZ Amailloux landfill topography gradually evolves over time, as new cells are opened, filled and then covered over with soil and geomembrane. The site features biogas collection infrastructure, in common with other European landfills (Daugela et al., 2020). The location of the ten System A loggers is provided in Fig. 15, with an example of field installation shown in Fig. 3. The loggers were typically positioned on covered soil, away from any direct point emission sources, except for LSCE003, which was placed near a leaking vent. Three loggers were moved from an "old"

to "new" location, due to site evolution: LSCE001 was moved between July and November 2021; LSCE010 was moved between February and March 2022; LSCE009 was moved on 28 April 2021.

As [CH_4] response (Sect. 3.4) and $R_{2\,ppm}$ (Sect. 3.3) characterisation tests have been performed on five sensors (LSCE001, LSCE003, LSCE005, LSCE007 and LSCE009), these five System A loggers will be the focus of subsequent analysis. These sensors sampled in the field between 20 March 2021 and 16 November 2021 (period 1) and then between 22 December 2021 and 27 March 2022 (period 2). Sensor testing was performed in-between these two sampling periods. LSCE005 stopped transmitting data on 19 October 2021. Other minor data gaps occurred due to data transmission issues.

4.2 Reference resistance modelling

For the five selected Figaro sensors, $R_{2\,ppm}$ was modelled for all field sampling, using Eq. (43). The ratio between measured resistance and $R_{2\,ppm}$ may then subsequently be used to derive [CH_4], following Eq. (65). The $R_{2\,ppm}$ model used, as input, raw measured T_A and derived [H_2O] ~~derived~~ from the SHT85 inside each System A enclosure. [H_2O] was derived using the same procedure outlined in Sect. 3.3, using Eq. (3) (Murray, 1967). Modelled $R_{2\,ppm}$ for the five System A loggers is presented in Fig. 16 for period 1 and in Fig. 17 for period 2. Measured resistance values are also presented in Fig. 16 and Fig. 17, which show a consistently elevated measured resistance above the 5 kΩ load resistance. It may therefore be better to use a higher load resistance in future work to provide better measurement sensitivity (see Sect. 2.1). Nevertheless, 5 kΩ is plainly sufficient for this work, as small peaks and troughs are clearly detectable.

Fig. 16 and Fig. 17 show that the Eq. (43) $R_{2\,ppm}$ model can replicate some features of measured resistance, due to the incorporation of water and temperature effects. The Person correlation coefficient (P) between measured resistance and $R_{2\,ppm}$ (given in Table 6) is greater than half for all bar one sensor (LSCE003), during both period 1 and period 2. Poor correlation for LSCE003 is hardly surprising, considering its placement near to a leaking vent. Yet for all five sensors there is a general disparity between modelled $R_{2\,ppm}$ and measured resistance, which outweighs any correlation, based on average resistance ratios for both periods, provided in Table 6. For reference, a ratio between measured resistance and $R_{2\,ppm}$ of one corresponds to [CH_4] of 2 ppm (standard air). Thus, Table 6 values should ~~thus~~ be close to one, or slightly less than one if generally sampling [CH_4] enhancements, as expected for LSCE003 which is near a methane leak. A ratio more than one (*i.e.* when $R_{2\,ppm}$ is less than measured resistance) corresponds to [CH_4] below 2 ppm, which is impossible in the absence of a potent CH_4 sink.

sensor	period 1 resistance ratio ($\Omega\ \Omega^{-1}$)	period 1 *P*	period 2 resistance ratio ($\Omega\ \Omega^{-1}$)	period 2 *P*
LSCE001	1.46±0.14	0.663	1.06±0.11	0.733
LSCE003	1.20±0.18	0.417	0.96±0.13	0.107
LSCE005	1.35±0.11	0.822	0.89±0.05	0.892
LSCE007	1.78±0.15	0.678	1.07±0.05	0.874
LSCE009	1.08±0.09	0.772	0.85±0.03	0.924

Table 6: The average ratio and *P* between System A measured resistance and derived standard 2 ppm [CH_4] Figaro reference resistance, while sampling at the SUEZ Amailloux landfill site during period 1 and period 2. Standard deviation uncertainties for resistance ratios are given.

Table 6 resistance ratio averages suggest that Eq. (43) $R_{2\,ppm}$ model performance is unsatisfactory for the ultimate purpose of estimating [CH_4], where an enhancement above the background of 1 ppm [CH_4] can correspond to a resistance drop of as little as 1%. Fig. 16 shows that during period 1, measured Figaro resistance was larger than $R_{2\,ppm}$ (a ratio greater than one) for all five sensors most of the time, except for some overlap for LSCE009 up to June 2021. Resistance disparity was particularly stark for LSCE007, with an average period 1 resistance enhancement of +(78±15)%, compared to $R_{2\,ppm}$. Conversely, for period 2, Fig. 17 shows that resistance ratios decreased for all five sensors and were closer to one (see Table 6), resulting in a generally better $R_{2\,ppm}$ agreement. However, Fig. 17 shows no period 2 improvement in capturing the nuances of daily temperature and [H_2O] variations. For LSCE005 and LSCE009, the period 2 resistance ratio was less than one (within the uncertainty range), which would imply consistently enhanced [CH_4] above 2 ppm, otherwise absent during period 1 (unlikely).

The reproduction of an $R_{2\,ppm}$ baseline, that can well-incorporate environmental variability, is essential to model [CH_4] enhancements above the 2 ppm standard background level, using Eq. (65). Based on model $R_{2\,ppm}$ and resistance measurements presented in Fig. 16 and Fig. 17, [CH_4] cannot be derived here in this way. There may be other factors causing resistance disparity, which must ~~be~~ first be addressed, before this sensor can be used to estimate parts-per-million level [CH_4] enhancements in future, which we discuss in Sect. 5.1.

5. Discussion

5.1 Field reference resistance disparity

In this section we attempt to understand the cause of poor agreement between $R_{2\,ppm}$ (modelled from temperature and [H_2O]) and measured resistance, as presented in Sect. 4.2, and the reasons why 2 ppm [CH_4] reference resistance disparity was different before sensor testing (period 1) compared to after sensor testing (period 2). From Sect. 3.3, the Eq. (34) model yielded excellent $R_{2\,ppm}$ agreement during chamber testing (see Table 2~~Fig. 8~~), with an $R_{2\,ppm}$ RMSE below ±1 kΩ for the five tested sensors and an R^2 of at least 0.96 ~~(see Table 2)~~. However, modelling $R_{2\,ppm}$ in the field was more challenging than in a controlled environment, with disparity between $R_{2\,ppm}$ and measured resistance up to the order of 10^1 kΩ. In addition, this resistance ratio decreased for all five sensors in period 2, though the cause of this change is not clear. As Eq. (4) model parameters were

derived using the same System A field loggers, supply voltage variation is not an issue. Furthermore, high-precision voltage regulators inside System A (see Sect. 2.2) ensure that Figaro supply voltage remains the same, regardless of using a charger (in the environmental chamber) instead of a solar panel (in the field) to charge the battery. Alternatively, c~~C~~hanges in the [CH_4] background level may have affected $R_{2\,ppm}$, but this was also unlikely to be responsible, as we also conducted regular onsite and offsite sampling campaigns (not shown), where no excessive abnormalities in general [CH_4] variability were observed. Thus, we expect emissions from the SUEZ Amailloux landfill site to remain at a relatively consistent order of magnitude throughout the year.

One possible cause of poor $R_{2\,ppm}$ fitting, was the composition of air during environmental chamber testing. On the one hand, no [CH_4] or [CO] irregularities were observed in the chamber by the Picarro G2401 HPR. However, the results presented in Fig. 5 point to the presence of a different reducing species in air, otherwise absent in clean synthetic gas (see Sect. 5.2 for further discussion). It is possible that the composition of these interfering compounds was different in the chamber compared to the landfill site, either through high-temperature chamber degassing or due to the natural ambient composition of the surrounding chamber environment. A cocktail of trace gas species (other than CH_4 and CO_2) can be emitted from landfill sites, including ~~species such as~~ sulphides, ammonia, alcohols, alkanes, alkenes and aromatics, which vary by many orders of magnitude in different landfill sites (Duan et al., 2020). Yet, the pronounced resistance ratio jump from period 1 to period 2 does not support this hypothesis as the principal cause of resistance disparity. If there were consistently poor $R_{2\,ppm}$ model parameters, one would expect field resistance to consistently exceed $R_{2\,ppm}$ and not to erroneously decrease in period 2.

Another possibility for poor $R_{2\,ppm}$ agreement with measured resistance, is differences in Figaro cooling dynamics in the environmental chamber, compared to the field. van den Bossche et al. (2017) showed that the location of a temperature measurement can be highly influential concerning its application in any correction model. We therefore used the same System A logger in both applications (chamber testing and field deployment) to minimise such effects. Yet, Figaro airflow may still vary depending on conditions exterior to System A ~~conditions~~. In the field, the logging enclosures faced downwards, where lateral winds could influence upwards airflow from the downwards facing fan, due to a vacuum effect. On the other hand, boxes faced sideward in the chamber, with a large chamber fan for air circulation. These two scenarios may have cooled the Figaro sensors inside the System A enclosure differently, such that the temperature gradient between the SHT85 environmental sensor and the Figaro varied, rendering the empirical Eq. (~~4~~3) $R_{2\,ppm}$ model unusable.

Sect. 4 shows that there is an unexplained jump in resistance ratio from period 1 to period 2. Yet, the above discussion suggests that the $R_{2\,ppm}$ model may be fundamentally flawed, either due to airflow effects or different levels of other interfering reducing gas species (see Sect. 5.2 for further discussion). Instead of resistance ratio, it may be better to analyse ~~at~~ raw resistance measurements. Maybe, cooler and drier period 2 conditions (largely coinciding with Boreal~~Northern Hemispheric~~ winter) erroneously exaggerated $R_{2\,ppm}$. The full T_A and [H_2O] measurement range is presented in Fig. 18 for both periods as box plots, for comparison, along with the measured Figaro resistance range. When actual resistance measurements are assessed, there is

a large overlap between period 1 and period 2 over the full sampling range. Nevertheless, Fig. 18 shows that measured resistance was significantly lower for all five sensors in period 2, considering the interquartile range, and particularly so for LSCE005 and LSCE007. Yet in view of an equally significant temperature and [H_2O] period 2 decrease, it is possible that these environmental effects may account for the period 2 resistance drop if a better $R_{2\,ppm}$ model were used, thus improving $R_{2\,ppm}$ agreement with measured resistance.

A final cause of disparity between $R_{2\,ppm}$ and measured resistance may be spontaneous variations in the sensor itself, causing the original $R_{2\,ppm}$ model parameters to become invalid. However, the fact that resistance ratio decreased for all five sensors in period 2 makes this hypothesis unlikely. Instead, something may have physically altered natural behaviour of multiple sensors during testing, such as the transfer from System A to System B or extreme [H_2O] or temperature conditions. Alternatively, high concentration exposure to certain gases can cause permanent sensor damage, which may have occurred some time between period 1 and period 2. While such effects may have been a contributory factor, the most likely cause of reference resistance disparity from actual resistance measurements (and the change in resistance ratio from period 1 to period 2) is a poor $R_{2\,ppm}$ model which did not suitably account for sampling conditions in the field.

5.2 Characterisation approach and future improvements

Here we discuss our general Figaro testing approach and compare our methods to other work conducted with the Figaro TGS 2611-E00, along with studies on other Figaro sensor types. In Sect 3.2, we derived $R_{2\,ppm}$ using an environmental chamber. However, characterising SMO sensors using an environmental chamber calibration has proved challenging in the past. For example, ~~Yet according to~~ Eugster et al. (2020)~~, who~~ attempted their own chamber characterisation of the less selective (but more sensitive) Figaro TGS 2600, but yielded unsatisfactory results~~chamber testing may not be suited for SMO sensors in general~~. They instead employed a long-term HPR field calibration (Eugster et al., 2020). Field calibration has proved popular for the TGS 2600, where ambient HPR measurements help to optimise model parameters (Eugster and Kling, 2012, Casey et al., 2019, Collier-Oxandale et al., 2019) in conditions with a similar environment and pollutant gas levels (Collier-Oxandale et al., 2018). An analogous approach can also be applied to ambient laboratory sampling, by simply leaving a sensor to sample in a laboratory alongside an HPR (Martinez Rivera et al., 2021), with an aim for subsequent field deployment (Riddick et al., 2020). Yet, ambient air sensor characterisation can be problematic if various calibration models are required in different conditions, for example in different humidity (Collier-Oxandale et al., 2018) or temperature (Eugster et al., 2020) regimes.

Despite this, the Figaro TGS 2611-E00 has successfully been tested in controlled conditions in the past, for example Cho et al. (2022) set an oven set to three precise temperatures, where [CH_4] and relative humidity were externally controlled to fill a 2 dm^3 test chamber. Although the application of their calibration model was tested in controlled conditions, it was not HPR field-tested (Cho et al., 2022). Furuta et al. (2022) designed a temperature-controlled TGS 2611-E00 testing chamber, by placing a heated inner enclosure inside a larger freezer, where pulses of methane were injected into ambient air at various

temperature settings. However, the sensors were not HPR field-tested, as this work was more focussed on sensor characterisation (Furuta et al, 2022). As this test lacked humidity control, large [H_2O] variability occurred due to condensation and evaporation of water from the chamber walls (Furuta et al, 2022). Bastviken et al. (2020) conducted chamber testing at various temperature and humidity settings up to 3.5% [H_2O] (humidity was indirectly controlled), where CH_4 was injected at each setting. As this calibration was designed to detect high [CH_4] in flux chambers, it was not extensively field-tested (Bastviken et al., 2020). van den Bossche et al. (2017) instead tested a Figaro sampling cell in a water bath, for improved temperature regulation. Elsewhere, Jørgensen et al. (2020) conducted laboratory tests at three different relative humidity settings, with no temperature control, assuming constant laboratory temperature. However, they could not use this test in the field (where zero-air served as a standard gas) and instead employed an HPR field calibration, assuming invariant environmental conditions (Jørgensen et al., 2020).

Yet, a key limitation of ambient air characterisation, is the requirement of an expensive HPR, co-located with each Figaro for a sufficient period of testing time, in order to derive a robust long-term model. Unless readily available, this can negate the central advantage of a cheap SMO sensor. Most of the System A loggers at the SUEZ Amilloux landfill site were isolated and distant from sources of mains power, typically required by a CH_4 HPR. Furthermore, the site is constantly evolving, which is conducive to the deployment of low-cost sensors powered by a solar panel, due to their mobility and ease of remote installation. Thus, we conducted Figaro characterisation in controlled conditions (*i.e.* not in the field). HPR ambient air testing of ten System A loggers is not logistically feasible. However, it is worth noting that it may be possible to characterise $R_{2\,ppm}$ for multiple Figaro sensors using a single HPR, by only selecting sampling during high winds, assuming the wind to sufficiently dilute any nearby methane emission source (although the influence of wind of sensor cooling would need to be accounted for in such an approach). Nevertheless, a [CH_4] field characterisation cannot be achieved in this way.

Instead, our controlled chamber calibration approach required the simulation of environmental field conditions. Based on our [O_2] test (see Sect. 3.7), atmospheric pressure was dismissed as a key factor effecting the TGS 2611-E00, in agreement with other work (van den Bossche et al., 2017, Rivera Martinez et al., 2021). However, environmental chamber tests revealed a strong [H_2O] and temperature resistance response, as observed elsewhere (Bastviken et al., 2020, Rivera Martinez et al., 2021, Cho et al., 2022). Temperature may also influence electronic measurement circuitry (Ferri et al., 2009). We found [H_2O] to dominate resistance, at fixed [CH_4]. We accounted for these environmental effects in our calibration approach by deriving a standard $R_{2\,ppm}$, following van den Bossche et al. (2017). Whereas van den Bossche et al. (2017) derived logarithmic relationships between environmental parameters and standard resistance, we found linear correlations to be suitable.

Conversely, in many past studies testing the TGS 2600 (Eugster and Kling, 2012, Collier-Oxandale et al., 2018, Eugster et al., 2020, Riddick et al., 2020), TGS 2602 (Casey et al., 2019, Collier-Oxandale et al., 2019) and TGS 2611-E00 (Bastviken et al., 2020, Jørgensen et al., 2020, Cho et al., 2022), a fixed reference resistance has been used, in contrast to our dynamic $R_{2\,ppm}$ approach. Temperature and water effects have then subsequently been incorporated into models, alongside resistance ratio, to

yield [CH_4] (Collier-Oxandale et al., 2018). Collier-Oxandale et al. (2019) and Casey et al., (2019) used this fixed reference approach to derive [CH_4] (as well as other gas mole fractions) by combining input from various sensors including a TGS 2600 and TGS 2602. Bastviken et al. (2020) used a combination TGS 2611-E00 environmental correction, where water and temperature were first incorporated into a dynamic reference resistance and then subsequently corrected from resistance ratio.

Despite our best efforts, our dynamic $R_{2\,ppm}$ model could not replicate field Figaro resistance measurements. One cause may have been a misrepresentative temperature measurement during testing, compared to field sampling (see Sect. 5.1 for specific discussion). In light of this temperature dependence, Eugster et al. (2020) proposed a TGS 2600 heat-loss model using wind speed, temperature and air heat capacities, however, this model could not predict [CH_4] any better than their original deterministic model. Elsewhere, Casey et al. (2019) found that low wind speeds adversely affected the performance of both linear and ANN [CH_4] models, whose TGS 2600 and TGS 2602 were also inside an enclosure. In light of this potential wind effect, we compared resistance ratio with increasing minute-average wind speed for LSCE007, as measured simultaneously by the LSCE007 System A anemometer (Fig. 19), where wind direction was between 180° and 270° (*i.e.* away from the active landfill). This shows that, there is no correlation between wind speed and resistance ratio, which therefore suggests that our $R_{2\,ppm}$ model is not fundamentally influenced by wind speed.

All types of Figaro TGS sensors are clearly affected by water (Furuta et al., 2022). Yet, when correcting for water effects, some researchers have used relative humidity (Eugster and Kling, 2012, van den Bossche et al., 2017, Jørgensen et al., 2020, Cho et al., 2022), some have used either [H_2O] or absolute humidity (Collier-Oxandale et al., 2018, Casey et al., 2019, Collier-Oxandale et al., 2019, Eugster et al., 2020, Rivera Martinez et al., 2021, Furuta et al., 2022, Rivera Martinez et al., 2022) and some have mixed both in model combinations (Bastviken et al., 2020). As these SMO sensors respond to absolute water content, we chose [H_2O] in our model, representing the fraction of water molecules in air. Absolute humidity is a mass fraction, similar to [H_2O]. On the other hand, relative humidity represents the proximity to water saturation (dew point), as a function of temperature. Thus [H_2O] or absolute humidity typically results in superior model fitting (Bastviken et al., 2020).

Figaro sensors in general require a sufficient warm-up time before testing (Honeycutt et al., 2019, Glöckler et al., 2020, Cho et al., 2022, Furuta et al., 2022). They may also slowly age over time (Eugster et al., 2020, Riddick et al., 2020), resulting in reduced sensitivity (Eugster and Kling, 2012, Collier-Oxandale et al., 2018). Collier-Oxandale et al. (2019) resolved ageing effects by including time as a reference resistance parameter. In principle, ageing can easily be corrected by fitting between calibrations performed at two time points (Eugster and Kling, 2012). While, Riddick et al. (2020) recommend bimonthly calibrations to account for time, ageing is unlikely to be an issue when targeting large (part-per-million level) [CH_4] enhancements (Rivera Martinez et al., 2022).

During testing, we characterised each Figaro individually. Previous work has shown that despite using the same Figaro type, individual sensors behave differently (Rivera Martinez et al., 2021, Rivera Martinez et al., 2022) due to variability in sensor

surface characteristics (Bastviken et al., 2020, Riddick et al., 2020, Sieczko et al., 2020). Our results plainly show that $R_{2\ ppm}$ (see Table 2) and CH_4 response (see Table 4) vary for each sensor. However, some sensors were more similar (for example LSCE001 and LSCE003) than others (LSCE009), possibly due to batch production with similar surface characteristics; sensors from the same production batch exhibit a similar CH_4 response (Furuta et al., 2022). The sensors tested in Sect. 3.4 come from various sources so they were most probably produced from at least two different batches. In the past, Cho et al. (2022) applied a single calibration model to 19 different TGS-2611-E00 sensors, but each sensor was assigned a unique fixed reference resistance. While this was crudely laboratory-tested, with an average 8 ppm [CH_4] deviation (sampling up to 190 ppm), it is not clear if this approach was valid in the field (Cho et al., 2022). Elsewhere, Collier-Oxandale et al. (2018) tested a universal TGS 2600 calibration model, which while promising, could not compete with a sensor specific model, supporting our approach.

Although our $R_{2\ ppm}$ model requires improvement, [CH_4] response was characterised very well up to 1 000 ppm in controlled conditions, with a resistance ratio RMSE of no more than ±1% $\Omega\ \Omega^{-1}$ for the five tested sensors and an R^2 of at least 0.997. Our Eq. (54) [CH_4] model is similar to the simple manufacturer-proposed power law (Eugster and Kling, 2012). However, as we use resistance ratio instead of raw resistance, we include a unity term. This satisfies the requirement that resistance ratio is equal to one in standard gas (*i.e.* when [CH_4] is 2 ppm). Furthermore, Eq. (54) allows other sensitive gases to be multiplicatively included.

Our Fig. 11 resistance decay curve is similar to the TGS 2611-C00 relationship overserved by Glöckler et al. (2020) up to 9 000 ppm [CH_4], although they did not derive a model fit. Honeycutt et al. (2019) proposed a Langmuirian fit in dry conditions, up to 1 000 ppm [CH_4], for various Figaro types. Instead of using a reference resistance, Furuta et al. (2022) devised a simple [CH_4] model for various Figaro types up to 10 ppm, based solely on [H_2O] and sensor resistance, resulting in ±1 ppm [CH_4] RMSE for three different tested TGS 2611-E00 units. Elsewhere, Rivera Martinez et al. (2021) found a clear resistance-~~[CH_4]~~ decline up to 9 ppm [CH_4], but Figaro TGS 2611-E00 resistance changes were less pronounced than for the TGS 2600 and TGS 2611-C00. van den Bossche et al. (2017) derived a linear TGS 2611-E00 [CH_4] calibration, by sampling six [CH_4] levels up to 9 ppm in fixed environmental conditions. Although TGS 2611-E00 resistance appears linear over a small [CH_4] range, non-linearity increases at higher [CH_4] (Honeycutt et al., 2019, Bastviken et al., 2020). Cho et al. (2022) derived a resistance power law up to ~~[CH_4]~~ 10 000 ppm [CH_4], at various temperature settings. Jørgensen et al. (2020) also observed a resistance ratio power fit up to 100 ppm [CH_4]. A similar fit was observed at three different relative humidity settings; however, this model did not include a unity term as in Eq. (55) (Jørgensen et al., 2020), meaning that resistance tends to infinity at standard [CH_4], rather than a limiting reference resistance ~~(Jørgensen et al., 2020)~~. A simple power law also limits the model to a single gas.

As Jørgensen et al. (2020) and Cho et al. (2022) targeted emissions where CH_4 is the primary reducing gas, their calibration models only included CH_4. We followed a similar approach for our landfill emission source, by simplifying Eq. (54) to Eq. (65). Alternatively, the TGS 2611-C00 or even the TGS 2600 may be used where only small interfering CO enhancements are

expected, as the lack of a CO filter amplifies CH_4 sensitivity (Eugster et al., 2020). In addition, Rivera Martinez et al. (2022) showed that the TGS 2611-C00 may be less noisy, making it easier to model [CH_4] enhancements above the background than the TGS 2611-E00. This improved TGS 2611-C00 sensitivity may augment an environmental $R_{2\,ppm}$ fit. In any case, our Eq. (54) model allows other gases to be included in future work if necessary. This may allow the TGS 2611-E00 to be deployed in industrial locations with high CO emissions. However, before considering such an approach, improvements in $R_{2\,ppm}$ characterisation are first required. The small resistance decrease (between 1.4% and 2.0% for the five tested sensors; see Table 4), in response to a 1 ppm [CH_4] enhancement above the background, emphasises the importance of accurately modelling $R_{2\,ppm}$.

Reference gas testing (Sect. 3.2) revealed that synthetic air and ambient air (from our laboratory), containing the same 2 ppm [CH_4], resulted in a different Figaro resistance response. A similar effect may have also contributed towards disparity between landfill Figaro measurements and $R_{2\,ppm}$, due to a different air composition in the environmental chamber, compared to the field. A precise gas analysis may identify Figaro-sensitive species in different gas sources, including ambient air at the landfill site (Duan et al., 2020), using techniques such as gas chromatography, Fourier-transform IR spectroscopy or proton-transfer-reaction mass spectrometry, which is particularly suited to detect volatile organic compounds. However, in reality, this would be arduous as it is not clear which interfering gases to look for, especially at a landfill site (Duan et al., 2020). CH_4 is the most abundant reducing gas in natural ambient air followed by CO, which were both measured by the Picarro G2401 HPR throughout testing in the environmental chamber and during the laboratory sensitivity test. Although other alkanes (for example, ethane, propane and butane) are reducing gases, with similar chemical properties to methane, they are present in very low quantities in ambient air. Furthermore, manufacturer testing with iso-butane up to 10 000 ppm revealed negligible Figaro resistance response (Figaro Engineering Inc., 2011), though straight-chain alkanes may behave differently. Similarly, alcohols may interfere with SMO sensors, but manufacturer testing up to 10 000 ppm of ethanol also showed negligible Figaro response (Figaro Engineering Inc., 2011). Hydrogen is the only other reducing gas~~,~~ known to affect the Figaro TGS 2611-E00 (Figaro Engineering Inc., 2011). Maybe different alcohols and alkanes (or some other volatile organic compounds, not discussed here) could play a role, but targeting a specific reducing species, with no obvious candidate, remains a challenge. Unfortunately, it is difficult to look to other SMO prototype sensors to help to identify Figaro-sensitive interfering compounds, as each SMO sensor is unique in its composition and behaviour. Therefore, we recommend a robust analysis of Figaro TGS 2611-E00 gas sensitivities in future work, to help to identify potential interfering gas species in ambient air. In this work, for simplicity, we used ambient air as a standard gas, rather than clean synthetic gas or zero-air when characterising $R_{2\,ppm}$. However, this assumes that the air composition during testing was similar to ambient air in the field. A thorough gas analysis may help to confirm this assumption. Alternatively, deploying a field logger containing a suite of low-cost SMO sensors with sensitivities to different gases (including and excluding methane) may help to shed some light on the nature of interfering reducing compounds (Casey et al., 2019, Collier-Oxandale et al., 2019). Such a~~This~~ future test may offer valuable insight into various Figaro sensitivities over a prolonged sampling period.

Another potential cause of resistance~~R_2~~ disparity between the $R_{2\,ppm}$ model and landfill Figaro sampling was the wind dynamics around the System A enclosure, as discussed above. This may be resolved by placing the Figaro sensor in a closed cell more akin to System B. This permits a controlled sensor airflow, resulting in consistent sensor cooling effects. It also buffers temperature changes and allows temperature measurements to be more repeatable in the laboratory compared to the field. This approach would also enable precise gas exposure during environmental $R_{2\,ppm}$ testing, rather than relying on potentially contaminated air in and around an environmental chamber. Furthermore, the Figaro sensor would not move between loggers, eliminating the chance of different loggers potentially causing spurious jumps in sensor behaviour. However, a closed cell logger requires a pump, which has substantially higher power requirements. This may push a solar panel power source to its limits, especially in the mid-latitude winter.

6. Conclusion

Ten Figaro TGS 2611-E00 sensors were deployed at a landfill site in France, of which five sensors were tested to characterise environmental and methane gas~~mole fraction~~ response. The~~With an~~ ultimate objective was to~~of~~ derive~~ing~~ methane mole fraction from sensor resistance.~~,~~ Our characterisation~~we took the~~ approach ~~of~~ first separated ~~incorporating~~ environmental effects by incorporating them into a standard reference resistance.~~,~~ Thi~~thu~~s enable~~ding~~ the independent~~separate~~ characterisation of sensor~~gas~~ response to individual reducing gas species.

Before characterising an environmental baseline resistance (independent of gas composition), w~~W~~e found that the choice of standard reference gas has a significant effect on Figaro resistance, despite each gas sample containing the same 2 ppm methane mole fraction: Figaro resistance was much lower in natural ambient air, compared to both synthetic air and a high concentration methane source diluted with zero-air (to target~~ing~~ 2 ppm methane mole fraction). We therefore used ambient laboratory air as our testing gas standard, which naturally contains 2 ppm of methane ~~mole fraction~~. Sensor response to t~~T~~emperature and water vapour mole fraction ~~effects~~ were then characterised in the field logging enclosure which was placed inside~~, using~~ a large environmental chamber. A four-parameter model was then used to yield reference resistance from w~~W~~ater vapour mole fraction and temperature, of which the former had the largest influence on resistance~~, but temperature also played a role~~.

This model was then applied to field sampling, where methane mole fraction was mostly at background levels (2 ppm). In spite of the capability~~quality~~ of the~~our~~ environmental chamber model fit to derive reference resistance under controlled conditions at 2 ppm methane mole fraction, ~~a reference (2 ppm) resistance, as observed in the chamber,~~reference resistance could not be replicated in field conditions for a variety of potential reasons. There may have been ~~field~~ differences in airflow around the logger in the field compared to the environmental chamber, the air composition may have been different during chamber testing or there may have been spontaneous sensor variability during transfer between various loggers and in different environments.

Nevertheless, our independent methane gas enhancement characterisation model provided an excellent fit in controlled conditions. This was achieved by taking the ratio between measured resistance and a reference (background methane) resistance, when sampling up to 1 000 ppm methane mole fraction in incremental steps. We conceived an adapted power fit between methane mole fraction and this resistance ratio, with a coefficient of determination of at least 0.999. When this model was inverted to make methane mole fraction the subject, we derived a root-mean-squared error of less than ±1 ppm, when limited to below 28 ppm. We also showed that the effect of carbon monoxide is minimal, during similar tests.

We propose that f~~F~~uture TGS 2611-E00 work should be conducted with great care, to ensure that environmental effects are well-characterised and that an appropriate~~good~~ choice of standard gas is used, to mirror field sampling conditions. With improvements in a reference (standard gas) resistance characterisation, it is evident that the Figaro TGS 2611-E00 sensor has great potential in detecting methane mole fraction with a parts-per-million level precision. A closed sampling cell with a pump may help to achieve this goal, although power requirements will have to be taken into consideration.

Funding

This work was supported by the Chaire Industrielle TRACE, which is co-funded by the *Agence Nationale de la Recherche* (ANR) French National Research Agency (grant number: ANR-17-CHIN-0004-01), SUEZ, TotalEnergies - OneTech and Thales Alenia Space. This work also received contributions in kind from the Integrated Carbon Observation System (ICOS) National Network France.

Author contributions

AS prepared the manuscript in collaboration with GB, PC, OL and EA, who edited the text. GB, PC, OL, RRM and EA provided support and ideas during the testing process. AS designed System B. AS, LL and OL conducted testing of System A and System B and installed System A in the field. EA helped to facilitate site access for field deployment. AS processed testing and field sampling data.

Competing interests

The authors declare that they have no conflict of interest.

Acknowledgements

We thank Mathis Lozano, Mali Chariot, Timothé Depelchin and Julien Moyé for support in System A field installation and Carole Philippon for support during laboratory testing. We thank Pierre Maso, Nicolas Caignard and Sébastien Ancelin at the Plateforme d'Intégration et de Tests at the Observatoire de Versailles Saint-Quentin-en-Yvelines for access and support in using the environmental chamber. We thank the operating staff at the SUEZ Amailloux landfill site for site access, assistance and support. We thank Scientific Aviation, Inc for complimentary System A data access and support.

Data availability

Data are available upon request from the corresponding author.

References

Baer, D. S., Paul, J. B., Gupta, M. and O'Keefe, A.: Sensitive absorption measurements in the near-infrared region using off-axis integrated-cavity-output spectroscopy. *Applied Physics B.* **75**, *pp*.261–265, https://doi.org/10.1007/s00340-002-0971-z. 2002.

Barsan, N., Koziej, D. and Weimar, U.: Metal oxide-based gas sensor research: How to?. *Sensors and Actuators B: Chemical*, **121**, *pp*.18-35, https://doi.org/10.1016/j.snb.2006.09.047. 2007.

Bastviken, D., Nygren, J., Schenk, J., Parellada Massana, R. and Duc, N. T.: Technical note: Facilitating the use of low-cost methane (CH4) sensors in flux chambers – calibration, data processing, and an open-source make-it-yourself logger. *Biogeosciences*, **17**, *pp*.3659–3667, https://doi.org/10.5194/bg-17-3659-2020, 2020.

Casey, J. G., Collier-Oxandale, A. and Hannigan, M.: Performance of artificial neural networks and linear models to quantify 4 trace gas species in an oil and gas production region with low-cost sensors. *Sensors and Actuators B: Chemical*, **283**, *pp*.504-514, https://doi.org/10.1016/j.snb.2018.12.049. 2019.

Chakraborty, S., Sen, A. and Maiti, H. S.: Selective detection of methane and butane by temperature modulation in iron doped tin oxide sensors. *Sensors and Actuators B: Chemical*, **115**, *pp*.610-613, https://doi.org/10.1016/j.snb.2005.10.046. 2006.

Cho, Y., Smits, K. M., Riddick, S. N. and Zimmerle, D. J.: Calibration and field deployment of low-cost sensor network to monitor underground pipeline leakage. *Sensors and Actuators B: Chemical*, **355**, article number: 131276, https://doi.org/10.1016/j.snb.2021.131276. 2022.

Collier-Oxandale, A., Casey, J. G., Piedrahita, R., Ortega, J., Halliday, H., Johnston, J. and Hannigan, M. P.: Assessing a low-cost methane sensor quantification system for use in complex rural and urban environments. *Atmospheric Measurement Techniques*, **11**, *pp*.3569-3594, https://doi.org/10.5194/amt-11-3569-2018. 2018.

Collier-Oxandale, A. M., Thorson, J., Halliday, H., Milford, J. and Hannigan, M.: Understanding the ability of low-cost MOx sensors to quantify ambient VOCs. *Atmospheric Measurement Techniques*, **12**, *pp*.1441-1460, https://doi.org/10.5194/amt-12-1441-2019. 2019.

Das, A., Bonu, V., Prasad, A. K., Panda, D., Dharaa, S. and Tyagia, A. K.: The role of SnO2 quantum dots in improved CH4 sensing at low temperature. *Journal of Materials Chemistry C*, **2**, *pp*.164-171, https://doi.org/10.1039/C3TC31728E. 2014.

Daugela, I., Suziedelyte Visockiene, J. and Kumpiene, J. Detection and analysis of methane emissions from a landfill using unmanned aerial drone systems and semiconductor sensors. *Detritus*, **10**, *pp*.127-138, https://doi.org/10.31025/2611-4135/2020.13942. 2020.

Dlugokencky, E. J., Steele, L. P., Lang, P. M. and Masarie, K. A.: The growth rate and distribution of atmospheric methane. *Journal of Geophysical Research*, **99**, *pp*.17021–17043, https://doi.org/10.1029/94jd01245. 1994.

~~Dlugokencky, E.: Carbon Monitoring Laboratory – Carbon Cycle Greenhouse Gases, available at: https://esrl.noaa.gov/gmd/ccgg/trends_ch4/, last access: 21 May 2022. 2022.~~

Duan, Z., Scheutz, C. and Kjeldsen, P.: Trace gas emissions from municipal solid waste landfills: A review. *Waste Management*, **119**, *pp*.39-62, https://doi.org/10.1016/j.wasman.2020.09.015.2020.

Eugster, W. and Kling, G. W.: Performance of a low-cost methane sensor for ambient concentration measurements in preliminary studies. *Atmospheric Measurement Techniques*, **5**, *pp*.1925-1934, https://doi.org/10.5194/amt-5-1925-2012. 2012.

Eugster, W., Laundre, J., Eugster, J. and Kling, G. W.: Long-term reliability of the Figaro TGS 2600 solid-state methane sensor under low-Arctic conditions at Toolik Lake, Alaska. *Atmospheric Measurement Techniques*, **13**, *pp*.2681-2695, https://doi.org/10.5194/amt-13-2681-2020. 2020.

Ferri, G., Di Carlo, C., Stornelli, V., De Marcellis, A., Flammini, A., Depari, A. and Jand, N.: A single-chip integrated interfacing circuit for wide-range resistive gas sensor arrays. *Sensors and Actuators B: Chemical*, **143**, *pp*.218-225, https://doi.org/10.1016/j.snb.2009.09.002. 2009.

Fleischer, M. and Meixner, H.: A selective CH4 sensor using semiconducting Ga2O3 thin films based on temperature switching of multigas reactions. *Sensors and Actuators B: Chemical*, **25**, *pp*.544-547, https://doi.org/10.1016/0925-4005(95)85118-6. 1995.

Figaro Engineering Inc.: tgs2611-e00_product infomation(en)_rev01.pdf, available at: https://www.figaro.co.jp/en/product/docs/tgs2611-e00_product%20infomation%28en%29_rev01.pdf, last access: 26 May 2022. 2021.

Frish, M. B.: Current and emerging laser sensors for greenhouse gas sensing and leak detection. *Proceedings of SPIE*, **9101**, article number: 91010H, https://doi.org/10.1117/12.2053181. 2014.

Furuta, D., Sayahi, T., Li, J., Wilson, B., Presto, A. A. and Li, J.: Characterization of inexpensive metal oxide sensor performance for trace methane detection. *Atmospheric Measurement Techniques*, **15**, *pp*.5117-5128, https://doi.org/10.5194/amt-15-5117-2022. 2022.

Gagaoudakis, E., Michail, G., Katerinopoulou, D., Moschovis, K., Iliopoulos, E., Kiriakidis, G., Binas, V. and Aperathitis, E.: Transparent p-type NiO:Al thin films as room temperature hydrogen and methane gas sensors. *Materials Science in Semiconductor Processing*, **109**, article number: 104922, https://doi.org/10.1016/j.mssp.2020.104922. 2020.

Glöckler, J., Jaeschke, C., Tütüncü, E., Kokoric, V., Kocaöz Y. and Mizaikoff, B.: Characterization of metal oxide gas sensors via optical techniques. *Analytical and Bioanalytical Chemistry*, **412**, *pp*.4575-4584, https://doi.org/10.1007/s00216-020-02705-6. 2020.

Gonzalez-Valencia, R., Magana-Rodriguez, F., Maldonado, E., Salinas, J. and Thalasso, F.: Detection of hotspots and rapid determination of methane emissions from landfills via a ground-surface method. *Environmental Monitoring and Assessment*, **187**, article number: 4083, https://doi.org/10.1007/s10661-014-4083-0. 2014.

Haridas, D. and Gupta, V.: Study of collective efforts of catalytic activity and photoactivation to enhance room temperature response of SnO2 thin film sensor for methane. *Sensors and Actuators B: Chemical*, **182**, *pp*.741-746, https://doi.org/10.1016/j.snb.2013.03.100. 2013.

Hodgkinson, J. and Tatam, R. P.: Optical gas sensing: a review. *Measurement Science and Technology*, **24**, article number: 012004, https://doi.org/10.1088/0957-0233/24/1/012004. 2013.

Honeycutt, W. T., Ley, M. T. and Materer, N. F.: Precision and Limits of Detection for Selected Commercially Available, Low-Cost Carbon Dioxide and Methane Gas Sensors. *Sensors*, **19**, article number: 3157, https://doi.org/10.3390/s19143157. 2019.

Honeycutt, W., Kim, T., Ley, M. T. and Materer, N. F.: Sensor array for wireless remote monitoring of carbon dioxide and methane near carbon sequestration and oil recovery sites. *RSC Advances*, **11**, *pp*.6972-6984, https://doi.org/10.1039/D0RA08593F. 2021.

Hong, T., Culp, J. T., Kim, K. J., Devkota, J., Sun, C. and Ohodnicki, P. R.: State-of-the-art of methane sensing materials: A review and perspectives. *Trends in Analytical Chemistry*, **125**, article number: 115820, https://doi.org/10.1016/j.trac.2020.115820. 2020.

Hummelgård, C., Bryntse, I., Bryzgalov, M., Henning, J., Martin, H., Norén, M. and Rödjegård, H. Low-cost NDIR based sensor platform for sub-ppm gas detection. *Urban Climate*, **14**, *pp*.342-350, https://doi.org/10.1016/j.uclim.2014.09.001. 2015.

Jackson, R. B, Saunois, M., Bousquet, P., Canadell, J. G., Poulter, B., Stavert, A. R., Bergamaschi, P., Niwa, Y., Segers, A. and Tsuruta, A.: Increasing anthropogenic methane emissions arise equally from agricultural and fossil fuel sources. *Environmental Research Letters*, **15**, article number: 071002, https://doi.org/10.1088/1748-9326/ab9ed2. 2020.

Jørgensen, C. J., Mønster, J., Fuglsang, K. and Christiansen, J. R.: Continuous methane concentration measurements at the Greenland ice sheet–atmosphere interface using a low-cost, low-power metal oxide sensor system. *Atmospheric Measurement Techniques*, **13**, *pp*.3319-3328, https://doi.org/10.5194/amt-13-3319-2020. 2020.

Kim, J. C., Jun, H. K., Huh, J. S. and Lee, D. D.: Tin oxide-based methane gas sensor promoted by alumina-supported Pd catalyst. *Sensors and Actuators B: Chemical*, **45**, *pp*.271-277, https://doi.org/10.1016/S0925-4005(97)00325-0. 1997.

Kim, Y. M., Park, M. H., Jeong, S., Lee, K. H. and Kim, J. Y.: Evaluation of error inducing factors in unmanned aerial vehicle mounted detector to measure fugitive methane from solid waste landfill. *Waste Management*, **124**, *pp*.368-376, https://doi.org/10.1016/j.wasman.2021.02.023. 2021.

Kohl, D.: Surface processes in the detection of reducing gases with SnO2-based devices. *Sensors and Actuators*, **1**, *pp*.71-113, https://doi.org/10.1016/0250-6874(89)87026-X. 1989.

Kohl, D.: The role of noble metals in the chemistry of solid-state gas sensors. *Sensors and Actuators B: Chemical*, **1**, *pp*.158-165, https://doi.org/10.1016/0925-4005(90)80193-4. 1990.

Kohl, D.: Function and applications of gas sensors. *Journal of Physics D: Applied Physics*, **34**, *pp*.R125-R149, https://doi.org/10.1088/0022-3727/34/19/201. 2001.

Kooti, M., Keshtkar, S., Askarieh, M. and Rashidibi, A.: Progress toward a novel methane gas sensor based on SnO2 nanorods-nanoporous graphene hybrid. *Sensors and Actuators B: Chemical*, **281**, *pp*.96-106, https://doi.org/10.1016/j.snb.2018.10.032. 2019.

Lan, X., Thoning, K. W. and Dlugokencky, E. J.: Global Monitoring Laboratory - Carbon Cycle Greenhouse Gases, available at: https://esrl.noaa.gov/gmd/ccgg/trends_ch4/, last access: 6 March 2023. 2023.

Mitchell, J. F. B: The "greenhouse" effect and climate change. *Reviews of Geophysics*, **27**, *pp*.115-139, https://doi.org/10.1029/RG027i001p00115. 1989.

Moalaghi, M., Gharesi, M., Ranjkesh, A. and Hossein-Babae, F.: Tin oxide gas sensor on tin oxide microheater for high-temperature methane sensing. *Materials Letters*, **263**, article number: 127196, https://doi.org/10.1016/j.matlet.2019.127196. 2020.

Murray, F. W.: On the Computation of Saturation Vapor Pressure. *Journal of Applied Meteorology and Climatology*, **6**, *pp*.203-204, https://doi.org/10.1175/1520-0450(1967)006<0203:OTCOSV>2.0.CO;2. 1967.

Navazani, S., Hassanisadi, M., Eskandari, M. M. and Talaei, Z.: Design and evaluation of SnO2-Pt/MWCNTs hybrid system as room temperature-methane sensor. *Synthetic Metals*, **260**, article number: 116267, https://doi.org/10.1016/j.synthmet.2019.116267. 2020.

Nisbet E. G., Dlugokencky, E. J. and Bousquet, P.: Methane on the Rise-Again. *Science*, **343**, *pp*.493-495, https://doi.org/10.1126/science.1247828. 2014.

Nisbet, E. G., Manning, M. R., Dlugokencky, E. J., Fisher, R. E., Lowry, D., Michel, S. E., Lund Myhre, C., Platt, M., Allen, G., Bousquet, P., Brownlow, R., Cain, M., France, J. L., Hermansen, O., Hossaini, R., Jones, A. E., Levin, I., Manning, A. C., Myhre, G., Pyle, J. A., Vaughn, B. H., Warwick, N. J. and White, J. W. C.: Very Strong. Atmospheric Methane Growth in the 4 Years 2014–2017: Implications for the Paris Agreement. *Global Biogeochemical Cycles*, **33**, *pp*.318–342, https://doi.org/10.1029/2018GB006009. 2019.

Picarro, Inc., G2401 Analyzer Datasheet | Picarro, available at: https://www.picarro.com/support/library/documents/g2401_analyzer_datasheet, last access: 2 July 2022. 2021.

Ponzoni, A., Baratto, C., Cattabiani, N., Falasconi, M., Galstyan, V., Nunez-Carmona, E., Rigoni, F., Sberveglieri, V., Zambotti, G. and Zappa, D.: Metal Oxide Gas Sensors, a Survey of Selectivity Issues Addressed at the SENSOR Lab, Brescia (Italy). *Sensors*, **17**, article number: 714, https://doi.org/10.3390/s17040714. 2017.

Reinelt, T., Delre, A., Westerkamp, T., Holmgren, M.A., Liebetrau, J and Scheutz, C.: Comparative use of different emission measurement approaches to determine methane emissions from a biogas plant. *Waste Management*, **68**, *pp*.173–185, https://doi.org/10.1016/j.wasman.2017.05.053. 2017.

Riddick, S. N, Mauzerall D. L., Celia, M., Allen, G., Pitt, J., Kang, M. and Riddick, J. C.: The calibration and deployment of a low-cost methane sensor. *Atmospheric Environment*, **230**, article number: 117450, https://doi.org/10.1016/j.atmosenv.2020.117440. 2020.

Rigby, R., Montzka, S. A., Prinn, R. G., White, J. W. C., Young, D., O'Doherty, S., Lunt, M. F., Ganesan, A. L., Manning, A. J., Simmonds, P. G., Salameh, P. K., Harth, C. M., Mühle, J., Weiss, R. F., Fraser, P. J., Steele, L. P., Krummel, P. B., McCulloch, A. and Park, S.: Role of atmospheric oxidation in recent methane growth. *Proceedings of the National Academy of Sciences of the United States of America*, **114**, *pp*.5373-5377, https://doi.org/10.1073/pnas.1616426114. 2007.

Rivera Martinez, R., Santaren, D., Laurent, O., Cropley, F., Mallet, C., Ramonet, M., Caldow, C., Rivier, L., Broquet, G., Bouchet, C., Juery, C. and Ciais, P.: The Potential of Low-Cost Tin-Oxide Sensors Combined with Machine Learning for

Estimating Atmospheric CH4 Variations around Background Concentration. *Atmosphere*, **12**, article number: 107, https://doi.org/10.3390/atmos12010107. 2021.

Rivera Martinez, R. A., Santaren, D., Laurent, O., Broquet, G., Cropley, F., Mallet, C., Ramonet, M., Shah, A., Rivier, L., Bouchet, C., Juery, C., Duclaux, O. and Ciais, P.: Reconstruction of high-frequency methane atmospheric concentration peaks from measurements using metal oxide low-cost sensors, *Atmospheric Measurement Techniques Discussions*, **in review**, https://doi.org/10.5194/amt-2022-200, 2022.

Sasakawa, M. Shimoyama, K., Machida, T., Tsuda, N., Suto, H., Arshinov, M., Davydov, D., Fofonov, A., Krasnov, O., Saeki, T., Koyama, Y. and Maksyutov, S.: Continuous measurements of methane from a tower network over Siberia, *Tellus B: Chemical and Physical Meteorology*, **62**, *pp*.403-416, https://doi.org/10.1111/j.1600-0889.2010.00494.x. 2010.

Saunois, M., Bousquet, P., Poulter, B., Peregon, A., Ciais, P., Canadell, J. G., Dlugokencky, E. J., Etiope, G., Bastviken, D., Houweling, S., Janssens-Maenhout, G., Tubiello, F. N., Castaldi, S., Jackson, R. B., Alexe, M., Arora, V. K., Beerling, D. J., Bergamaschi, P., Blake, D. R., Brailsford, G., Brovkin, V., Bruhwiler, L., Crevoisier, C., Crill, P., Covey, K., Curry, C., Frankenberg, C., Gedney, N., Höglund-Isaksson, L., Ishizawa, M., Ito, A., Joos, F., Kim, H. S., Kleinen, T., Krummel, P., Lamarque, J. F., Langenfelds, R., Locatelli, R., Machida, T., Maksyutov, S., McDonald, K. C., Marshall, J., Melton, J. R., Morino, I., Naik, V., O'Doherty, S., Parmentier, F. J. W., Patra, P. K., Peng, C., Peng, S., Peters, G. P., Pison, I., Prigent, C., Prinn, R., Ramonet, M., Riley, W. J., Saito, M., Santini, M., Schroeder, R., Simpson, I. J., Spahni, R., Steele, P., Takizawa, A., Thornton, B. F., Tian, H., Tohjima, Y., Viovy, N., Voulgarakis, A., van Weele, M., van der Werf, G. R., Weiss, R., Wiedinmyer, C., Wilton, D. J., Wiltshire, A., Worthy, D., Wunch, D., Xu, X., Yoshida, Y., Zhang, B., Zhang, Z. and Zhu, Q.: The global methane budget 2000–2012. *Earth System Science Data*, **8**, *pp*.697-751, https://doi.org/10.5194/essd-8-697-2016. 2016.

Schuyler, T. J. and Guzman, M. I.: Unmanned Aerial Systems for Monitoring Trace Tropospheric Gases. *Atmosphere*, **8**, article number: 206, https://doi.org/10.3390/Atmos8100206. 2017.

Sieczko, A. K., Duc N. T., Schenk, J., Pajala, G., Rudberg, D., Sawakuchi, H. O. and Bastviken, D.: Diel variability of methane emissions from lakes. *Proceedings of the National Academy of Sciences of the United States of America*, **117**, *pp*.21488-21494, https://doi.org/10.1073/pnas.2006024117. 2020.

Shah, A., Pitt, J. R., Kabbabe, K. and Allen, G.: Suitability of a Non-Dispersive Infrared Methane Sensor Package for Flux Quantification Using an Unmanned Aerial Vehicle. *Sensors*, **19**, article number: 4705, https://doi.org/10.3390/s19214705. 2019.

Suto, H. and Inoue, G.: A New Portable Instrument for In Situ Measurement of Atmospheric Methane Mole Fraction by Applying an Improved Tin Dioxide–Based Gas Sensor. *Journal of Atmospheric and Oceanic Technology*, **27**, *pp*.1175-1184, https://doi.org/10.1175/2010JTECHA1400.1. 2010.

Turner, A. J., Frankenberg, C. and Kort, E. A.: Interpreting contemporary trends in atmospheric methane. *Proceedings of the National Academy of Sciences of the United States of America*, **116**, *pp*.2805-2813, https://doi.org/10.1073/pnas.1814297116. 2019.

van den Bossche, M., Rose, N. T. and De Wekker, S. F. J.: Potential of a low-cost gas sensor for atmospheric methane monitoring. *Sensors and Actuators B: Chemical*, **238**, *pp*.501-509, https://doi.org/10.1016/j.snb.2016.07.092. 2017.

Wang, C., Yin, L., Zhang, L., Xiang, D. and Gao, R.: Metal Oxide Gas Sensors: Sensitivity and Influencing Factors. *Sensors*, **10**, *pp*.2088-2106, https://doi.org/10.3390/s100302088. 2010.

Xue, D., Wang, P., Zhang, Z. and Wang, Y.: Enhanced methane sensing property of flower-like SnO2 doped by Pt nanoparticles: A combined experimental and first-principle study. *Sensors and Actuators B: Chemical*, **296**, article number: 126710, https://doi.org/10.1016/j.snb.2019.126710. 2019.

Yang, B., Zhang, Z., Tian, C., Yuan, W., Hua, Z., Fan, S., Wu, X. and Tian, X.: Selective detection of methane by HZSM-5 zeolite/Pd-SnO2 gas sensors. *Sensors and Actuators B: Chemical*, **321**, article number: 128567, https://doi.org/10.1016/j.snb.2020.128567. 2020.

Yver Kwok, C., Laurent, O., Guemri, A., Philippon, C. Wastine, B., Rella C. W., Vuillemin, C., Truong, F., Delmotte, M., Kazan, V., Darding, M., Lebègue, B., Kaiser, C., Xueref-Rémy, I. and Ramonet, M.: Comprehensive laboratory and field testing of cavity ring-down spectroscopy analyzers measuring H2O, CO2, CH4 and CO. *Atmospheric Measurement Techniques*, **8**, *pp*.3867–3892, https://doi.org/10.5194/amt-8-3867-2015. 2015.

Zhang, S., Li, Y., Sun, G., Zhang, B., Wang, Y., Cao, J. and Zhang, Z.: Enhanced methane sensing properties of porous NiO nanaosheets by decorating with SnO2. *Sensors and Actuators B: Chemical*, **288**, *pp*.373-382, https://doi.org/10.1016/j.snb.2019.03.024. 2019.

Appendix A: Influence of supply voltage

The influence of power supply voltage on both resistance and CH_4 sensitivity was characterised by testing a Figaro sensor (LSCE009) in System B in our air-conditioned laboratory. V_s was adjusted from the high-precision power supply unit (T3PS23203P, Teledyne LeCroy Inc.) in four tests: test 1 was at a V_s of 5.00 V, test 2 was at a V_s of 5.10 V, test 3 was at a V_s of 5.00 V and test 4 was at a V_s of 5.10 V. During each test, gas from the zero-air generator was first sampled for at least ~~an~~ 1 hour. Then an ambient target gas cylinder filled with outside air (1.6 ppm [CO], 2.2 ppm [CH_4] and 434 ppm [CO_2]) was sampled in four 15-minute intervals. Each ambient target gas interval was followed by 15 minutes of sampling zero-air generator gas. A fixed 8° C dew point was used throughout testing. Gas at this dew point was sampled from at least 24 hours in advance of test 1.

Figaro resistance results for the four tests are presented in Fig. A1. For each test, a 2-minute average was taken at the end each 15-minute ambient target gas sampling interval, except the first (see Fig. A1). A 0 ppm reference resistance baseline was then derived by fitting a second order polynomial to the final 2 minutes of the each 15-minute zero-air sampling period. [H_2O] was on average (0.975±0.001)% during these 2-minute zero-air periods for all four tests, according to the Picarro G2401, and System B temperature was on average (27.9±0.1)° C, according to the SHT85 sensor inside the sampling cell.

The ratio between each 2-minute average ambient target gas resistance and its corresponding modelled zero-air reference resistance was acquired. Each of the four tests yielded three resistance ratios (see Table A1). In addition, for each test, all zero-air and ambient target gas 2-minute average resistance measurements were combined and averaged in Table A1. These results show that Figaro resistance is consistently lower at higher V_s, for example, zero-air resistance at 5.00 V is 35 kΩ whereas at 5.10 V it drops to 31 kΩ. This test also shows that Figaro sensitivity is consistently lower at a higher voltage, owing to a lower resistance ratio. At 5.00 V, the resistance decreases by 22% when transitioning from zero-air to ambient target gas, whereas at 5.10 V, there is a smaller 19% resistance decrease.

test	supply voltage	average baseline (zero-air) resistance (kΩ)	average target gas resistance (kΩ)	resistance ratios (Ω Ω^{-1})
test 1	5.00 V	35.3±0.3	27.7±0.4	0.7837±0.0003; 0.7832±0.0003; 0.7824±0.0003
test 2	5.10 V	31.4±0.5	25.5±0.6	0.8125±0.0003; 0.8105±0.0003; 0.8096±0.0003
test 3	5.00 V	35.2±0.2	27.4±0.1	0.7796±0.0003; 0.7788±0.0003; 0.7784±0.0003
test 4	5.10 V	31.3±0.6	25.3±0.4	0.8083±0.0003; 0.8080±0.0003; 0.8080±0.0003

Table A1: Average zero-air and ambient target gas resistances during 2-minute averaging periods for four tests at two different supply voltage settings. The resistance ratio for each 2-minute ambient target gas average is given, compared to a zero-air baseline reference resistance.

This resistance and sensitivity decrease at 5.10 V emphasises the importance of maintaining a fixed and reliable 5 V V_s, to maintain consistency between sensor testing and field application. This effect is possibly due to a higher heater temperature at higher V_s, resulting in lower resistance, as proposed in Eq. (43). Similarly, van den Bossche et al. (2017) found that a 10 mV change in heater voltage resulted in a roughly 1 ppm error in their [CH_4] estimate, at constant ambient temperature. However, this does not explain reduced Figaro sensitivity. This sensitivity effect may be caused by a change in the density of electrons within the SMO conduction band under an elevated potential difference.

Appendix B: Water response delay

Figaro sensors exhibit a delayed response to [H_2O] changes. Fig. B1 shows an example of [H_2O] decrease, while a Figaro sensor (LSCE010) continuously sampled gas from the zero-air generator in System B. The dew-point setting was abruptly reduced from 20° C to 8° C, resulting in a 1% [H_2O] drop. Sensor resistance appeared to overshoot in response to this [H_2O] change and slowly decayed back to a stable level, over many hours. [H_2O] was (1.116±0.002)% between 07:30 and 14:30 (UTC), according to the Picarro G2401, while System B temperature was (30.2±0.2)° C, according to the SHT85 inside the cell, with a small 0.07° C hour^{-1} increase (when applying a linear fit). This negligible temperature change suggests that the observed resistance decay is predominantly an artefact of the water transition. The cause of this effect is not fully understood. It may be related to water desorption dynamics on the surfaces between grain boundaries. Water desorption may not be homogenous throughout the sensor, causing a prolonged delay in reaching a resistance equilibrium. Whereas Rivera Martinez et al. (2021) allowed 35 minutes and van den Bossche et al. (2017) allowed 70 minutes for [H_2O] stabilisation, our test shows that many hours of sampling at fixed [H_2O] are needed for sufficient water stabilisation. One full day of constant Figaro exposure~~sampling~~ is recommended.

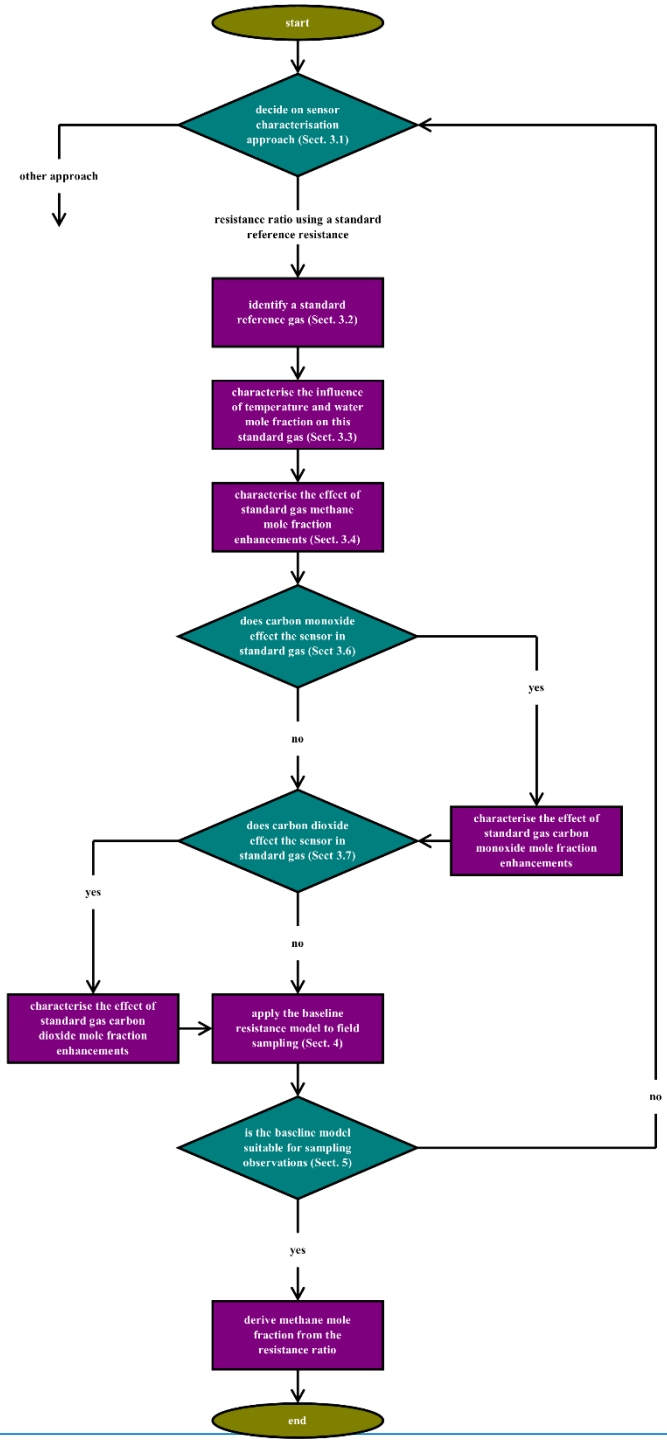
start
decide on sensor characterisation approach (Sect. 3.1)
other approach
resistance ratio using a standard reference resistance
identify a standard reference gas (Sect. 3.2)
characterise the influence of temperature and water mole fraction on this standard gas (Sect. 3.3)
characterise the effect of standard gas methane mole fraction enhancements (Sect. 3.4)
does carbon monoxide effect the sensor in standard gas (Sect 3.6)
yes
no
characterise the effect of standard gas carbon monoxide mole fraction enhancements
does carbon dioxide effect the sensor in standard gas (Sect 3.7)
yes
no
characterise the effect of standard gas carbon dioxide mole fraction enhancements
apply the baseline resistance model to field sampling (Sect. 4)
is the baseline model suitable for sampling observations (Sect. 5)
no
yes
derive methane mole fraction from the resistance ratio
end

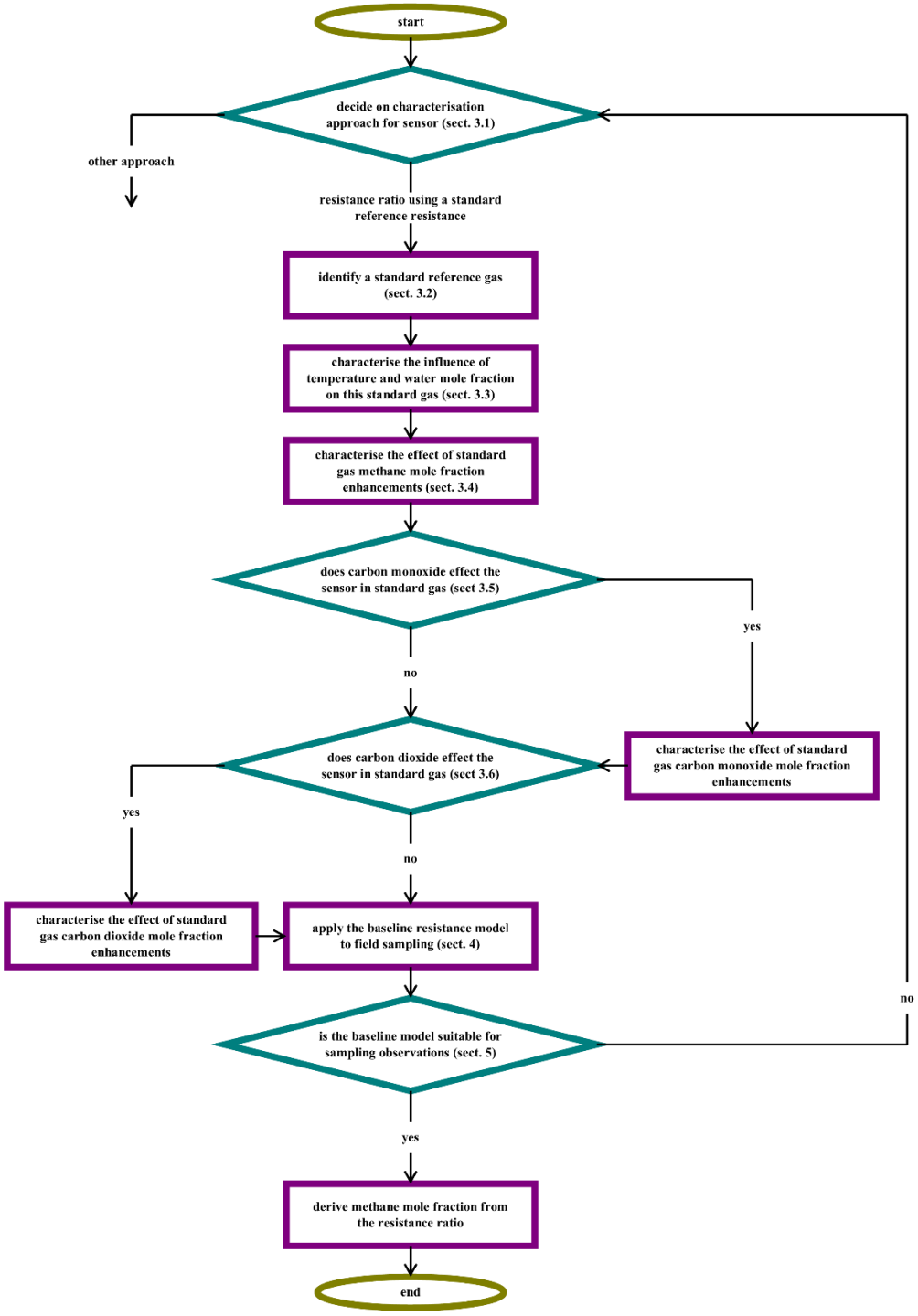

Figure 1: A flow chart illustrating the various steps that we followed in order to derive methane mole fraction from the Figaro TGS 2611-E00.

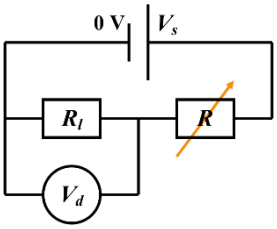

Figure 2: Circuitry used to measure the resistance of the Figaro sensing element. See text for labels.

Figure 3: System A autonomous field logger (LSCE007) installed at the SUEZ Amailloux landfill site in March 2021 (see text for description). This system includes a two-dimensional anemometer.

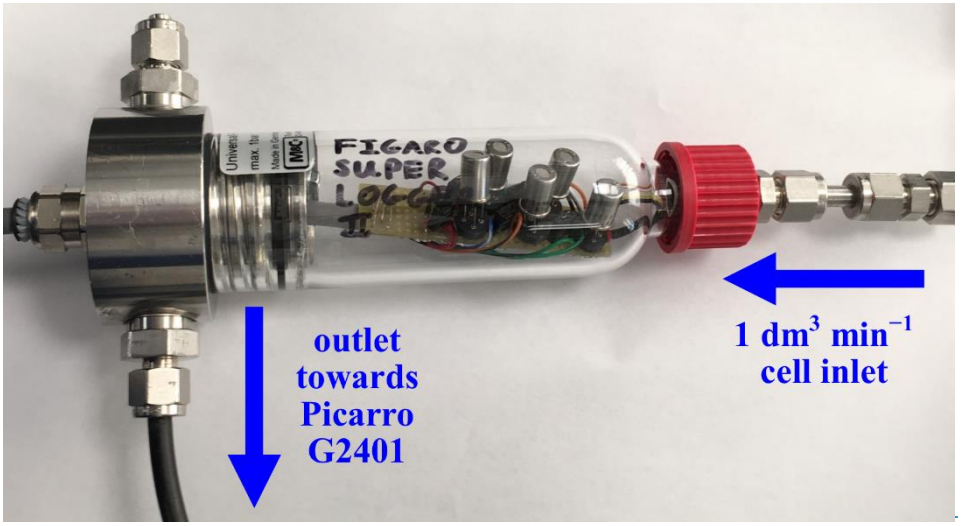

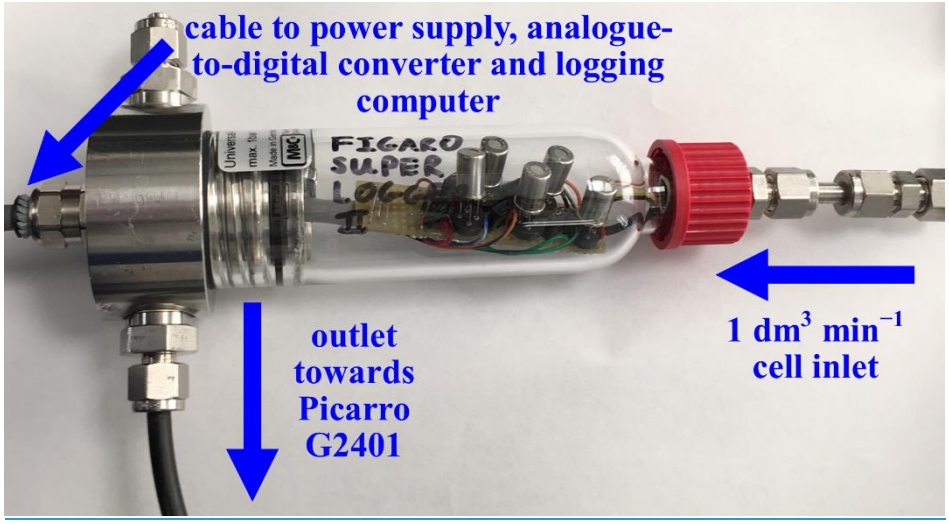

Figure 4: System B laboratory testing logging cell~~r~~ (logging computer and power supply not shown). Five Figaro sensors are plugged into the cell circuit board in this photograph.

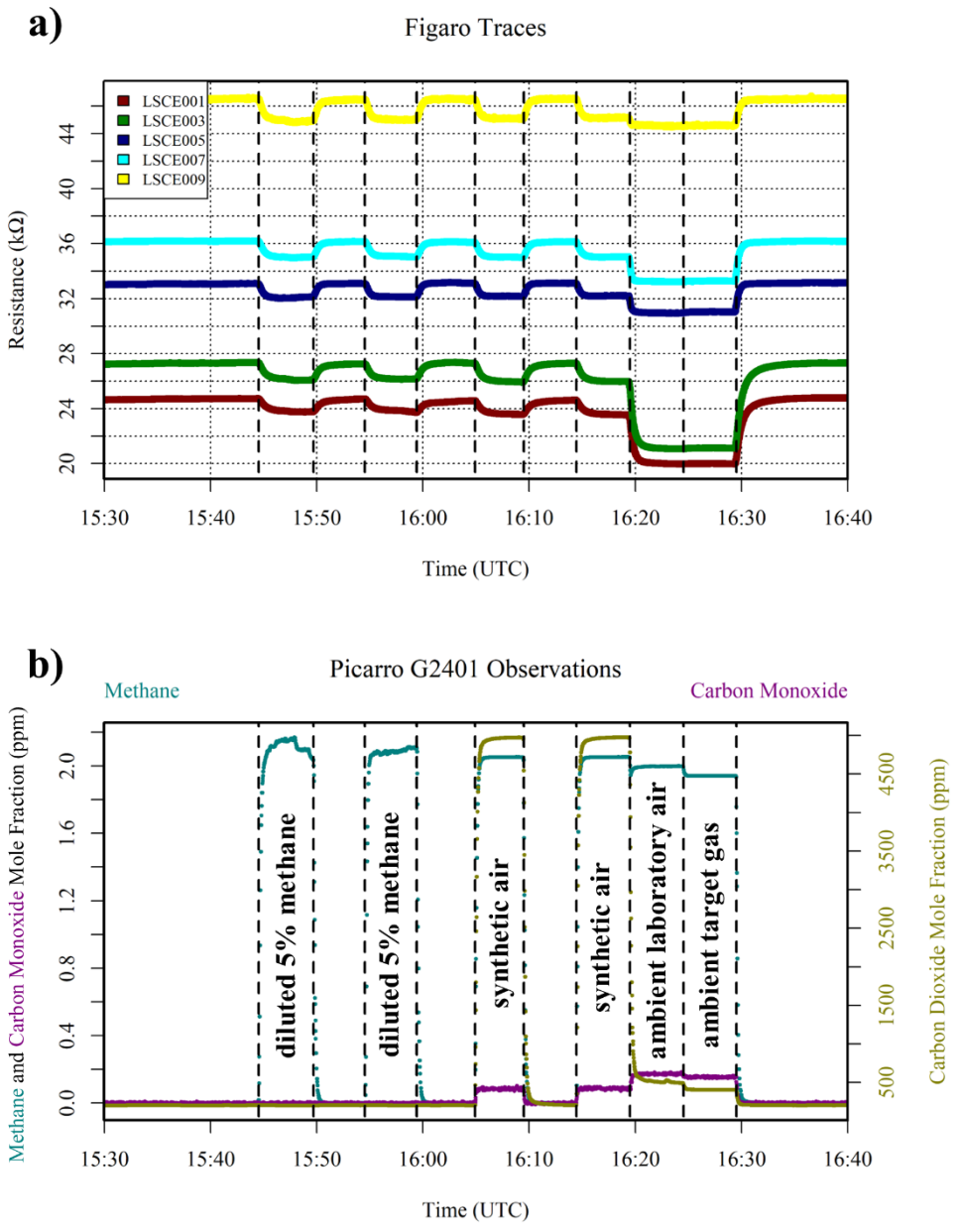
a)
Figaro Traces
LSCE001
LSCE003
LSCE005
LSCE007
LSCE009
Resistance (kΩ)
20
24
28
32
36
40
44
15:30
15:40
15:50
16:00
16:10
16:20
16:30
16:40
Time (UTC)
b)
Picarro G2401 Observations
Methane
Carbon Monoxide
Methane and Carbon Monoxide Mole Fraction (ppm)
0.0
0.4
0.8
1.2
1.6
2.0
Carbon Dioxide Mole Fraction (ppm)
500
1500
2500
3500
4500
diluted 5% methane
diluted 5% methane
synthetic air
synthetic air
ambient laboratory air
ambient target gas
15:30
15:40
15:50
16:00
16:10
16:20
16:30
16:40
Time (UTC)

1105

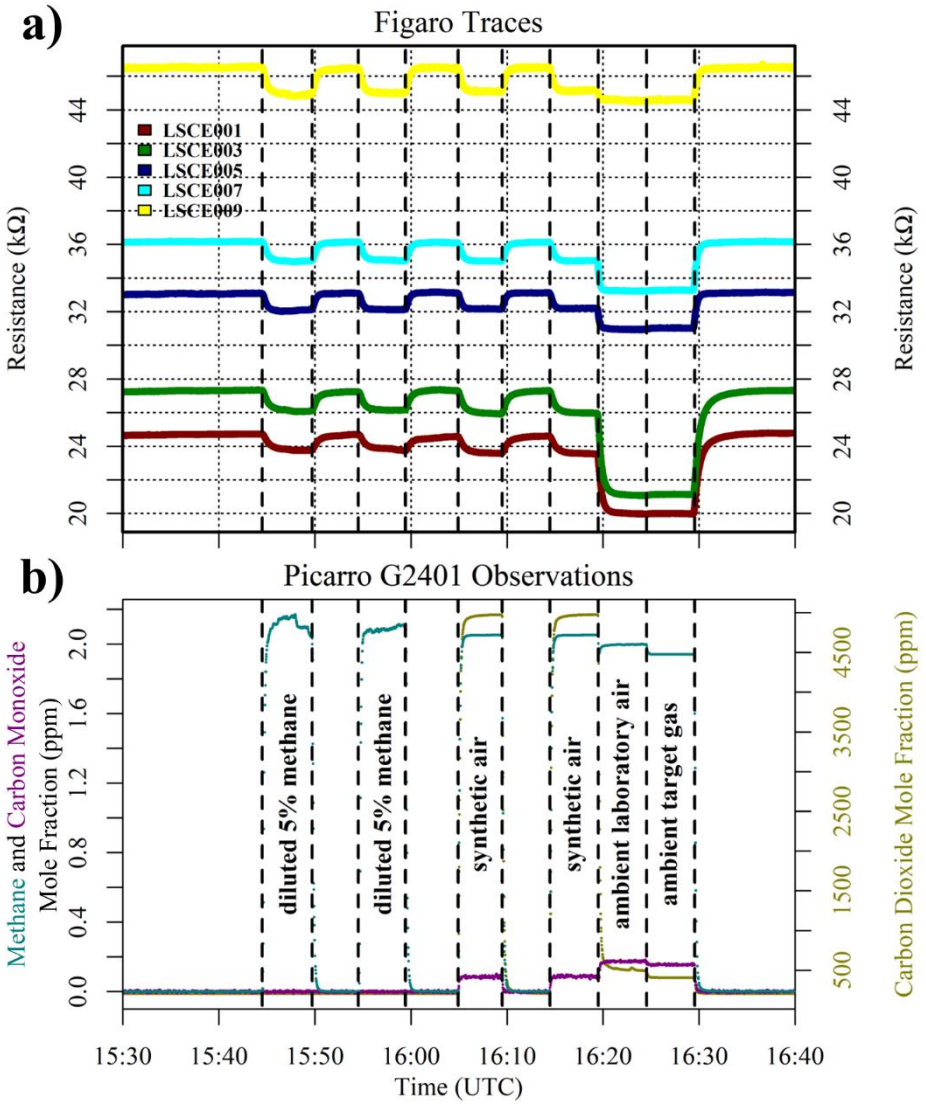

Figure 5: (a) Measured resistance for five Figaro sensors in System B (coloured dots; see legend) under exposure to various sources of 2 ppm methane mole fraction, compared to gas from a zero-air generator. (b) Corresponding Picarro G2401 mole fraction observations, with annotations indicating the sampled 2 ppm methane source. Areas not annotated correspond to gas from the zero-air generator. Methane (dark cyan) and carbon monoxide (dark magenta) mole fraction measurements are plotted on the left-hand axis. Carbon dioxide (dark yellow) mole fraction measurements are plotted on the right-hand axis.

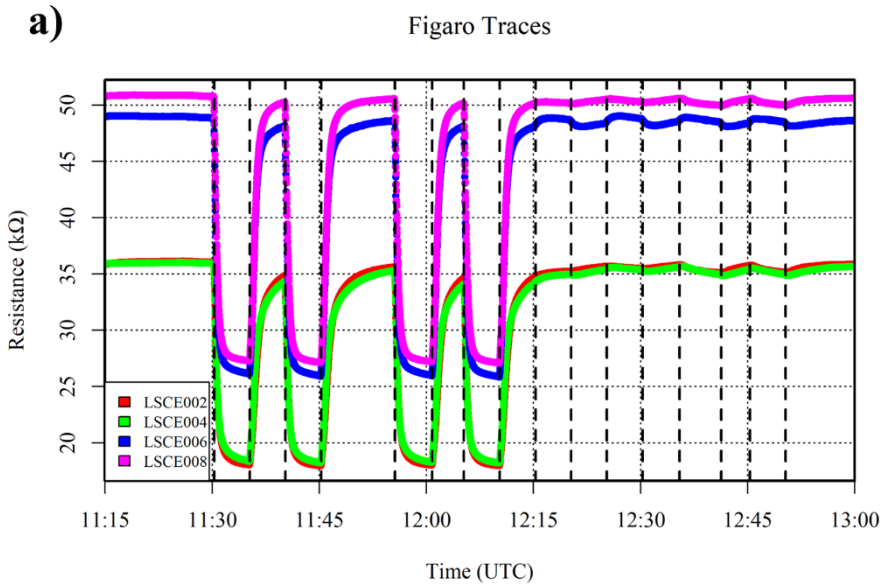
a)
Figaro Traces
Resistance (kΩ)
20
25
30
35
40
45
50
LSCE002
LSCE004
LSCE006
LSCE008
11:15
11:30
11:45
12:00
12:15
12:30
12:45
13:00
Time (UTC)

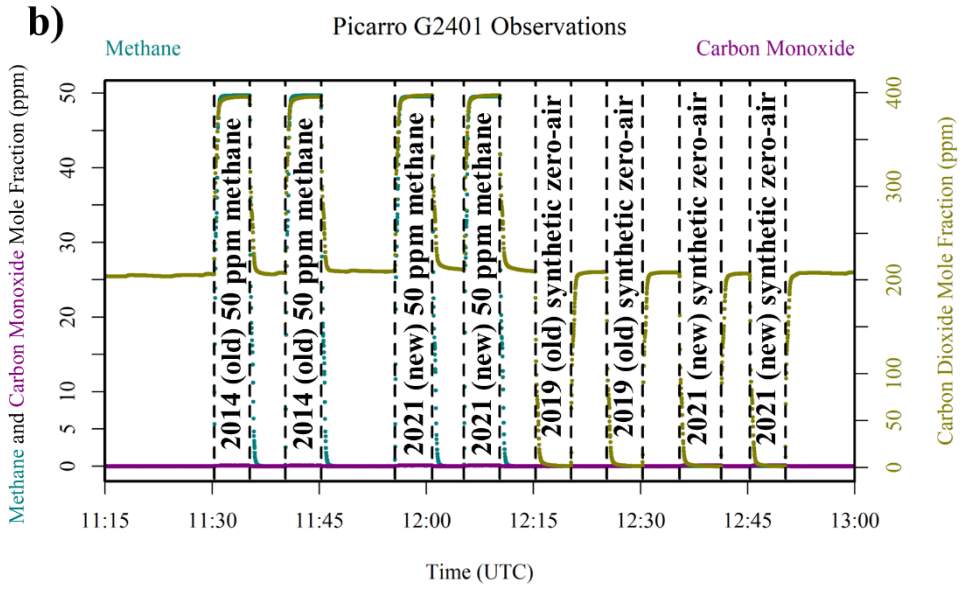
b)
Picarro G2401 Observations
Methane
Carbon Monoxide
Methane and Carbon Monoxide Mole Fraction (ppm)
Carbon Dioxide Mole Fraction (ppm)
0
5
10
20
30
40
50
0
50
100
200
300
400
2014 (old) 50 ppm methane
2014 (old) 50 ppm methane
2021 (new) 50 ppm methane
2021 (new) 50 ppm methane
2019 (old) synthetic zero-air
2019 (old) synthetic zero-air
2021 (new) synthetic zero-air
2021 (new) synthetic zero-air
11:15
11:30
11:45
12:00
12:15
12:30
12:45
13:00
Time (UTC)

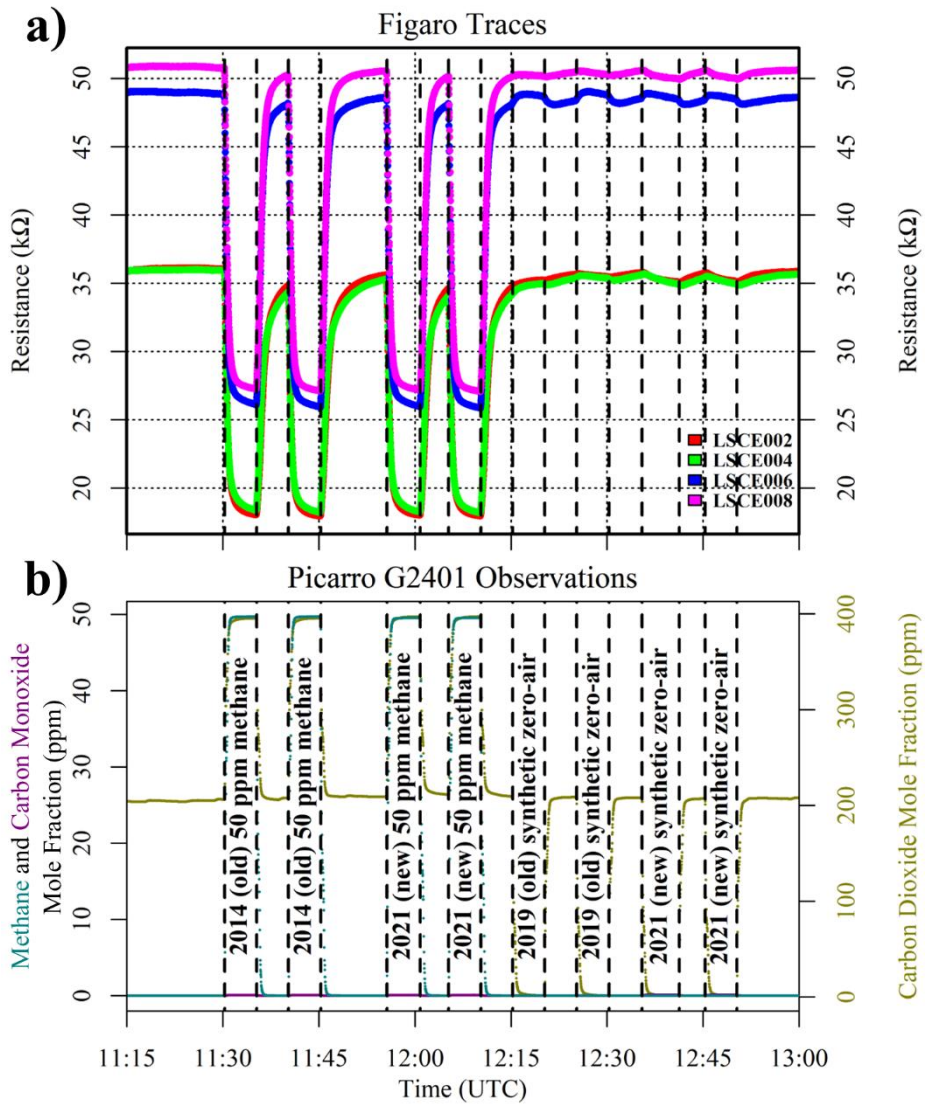

Figure 6: (a) Measured resistance for four Figaro sensors in System B (coloured dots; see legend), under exposure to two sources of 50 ppm methane mole fraction and two sources of synthetic zero-air, compared to gas from a zero-air generator. (b) Corresponding Picarro G2401 mole fraction observations, with annotations indicating the synthetic cylinder type. Areas not annotated correspond to gas from the zero-air generator. Methane (dark cyan) and carbon monoxide (dark magenta) mole fraction measurements are plotted on the left-hand axis. Carbon dioxide (dark yellow) mole fraction measurements are plotted on the right-hand axis.

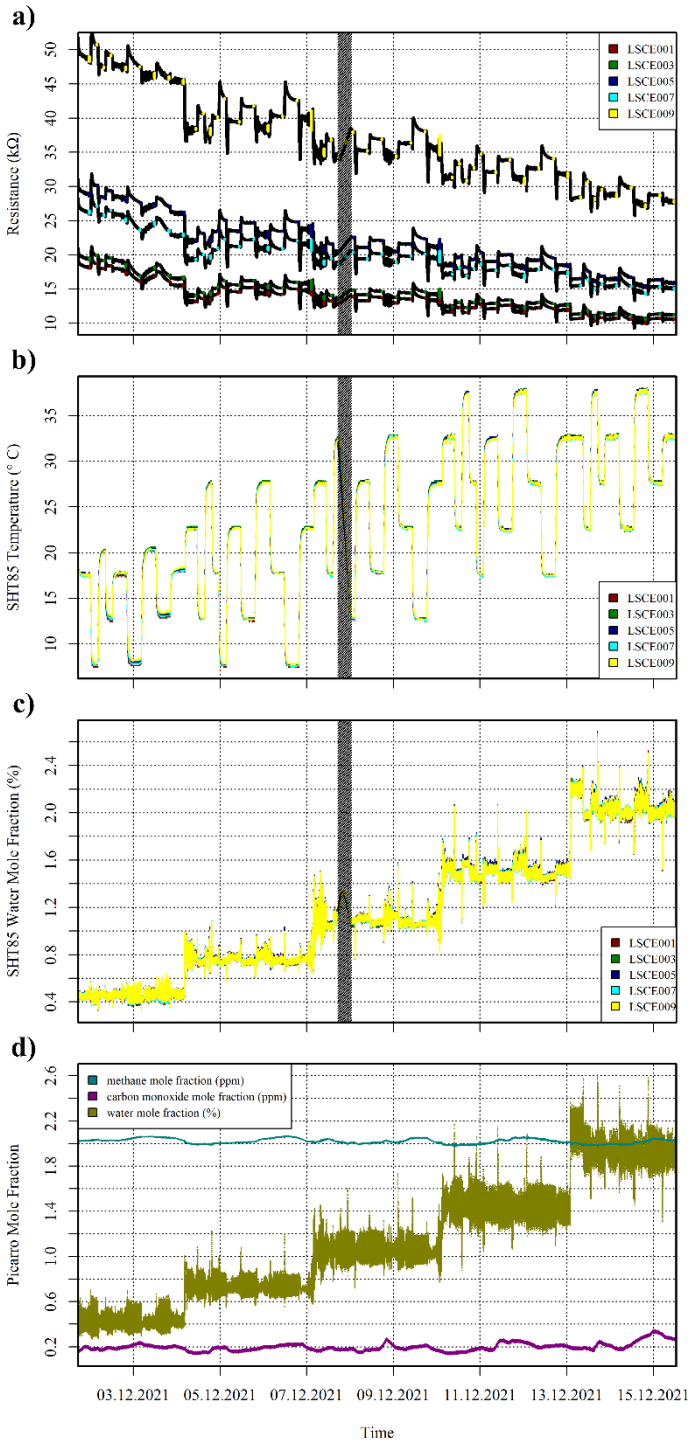
a)
Resistance (kΩ)
10
15
20
25
30
35
40
45
50
LSCE001
LSCE003
LSCE005
LSCE007
LSCE009
b)
SHT85 Temperature (° C)
10
15
20
25
30
35
LSCE001
LSCE003
LSCE005
LSCE007
LSCE009
c)
SHT85 Water Mole Fraction (%)
0.4
0.8
1.2
1.6
2.0
2.4
LSCE001
LSCE003
LSCE005
LSCE007
LSCE009
d)
Picarro Mole Fraction
0.2
0.6
1.0
1.4
1.8
2.2
2.6
methane mole fraction (ppm)
carbon monoxide mole fraction (ppm)
water mole fraction (%)
03.12.2021
05.12.2021
07.12.2021
09.12.2021
11.12.2021
13.12.2021
15.12.2021
Time

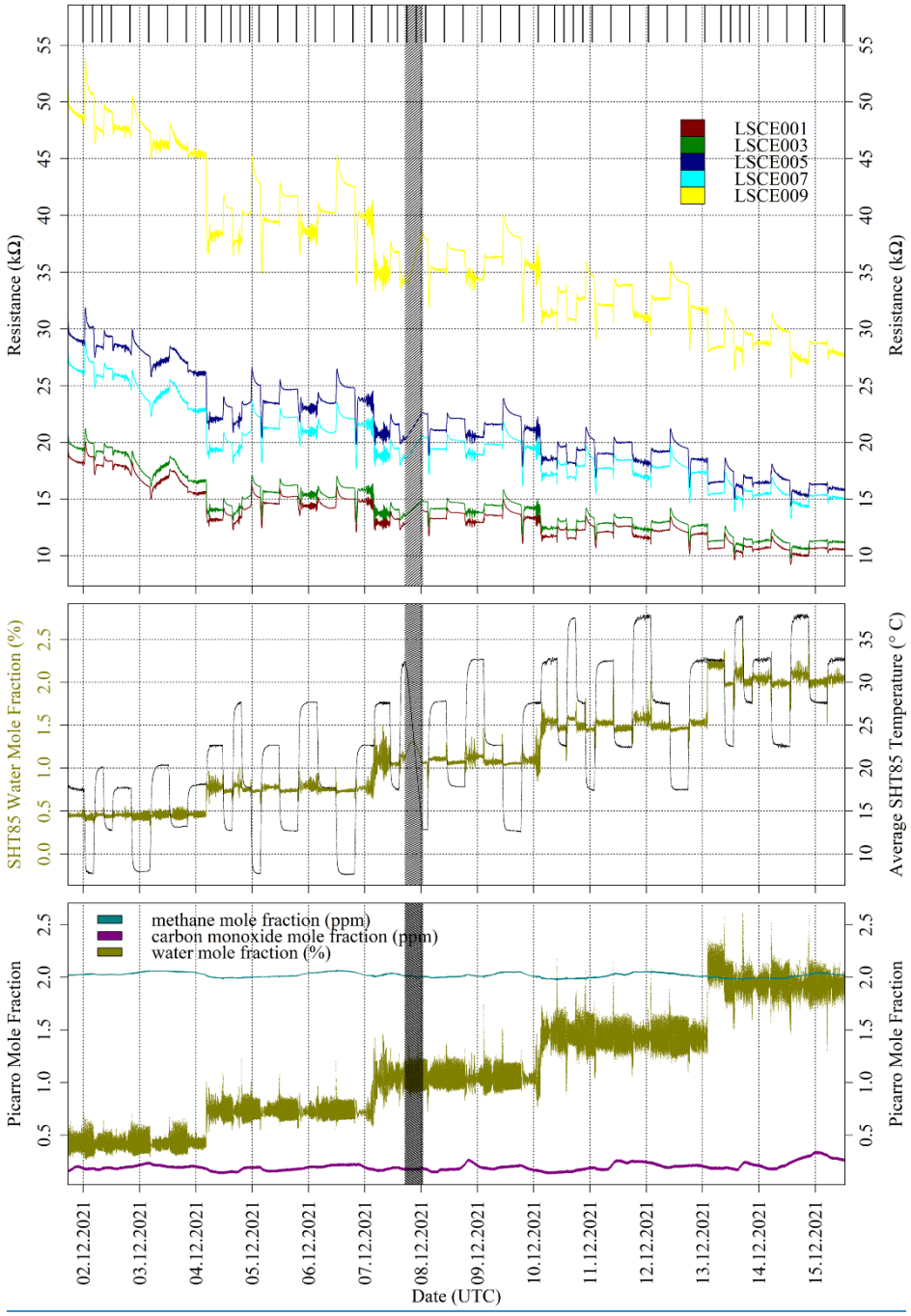

Figure 7: (top) Resistance for five Figaro sensors, sampling inside the environmental chamber (coloured ~~black~~ dots; see legend). The black bars at the top of the plot indicate periods used ~~Coloured dots indicate data used~~ to derive 30-minute averages for each sampling period ~~(see legend for sensor colours)~~. The shaded area indicates a data transmission gap. (~~b~~middle) Derived SHT85 water vapour mole fraction (dark yellow dots) averaged from all five system A boxes plotted against the left-hand axis (see text for

derivation details) and m~~M~~easured SHT85 temperature averaged from all five ~~each~~ System A boxes (black dots) plotted on the right-hand axis. ~~(c) Derived SHT85 water mole fraction (see text for derivation details) from each System A box.~~ (~~d~~bottom) Picarro G2401 measurements from inside the chamber. Methane (dark cyan) and carbon monoxide (dark magenta) mole fraction are plotted in parts-per-million; water (dark yellow) mole fraction is plotted in percent.

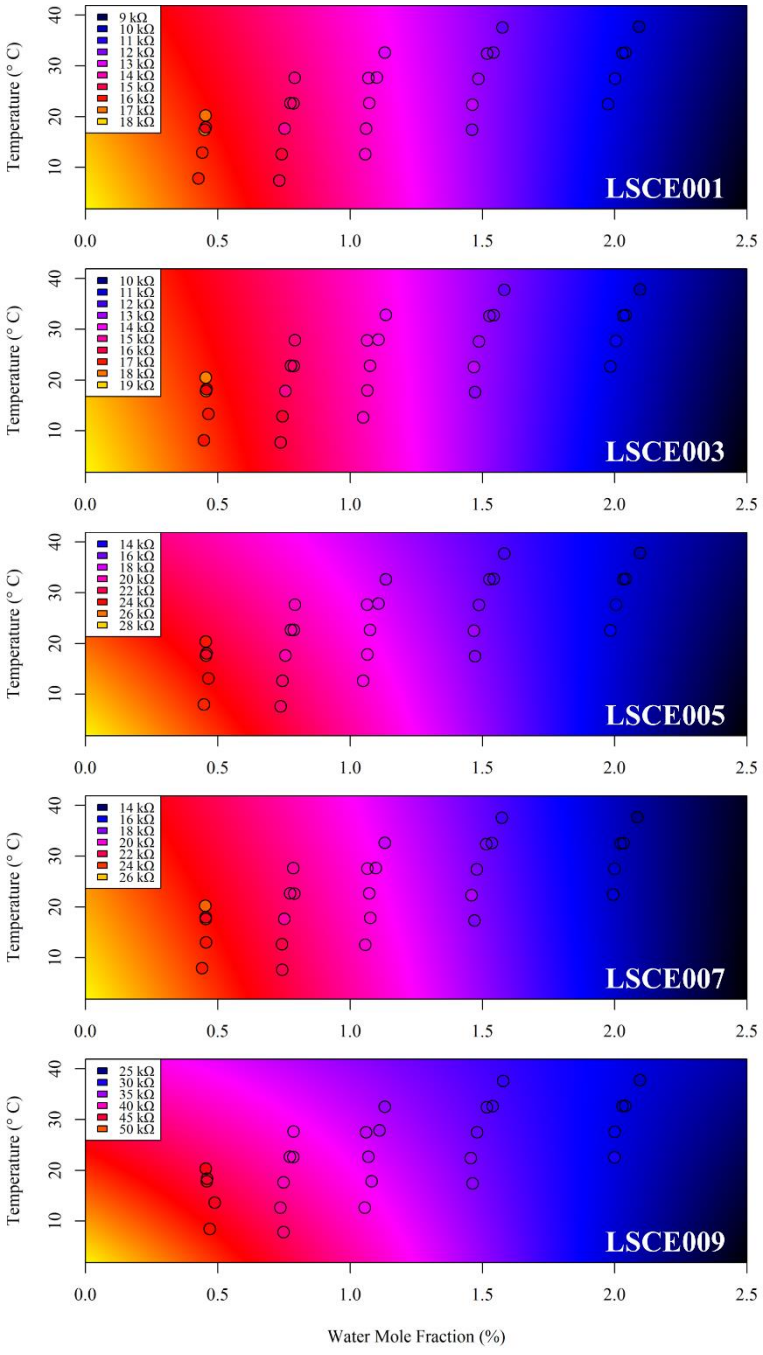
9 kΩ
10 kΩ
11 kΩ
12 kΩ
13 kΩ
14 kΩ
15 kΩ
16 kΩ
17 kΩ
18 kΩ
LSCE001
10 kΩ
11 kΩ
12 kΩ
13 kΩ
14 kΩ
15 kΩ
16 kΩ
17 kΩ
18 kΩ
19 kΩ
LSCE003
14 kΩ
16 kΩ
18 kΩ
20 kΩ
22 kΩ
24 kΩ
26 kΩ
28 kΩ
LSCE005
14 kΩ
16 kΩ
18 kΩ
20 kΩ
22 kΩ
24 kΩ
26 kΩ
LSCE007
25 kΩ
30 kΩ
35 kΩ
40 kΩ
45 kΩ
50 kΩ
LSCE009
Temperature (° C)
10
20
30
40
0.0
0.5
1.0
1.5
2.0
2.5
Water Mole Fraction (%)

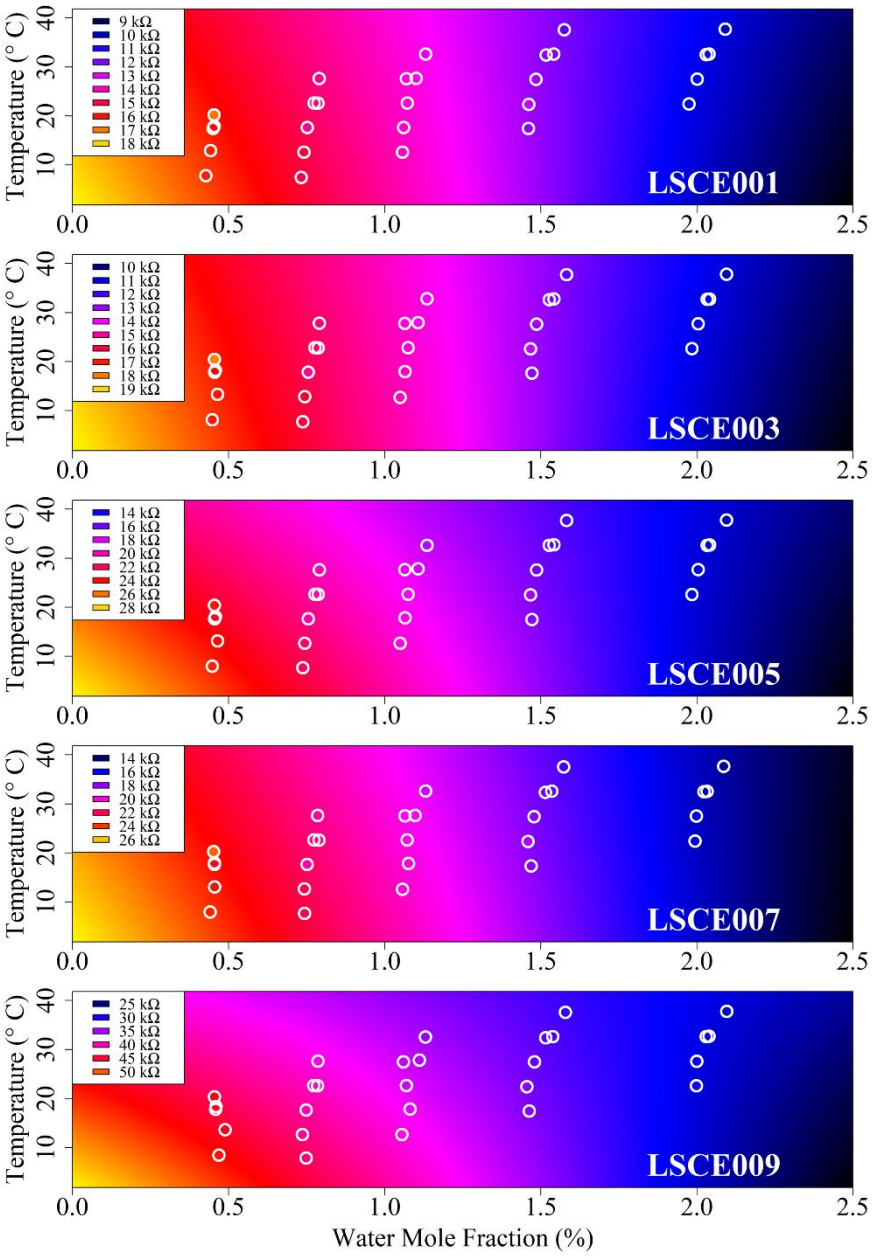

Figure 8: Modelled reference resistance at 2 ppm methane mole fraction (standard gas) for LSCE001, LSCE003, LSCE005, LSCE007 and LSCE009 (coloured background). Points inside ~~black~~white circles represent 30-minute measured resistance averages. Each plot has a unique colour scale (see legend).

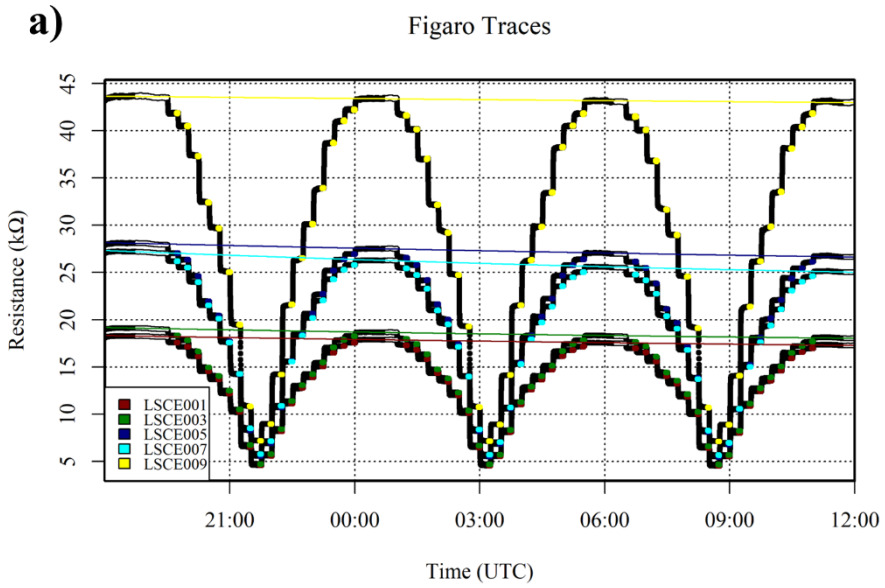
a)
Figaro Traces
Resistance (kΩ)
5
10
15
20
25
30
35
40
45
LSCE001
LSCE003
LSCE005
LSCE007
LSCE009
21:00
00:00
03:00
06:00
09:00
12:00
Time (UTC)

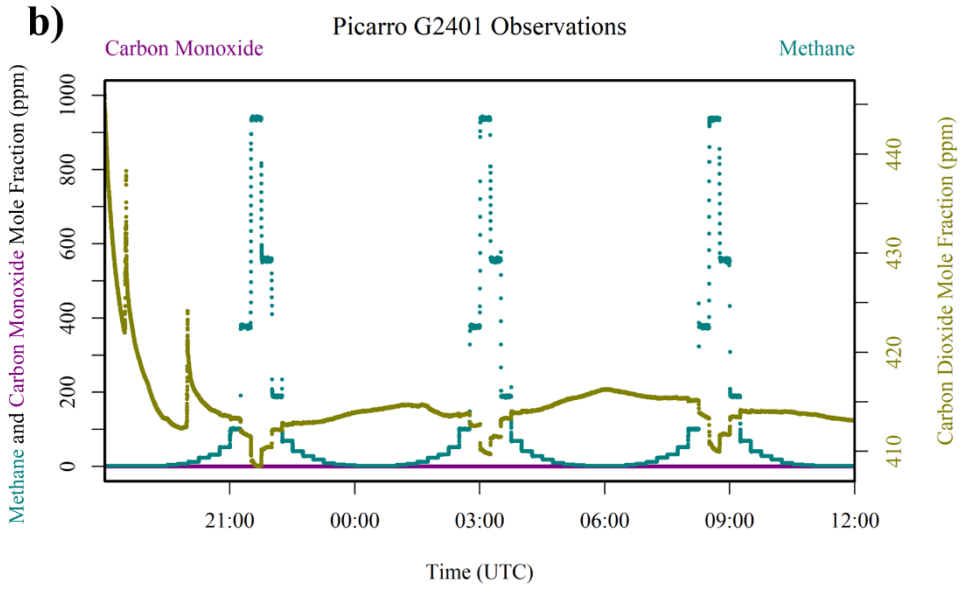
b)
Picarro G2401 Observations
Carbon Monoxide
Methane
Methane and Carbon Monoxide Mole Fraction (ppm)
0
200
400
600
800
1000
Carbon Dioxide Mole Fraction (ppm)
410
420
430
440
21:00
00:00
03:00
06:00
09:00
12:00
Time (UTC)

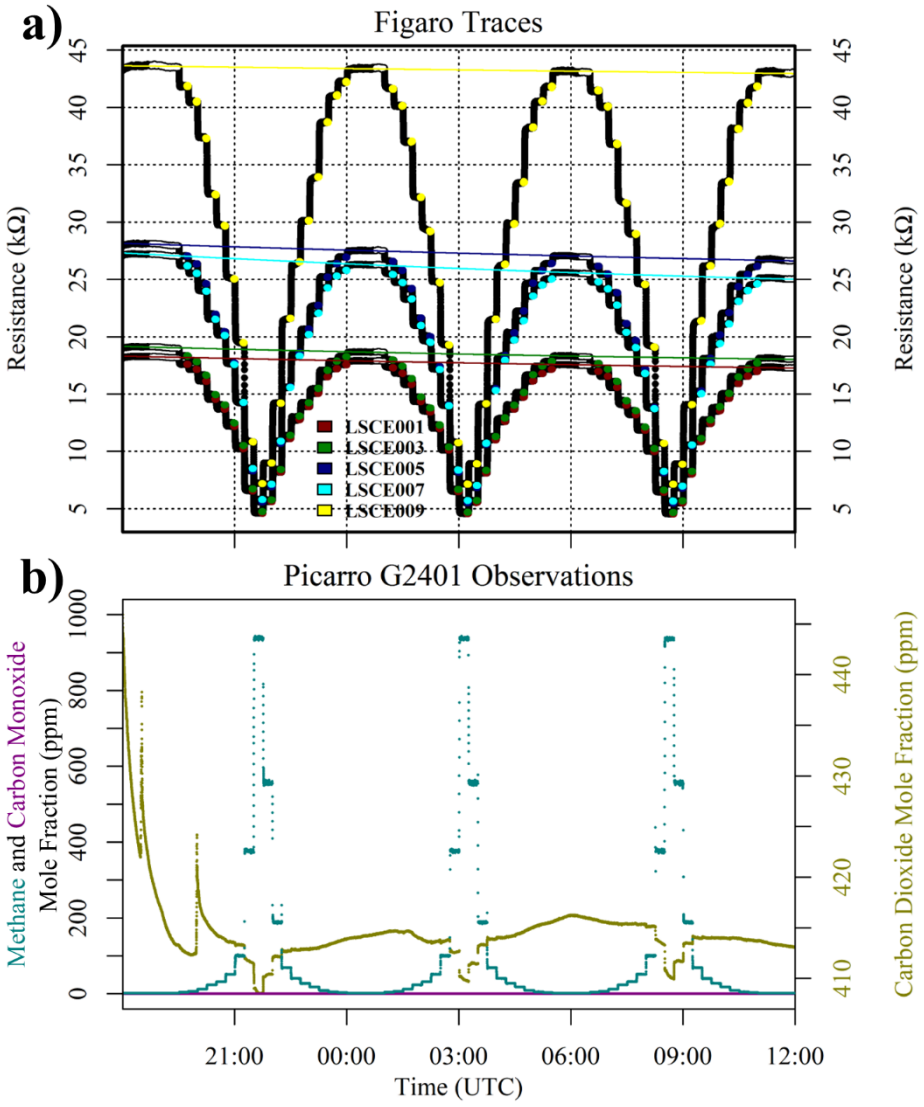

Figure 9: (a) Measured resistance for five Figaro sensors (black dots), under exposure to various methane mole fraction intervals up to 1 000 ppm. Highlighted ~~C~~coloured dots represent 2-minute periods used to derive average resistance values for each methane step (see legend for corresponding sensor colours). White-highlighted dots indicate periods used to derive standard gas reference resistances for each sensor and coloured lines show respective polynomial reference resistance fits. (b) Corresponding mole fraction observations from the Picarro G2401. Methane (dark cyan) and carbon monoxide (dark magenta) mole fraction measurements are plotted on the left-hand axis. Carbon dioxide (dark yellow) mole fraction measurements are plotted on the right-hand axis. Carbon dioxide measurements become unreliable at high methane mole fraction due to spectral overlap.

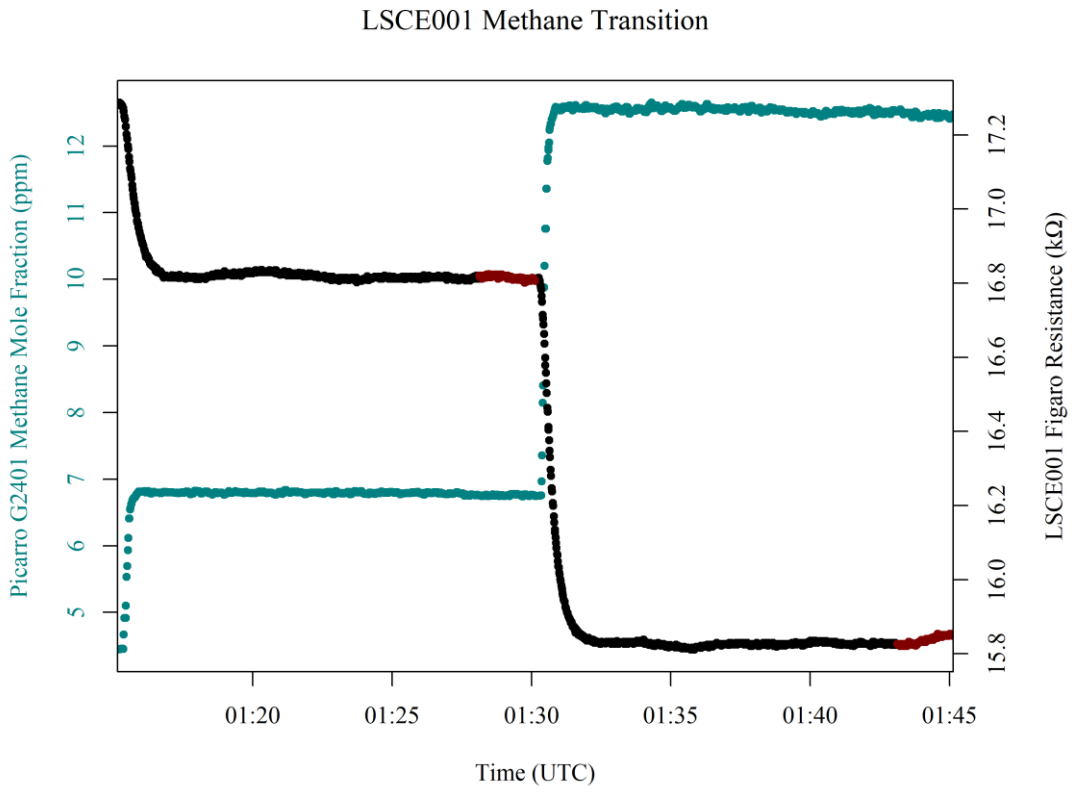
LSCE001 Methane Transition
Picarro G2401 Methane Mole Fraction (ppm)
5
6
7
8
9
10
11
12
LSCE001 Figaro Resistance (kΩ)
15.8
16.0
16.2
16.4
16.6
16.8
17.0
17.2
01:20
01:25
01:30
01:35
01:40
01:45
Time (UTC)

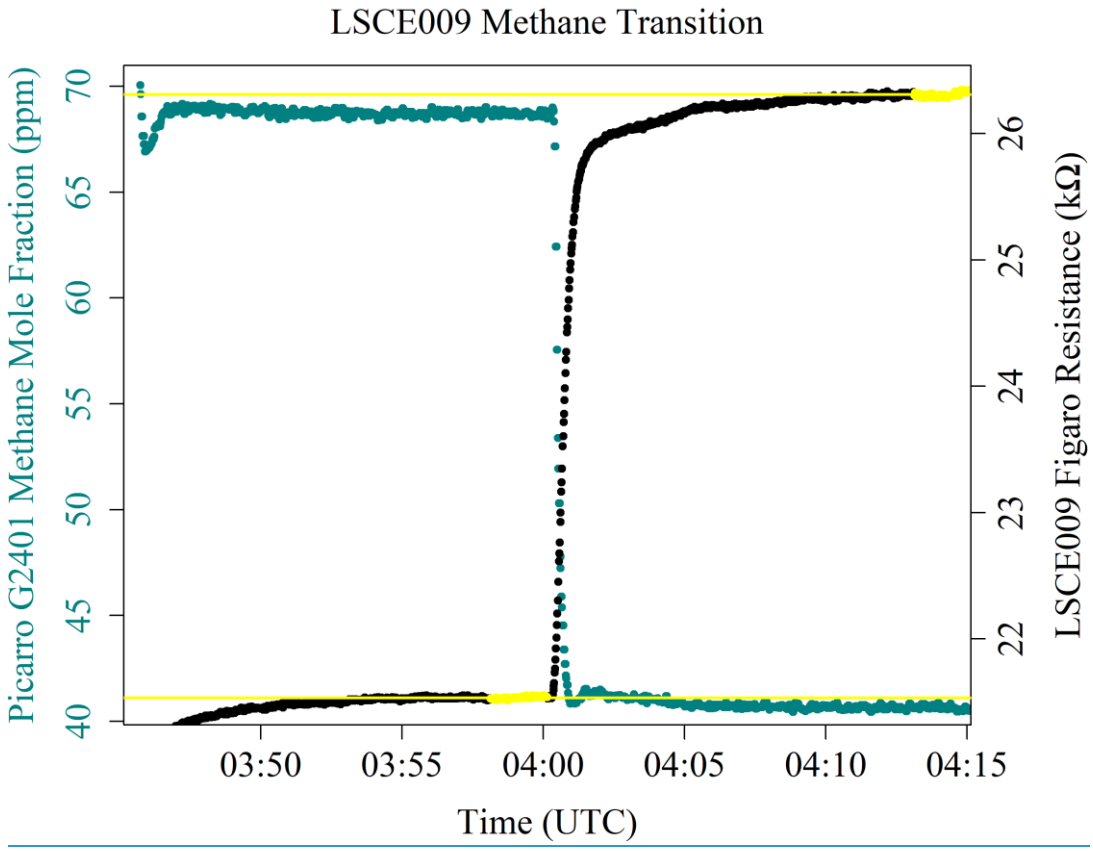

Figure 10: A methane mole fraction transition from ~~7~~69 ppm to ~~12~~41 ppm as recorded by the Picarro G2401 (dark cyan dots on left-hand axis) with corresponding LSCE00~~91~~ Figaro resistance measurements made in System B (black dots on right-hand axis). 2-minutes of stable Figaro resistance sampling from the end of each sampling period (highlighted yellow dots) were used to derive resistance averages (horizontal yellow lines)~~from the end of each sampling period are coloured as dark red dots~~.

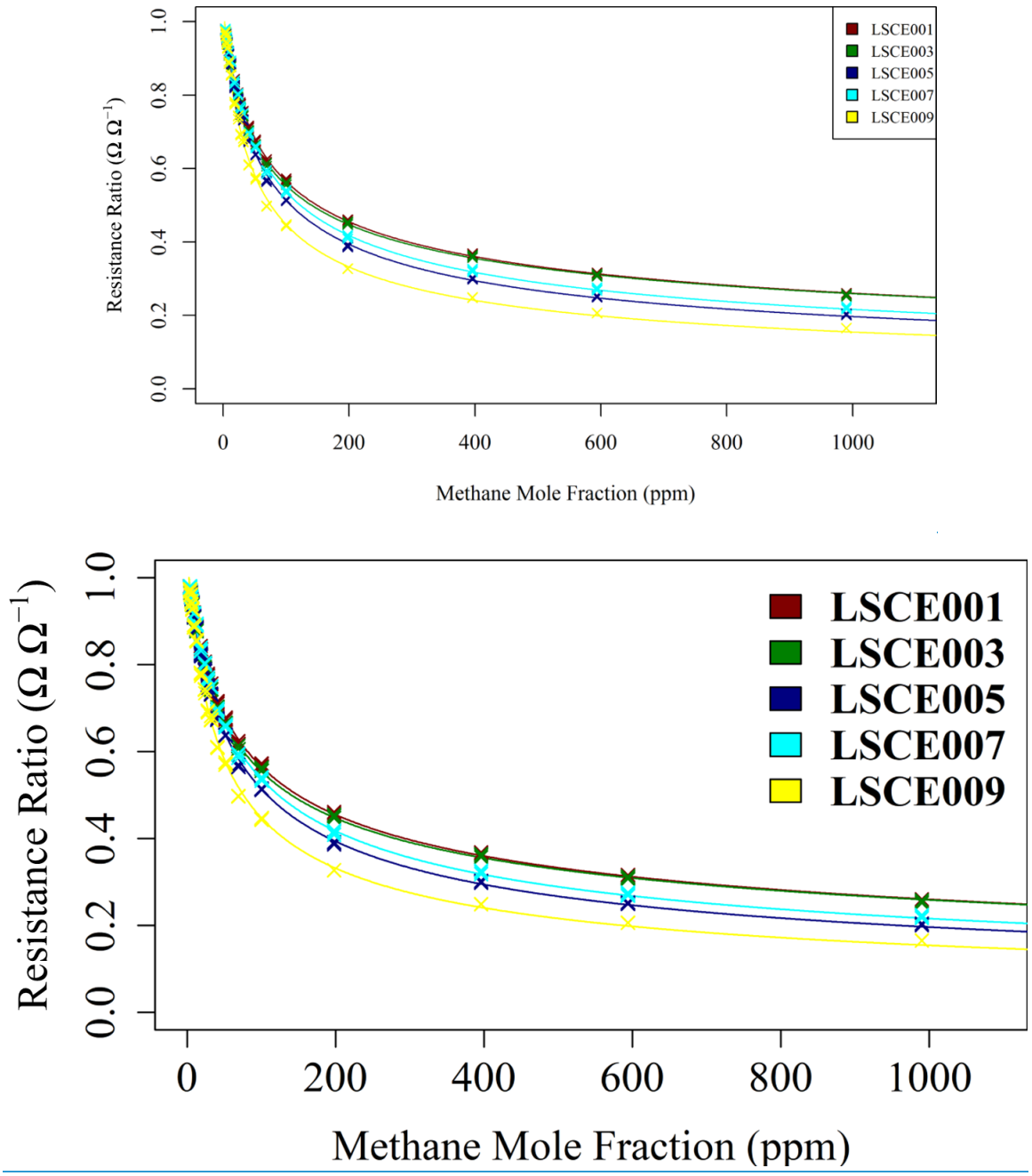

Figure 11: The ratio between each 2-minute average Figaro resistance (from 15-minute sampling intervals) and its corresponding reference resistance estimate (crosses), plotted against methane mole fraction for five Figaro sensors (see legend for respective colours). A model fit for each sensor (coloured lines) is plotted, according to Eq. (65).

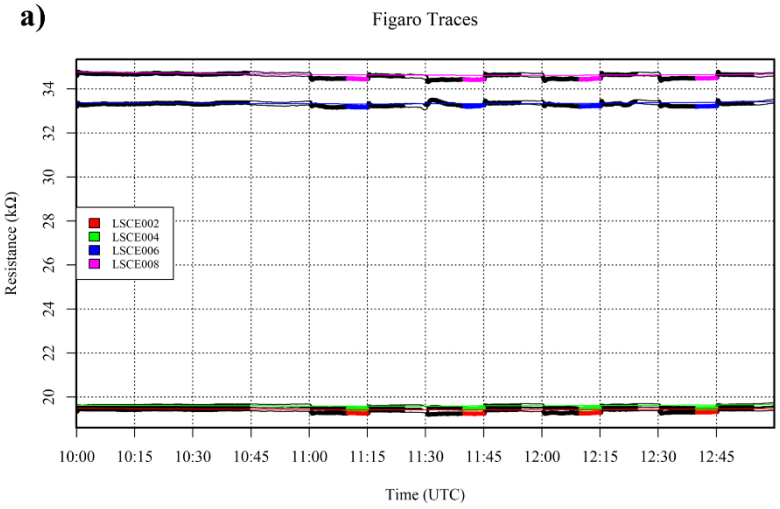
a)
Figaro Traces
Resistance (kΩ)
LSCE002
LSCE004
LSCE006
LSCE008
Time (UTC)

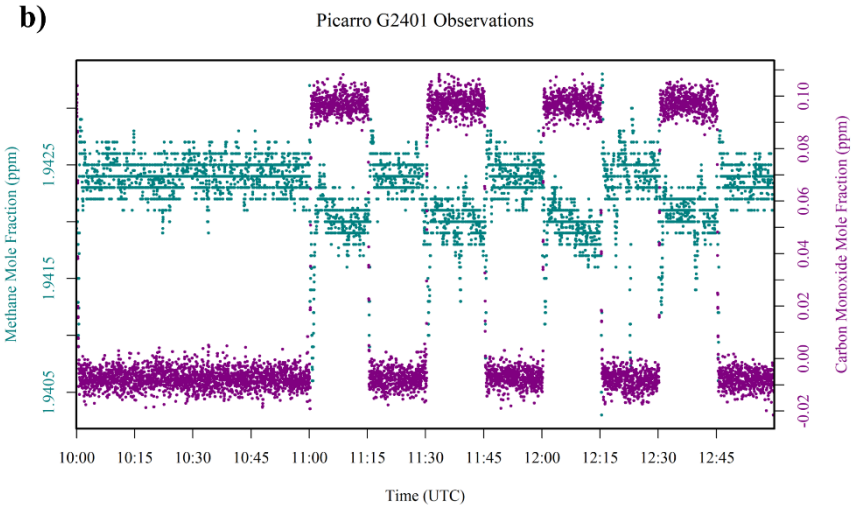
b)
Picarro G2401 Observations
Methane Mole Fraction (ppm)
Carbon Monoxide Mole Fraction (ppm)
Time (UTC)

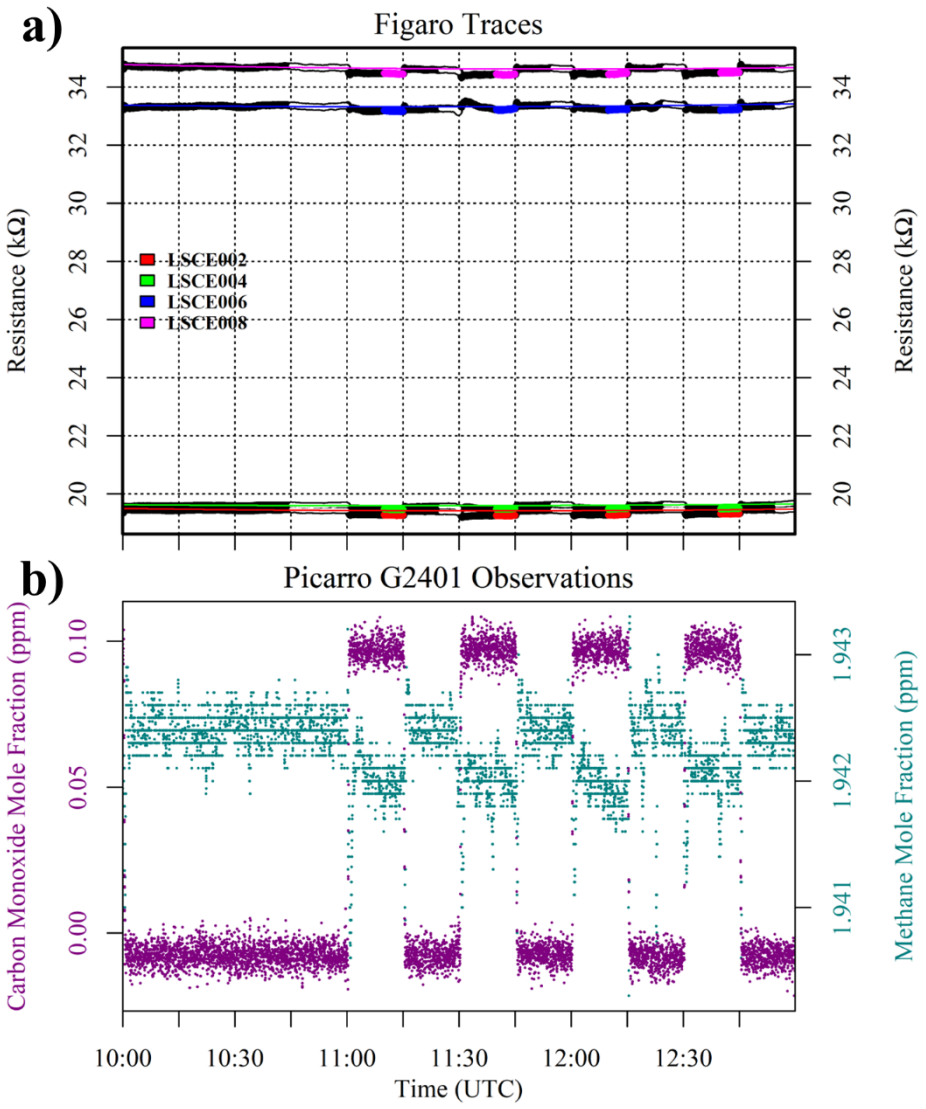

Figure 12: (a) Measured resistance for five Figaro sensors (black dots), when varying between 0.0 ppm and 0.1 ppm carbon monoxide mole fraction in standard gas. Highlighted c~~C~~oloured dots represent 5-minute periods used to derive an average resistance for each 0.1 ppm interval (see legend for corresponding sensor colours). White-highlighted dots indicate periods used to derive 0 ppm reference resistances for each sensor and coloured lines show respective polynomial reference resistance fits. (b) Corresponding Picarro G2401 observations. Methane (dark cyan) mole fraction measurements are plotted on the left-hand axis and carbon monoxide (dark magenta) mole fraction measurements are plotted on the right-hand axis.

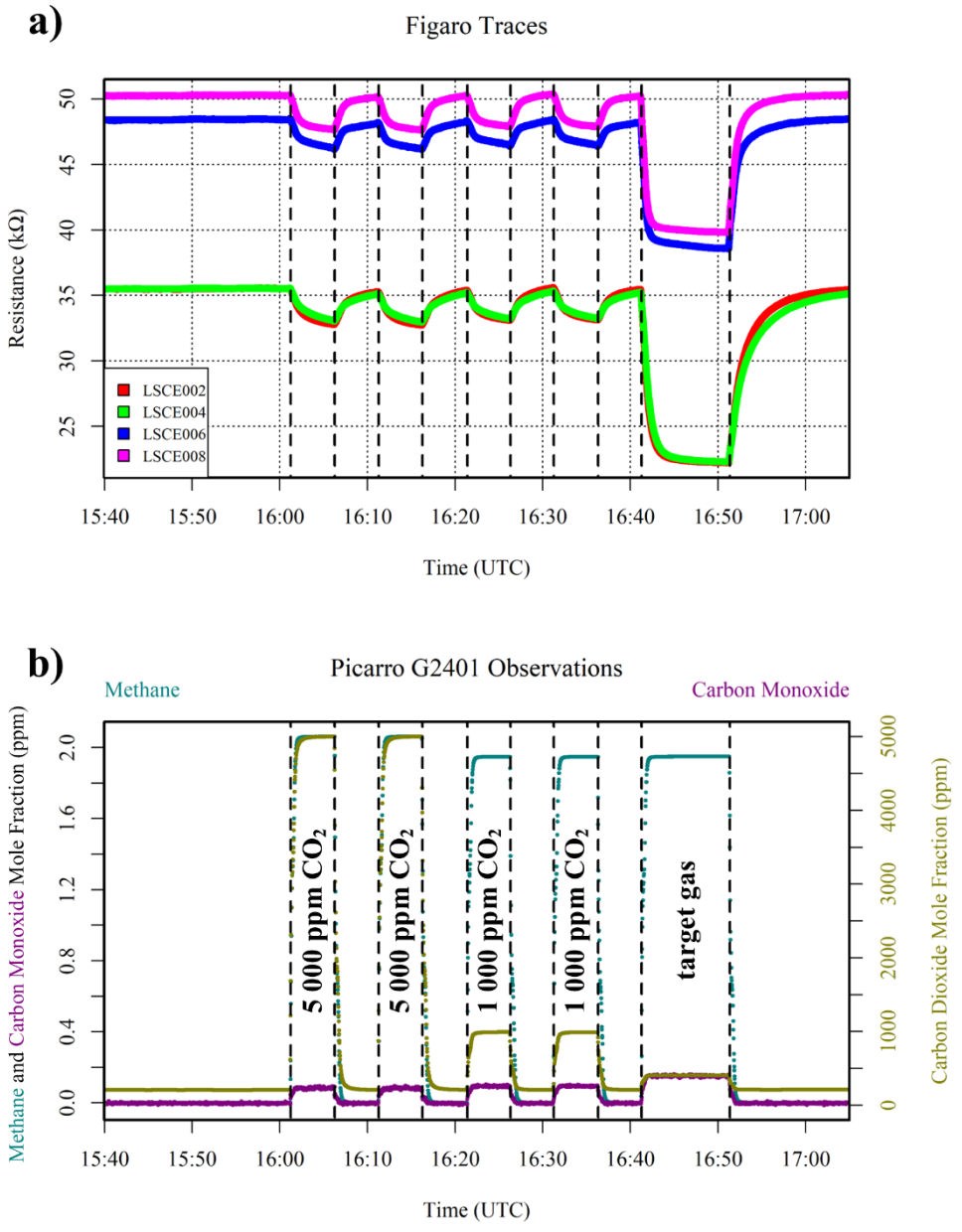
a)
Figaro Traces
Resistance (kΩ)
25
30
35
40
45
50
LSCE002
LSCE004
LSCE006
LSCE008
15:40
15:50
16:00
16:10
16:20
16:30
16:40
16:50
17:00
Time (UTC)
b)
Picarro G2401 Observations
Methane
Carbon Monoxide
Methane and Carbon Monoxide Mole Fraction (ppm)
0.0
0.4
0.8
1.2
1.6
2.0
5 000 ppm CO2
5 000 ppm CO2
1 000 ppm CO2
1 000 ppm CO2
target gas
0
1000
2000
3000
4000
5000
Carbon Dioxide Mole Fraction (ppm)
15:40
15:50
16:00
16:10
16:20
16:30
16:40
16:50
17:00
Time (UTC)

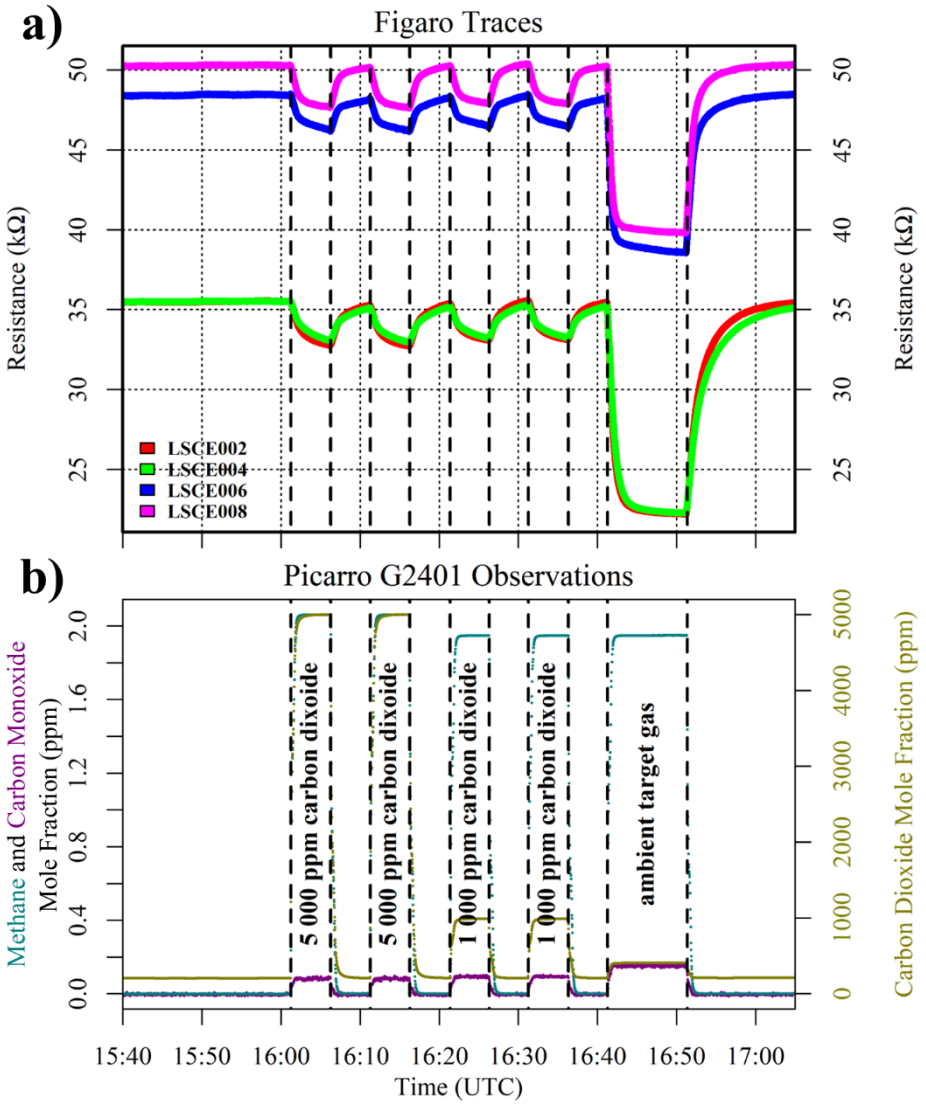

Figure 13: (a) Measured resistance for four Figaro sensors (coloured dots; see legend) in System B, under exposure to 5 000 ppm and 1 000 ppm carbon dioxide mole fraction, compared to gas from a zero-air generator. (b) Corresponding Picarro G2401 observations, with annotations indicating the sampled cylinder type. Areas not annotated correspond to gas from the zero-air generator. Methane (dark cyan) and carbon monoxide (dark magenta) mole fraction measurements are plotted on the left-hand axis. Carbon dioxide (dark yellow) mole fraction measurements are plotted on the right-hand axis.

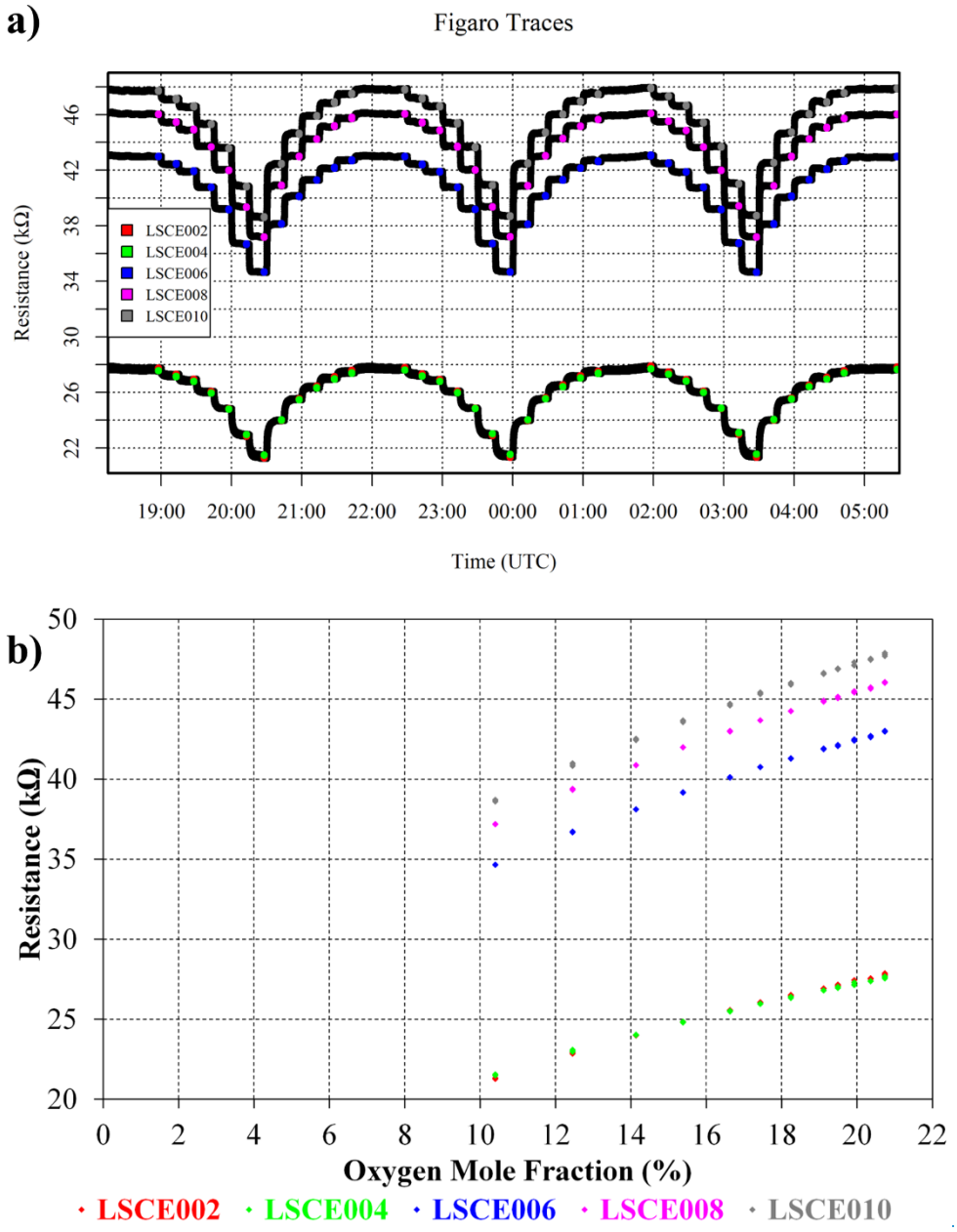
a)
Figaro Traces
Resistance (kΩ)
22
26
30
34
38
42
46
LSCE002
LSCE004
LSCE006
LSCE008
LSCE010
19:00
20:00
21:00
22:00
23:00
00:00
01:00
02:00
03:00
04:00
05:00
Time (UTC)
b)
Resistance (kΩ)
20
25
30
35
40
45
50
0
2
4
6
8
10
12
14
16
18
20
22
Oxygen Mole Fraction (%)
LSCE002
LSCE004
LSCE006
LSCE008
LSCE010

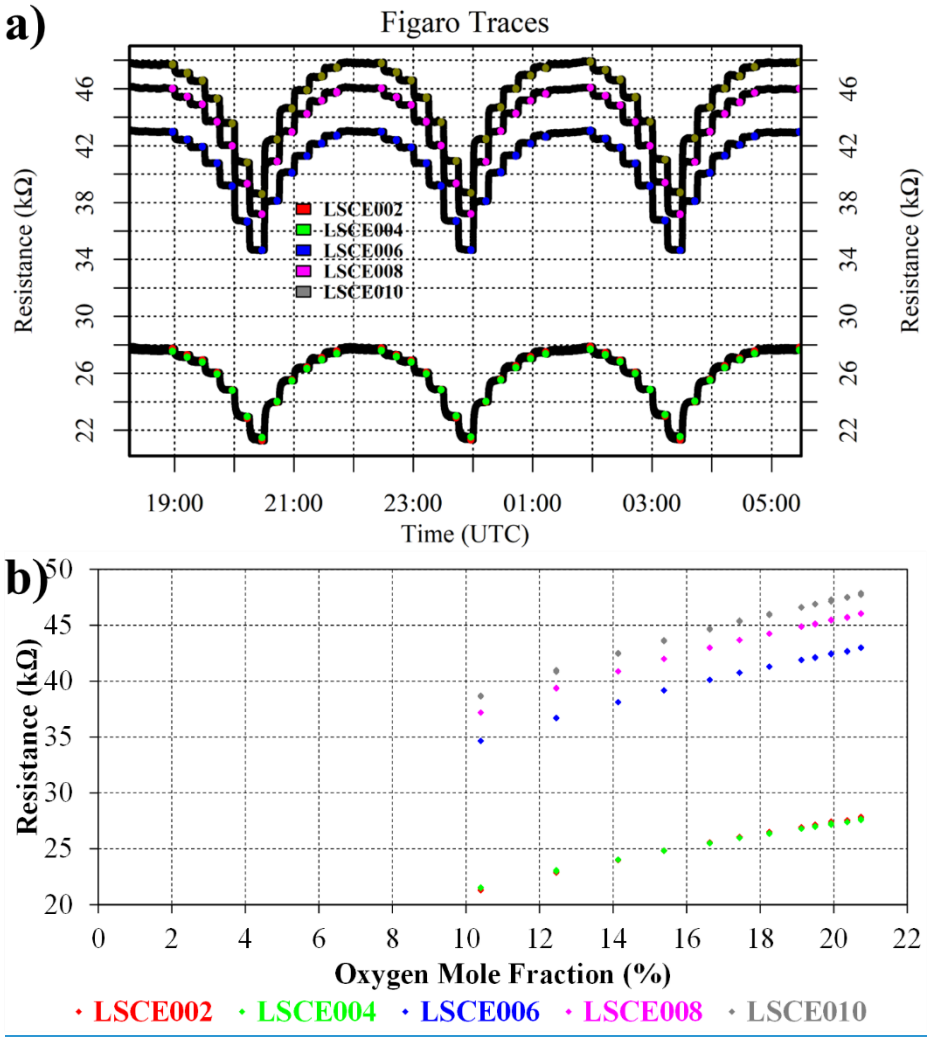

Figure 14: (a) Measured resistance for five Figaro sensors (black dots), when depleting the oxygen content of gas from a zero-air generator with nitrogen gas. Highlighted c~~C~~oloured dots represent periods used to derive 2-minute average resistance value for each interval (see legend for corresponding sensor colours). (b) Figaro 2-minute resistance averages against corresponding oxygen mole fraction.

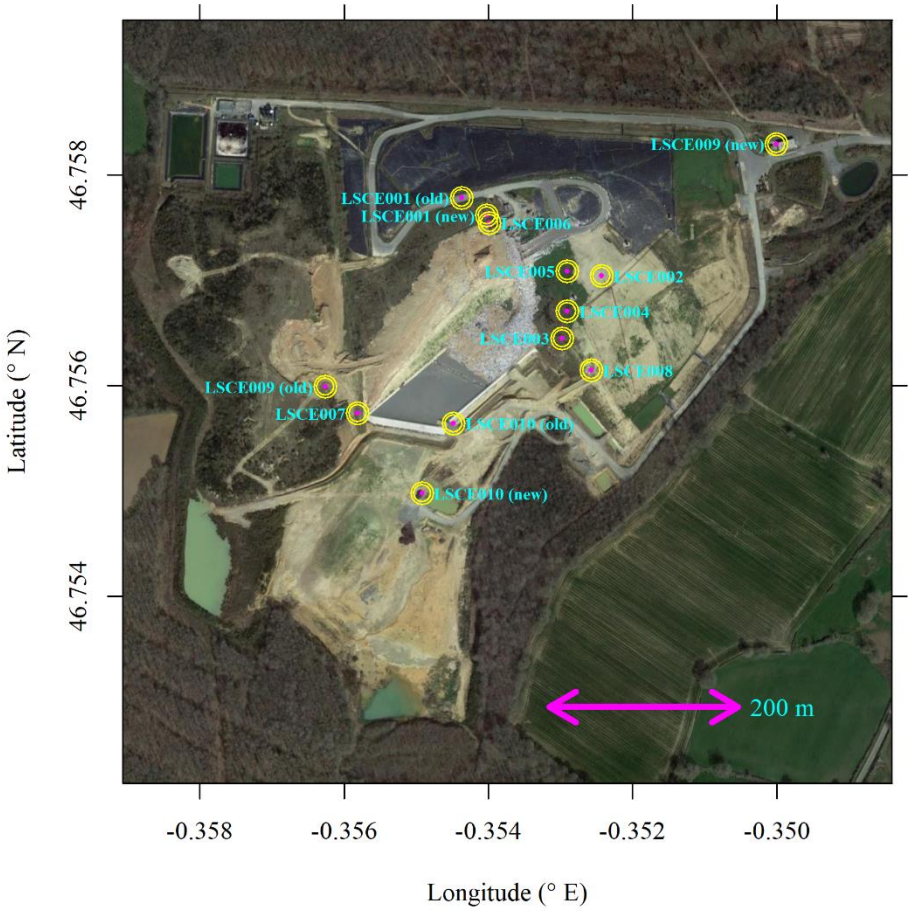

1175

Figure 15: System A logger locations at the SUEZ Amailloux landfill site. Three sensors were moved from location "old" to location "new" (see text for details). The background image is taken from Google Maps (imagery (2021): CNES/Airbus, Maxar Technologies).

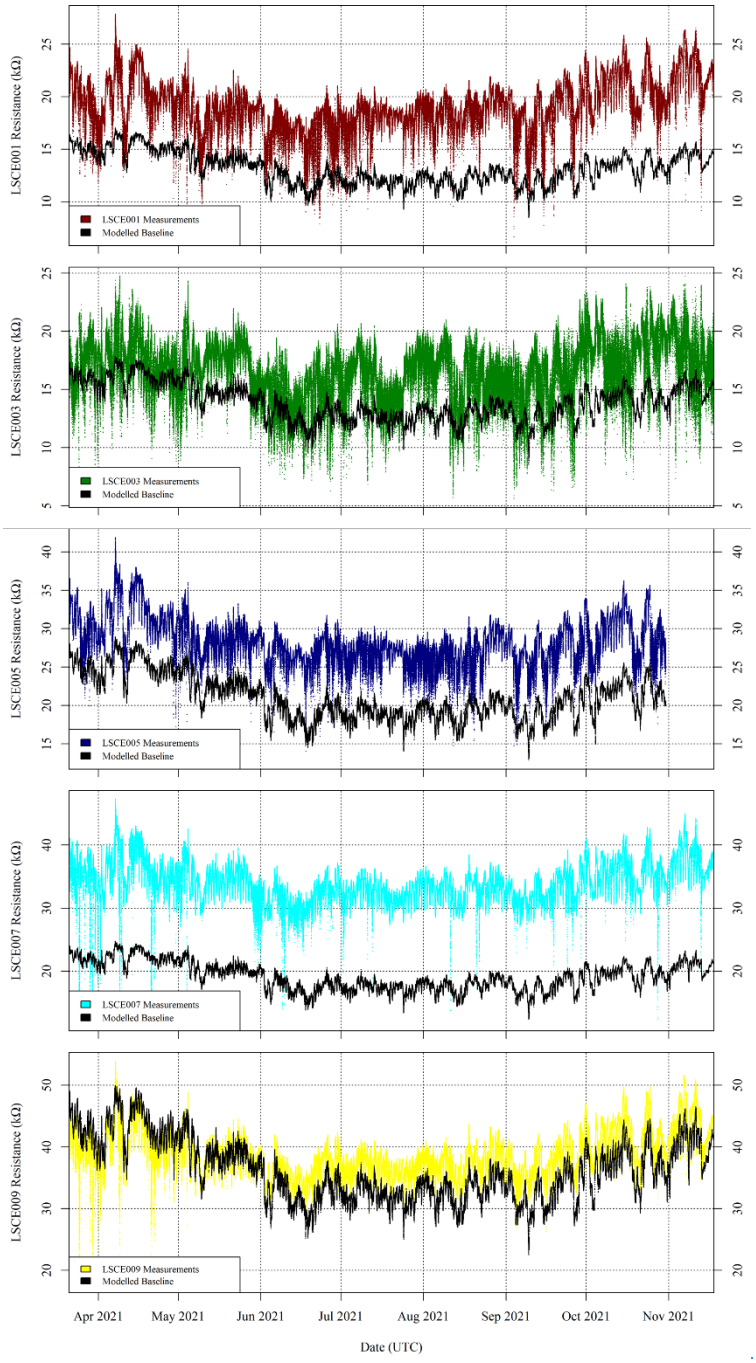
LSCE001 Resistance (kΩ)
LSCE001 Measurements
Modelled Baseline
LSCE003 Resistance (kΩ)
LSCE003 Measurements
Modelled Baseline
LSCE005 Resistance (kΩ)
LSCE005 Measurements
Modelled Baseline
LSCE007 Resistance (kΩ)
LSCE007 Measurements
Modelled Baseline
LSCE009 Resistance (kΩ)
LSCE009 Measurements
Modelled Baseline
Apr 2021
May 2021
Jun 2021
Jul 2021
Aug 2021
Sep 2021
Oct 2021
Nov 2021
Date (UTC)

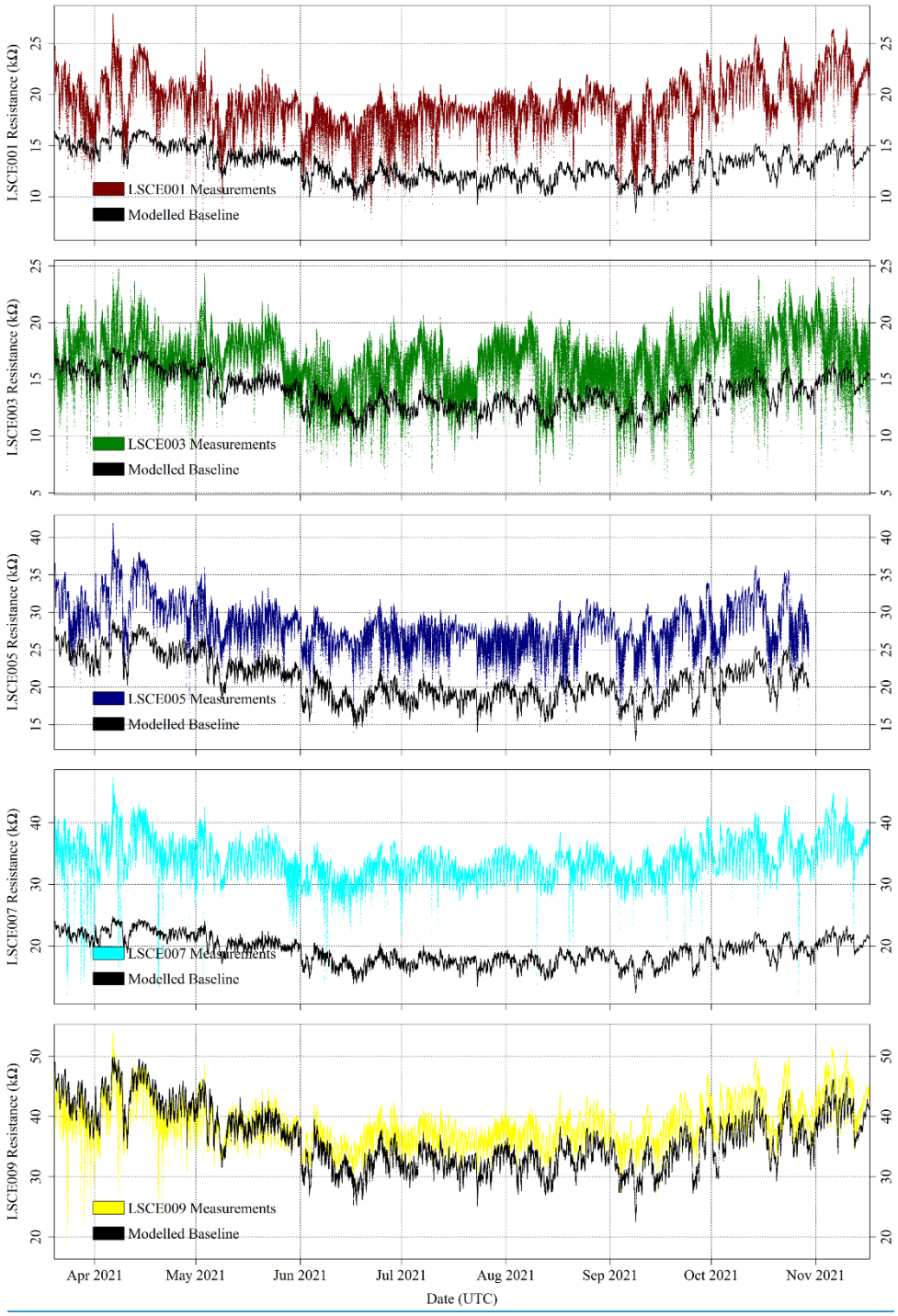

Figure 16: Measured System A Figaro resistance (coloured dots) and modelled standard 2 ppm [CH_4] reference resistance (black dots) from the SUEZ Amailloux landfill site for LSCE001, LSCE003, LSCE005, LSCE007 and LSCE009 (top to bottom) between 20 March 2021 and 17 November 2021 (period 1).

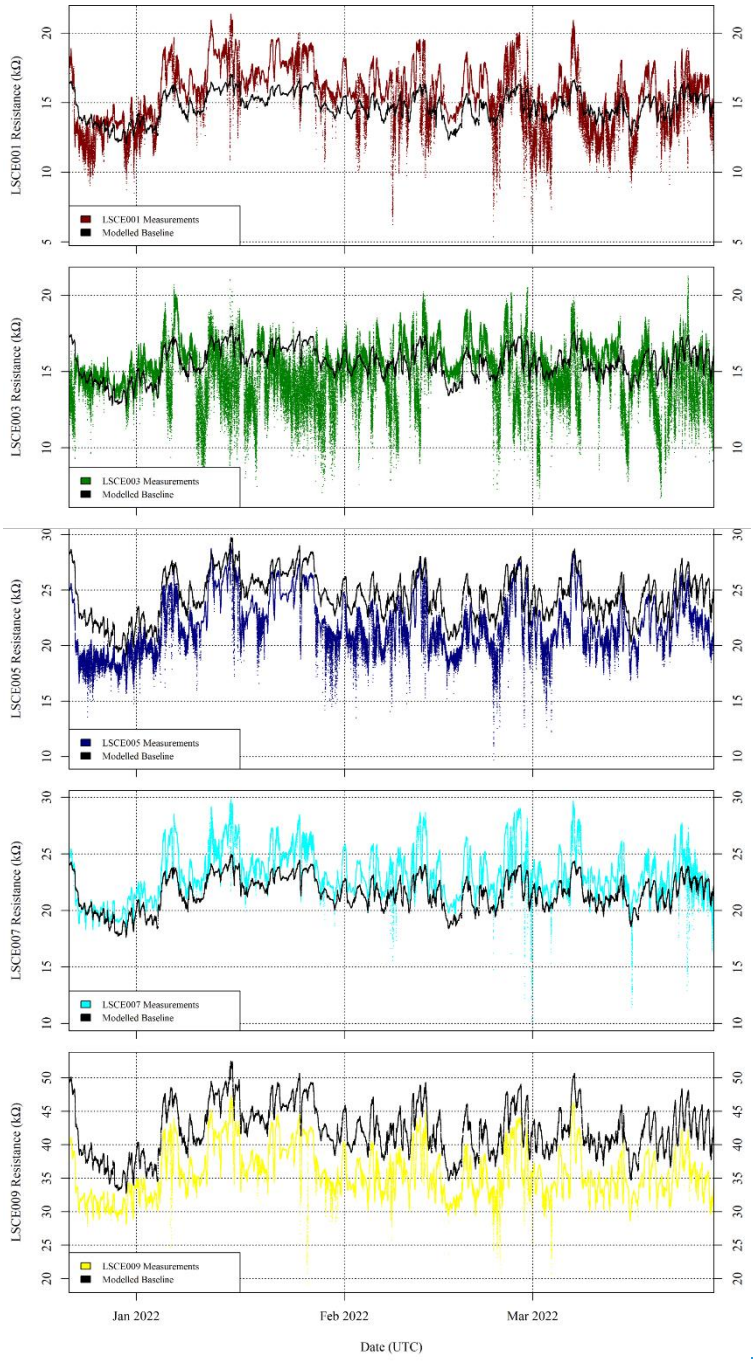
LSCE001 Resistance (kΩ)
LSCE001 Measurements
Modelled Baseline
LSCE003 Resistance (kΩ)
LSCE003 Measurements
Modelled Baseline
LSCE005 Resistance (kΩ)
LSCE005 Measurements
Modelled Baseline
LSCE007 Resistance (kΩ)
LSCE007 Measurements
Modelled Baseline
LSCE009 Resistance (kΩ)
LSCE009 Measurements
Modelled Baseline
Jan 2022
Feb 2022
Mar 2022
Date (UTC)

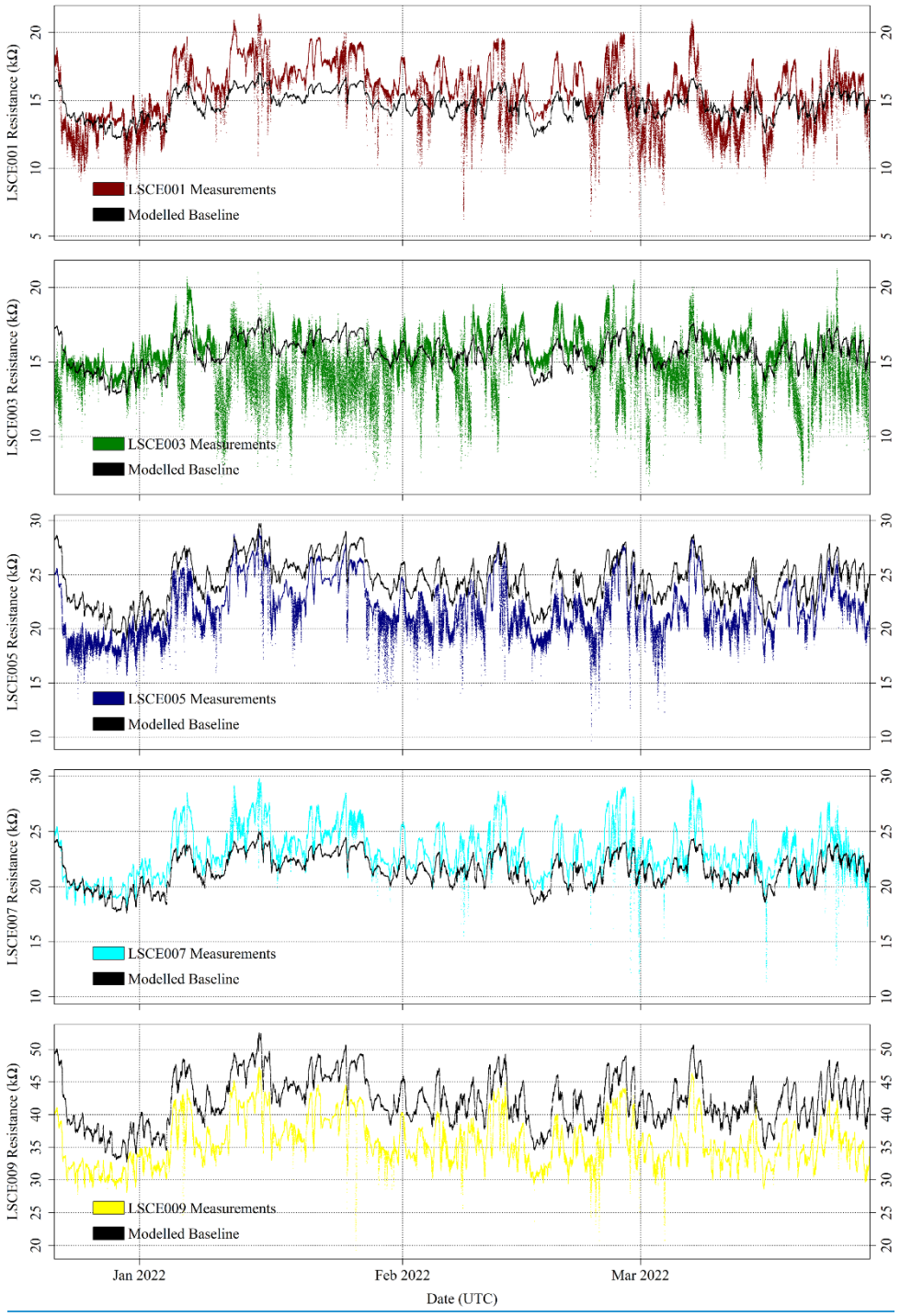

1185 **Figure 17: Measured System A Figaro resistance (coloured dots) and standard 2 ppm [CH_4] reference resistance (black dots) from the SUEZ Amailloux landfill site for LSCE001, LSCE003, LSCE005, LSCE007 and LSCE009 (top to bottom) between 22 December 2021 and 27 March 2021 (period 2).**

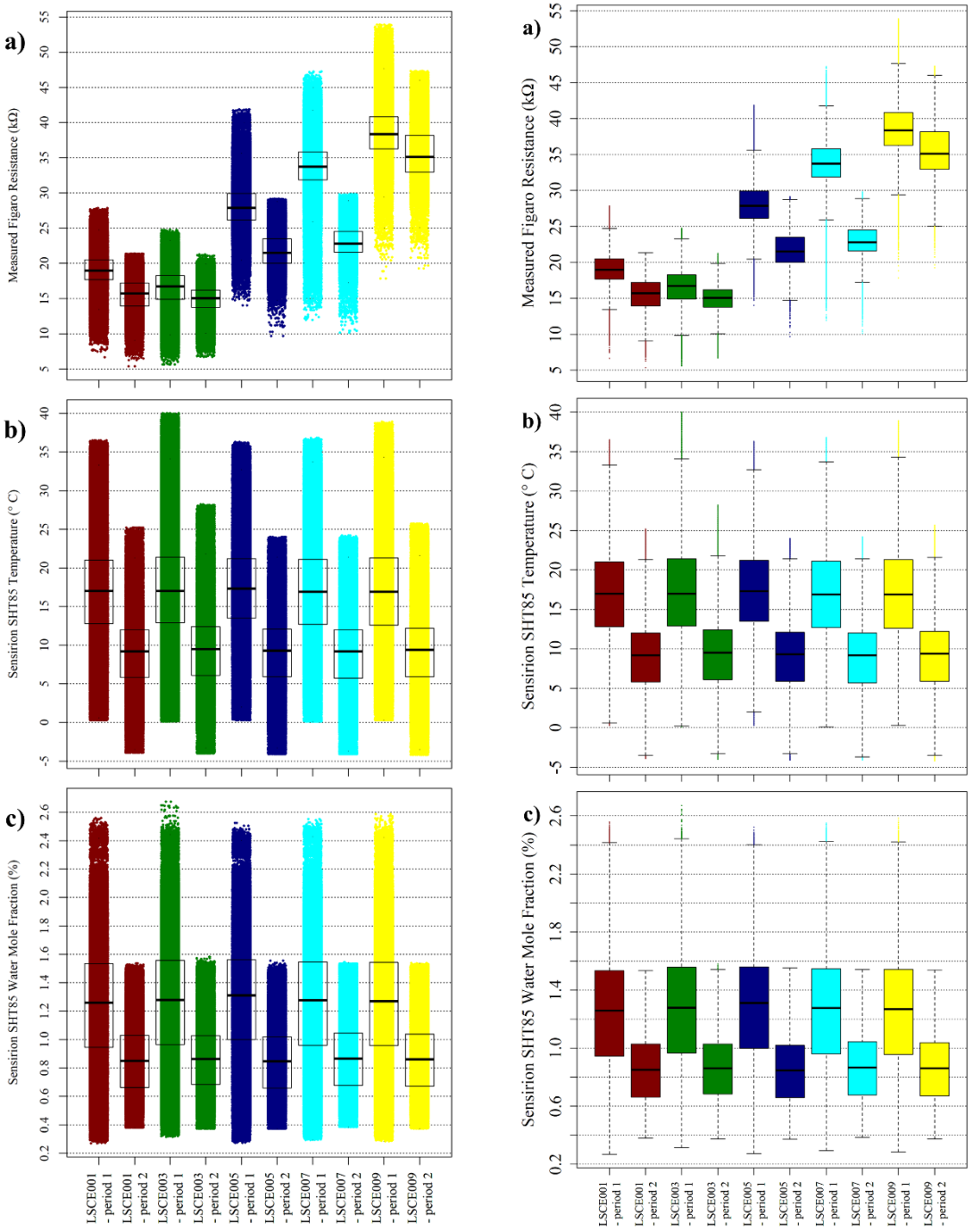

Figure 18: (a) Measured Figaro resistance, (b) measured SHT85 temperature and (c) derived SHT85 water vapour mole fraction (see text for derivation details), from inside each LSCE001, LSCE003, LSCE005, LSCE007 and LSCE009 System A enclosure at the

SUEZ Amailloux landfill site, shown as box plots, with outliers presented as (coloured dots). Data for period 1 and period 2 are plotted separately. The mean and interquartile range for each period are shown in black.

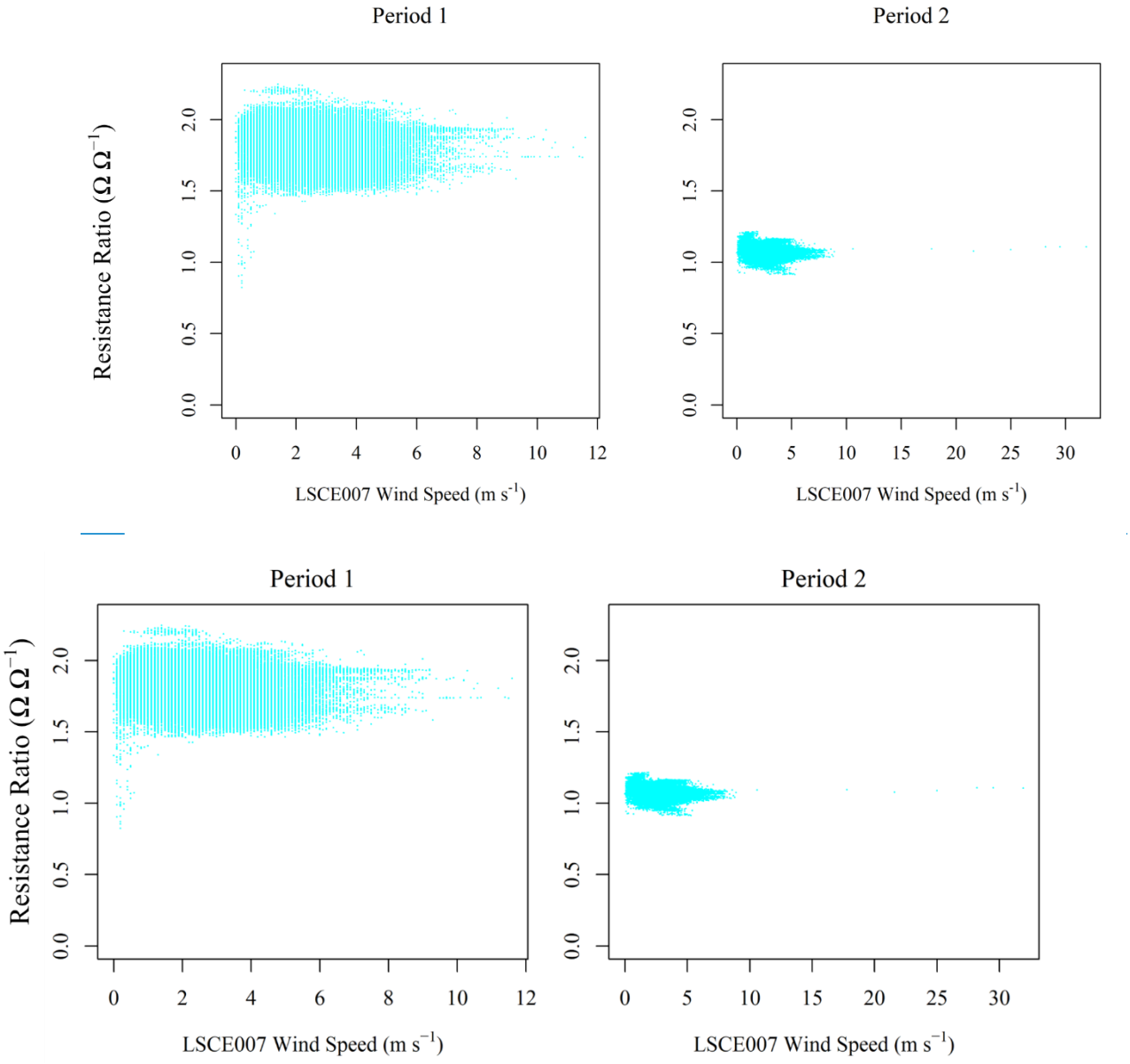

Figure 19: The ratio between measured Figaro resistance and standard 2 ppm [CH_4] reference resistance (cyan dots) from the SUEZ Amailloux landfill site for LSCE007, plotted against minute-averaged wind speed as measured by the LSCE007 anemometer, for wind directions between 180° and 270°. Data from period 1 is plotted on the left and data from period 2 is plotted on the right.

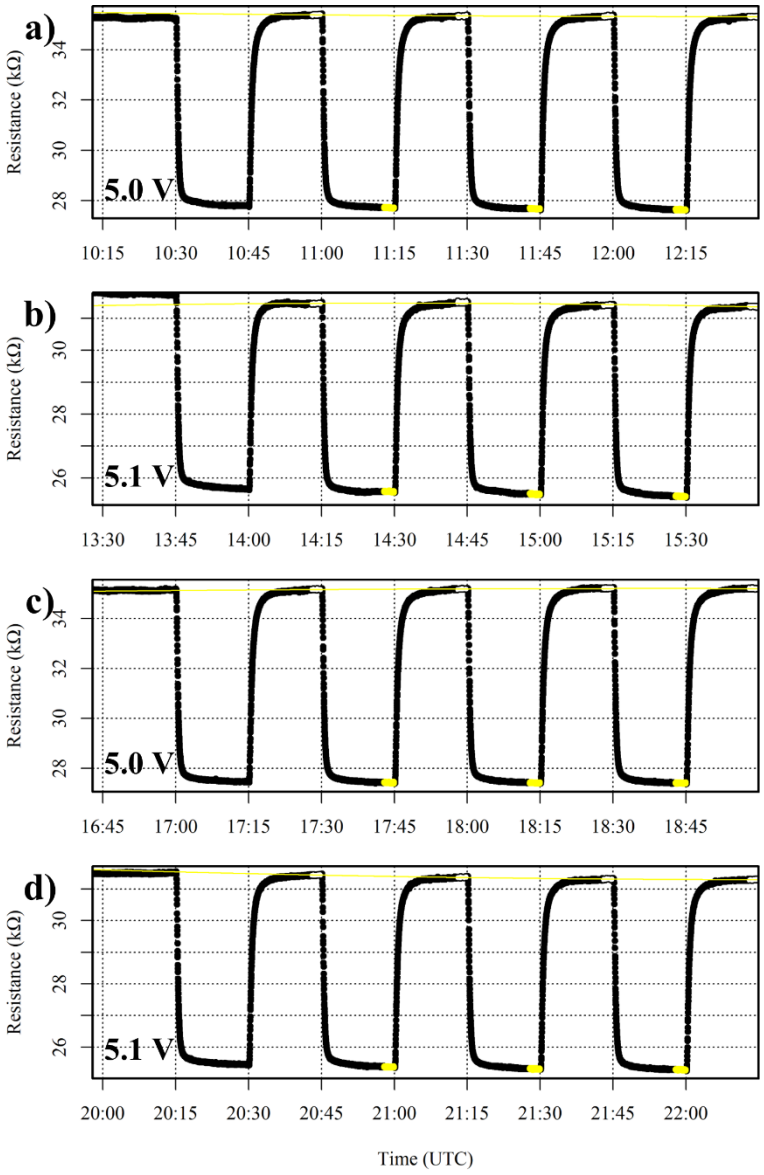

Figure A1: Measured LSCE009 resistance (black dots), when varying between zero-air and ambient target gas for (a) test 1 at 5.00 V, (b) test 2 at 5.10 V, (c) test 3 at 5.00 V and (d) test 4 at 5.10 V supply voltage. Highlighted y~~Y~~ellow dots show 2-minute periods used to derive an average resistance value for three ambient target gas sampling periods. White-highlighted dots indicate periods used to derive zero-air baseline resistances and yellow lines show respective polynomial baseline fits.

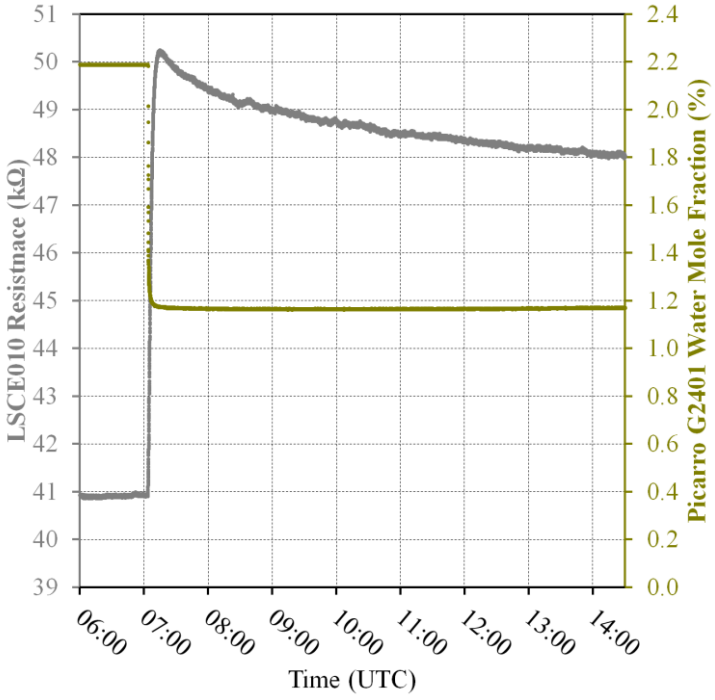
LSCE010 Resistnace (kΩ)
Picarro G2401 Water Mole Fraction (%)
Time (UTC)
51
50
49
48
47
46
45
44
43
42
41
40
39
2.4
2.2
2.0
1.8
1.6
1.4
1.2
1.0
0.8
0.6
0.4
0.2
0.0
06:00
07:00
08:00
09:00
10:00
11:00
12:00
13:00
14:00

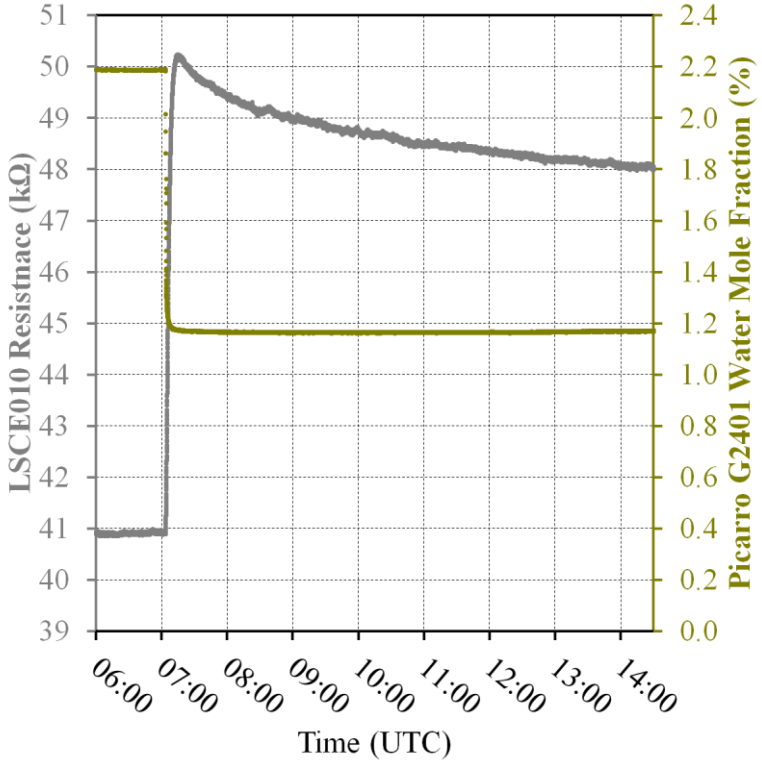
LSCE010 Resistnace (kΩ)
Picarro G2401 Water Mole Fraction (%)
Time (UTC)
51
50
49
48
47
46
45
44
43
42
41
40
39
2.4
2.2
2.0
1.8
1.6
1.4
1.2
1.0
0.8
0.6
0.4
0.2
0.0
06:00
07:00
08:00
09:00
10:00
11:00
12:00
13:00
14:00

Figure B1: Figaro LSCE010 measured resistance (grey points; left-hand axis) in response to a water vapour mole fraction ~~(dark yellow points; right-hand axis)~~ drop ~~in System B~~, as measured by the Picarro G2401 (dark yellow points; right-hand axis), while sampling zero-air generator gas inside System B.